UNIVERSITY OF CALIFORNIA
RIVERSIDE

Role of Endothelial Cell Stiffening in Choroidal Atrophy Associated with Dry Age-Related Macular Degeneration

A Dissertation submitted in partial satisfaction
of the requirements for the degree of

Doctor of Philosophy

in

Bioengineering

by

Andrea Paulina Cabrera

September 2018

Dissertation Committee:
Dr. Kaustabh Ghosh, Chairperson
Dr. Dimitrios Morikis
Dr. Joshua Morgan

The Dissertation of Andrea Paulina Cabrera is approved:

Committee Chairperson

University of California, Riverside

ACKNOLWDGEMENTS

I would like to express my utmost gratitude and appreciation to my committee chairperson, Professor Kaustabh Ghosh, who has been patient and helpful in guiding me towards the completion of this dissertation and most importantly, helped open my mind. This is a gift that will remain with me for the remainder of this lifetime. I would like to thank my committee members, Professor Dimitrios Morikis and Professor Joshua Morgan, whose kind words of encouragement made the world of difference and made me feel supported when I needed it the most.

I would also like to thank Soroush Ardekani, Harry Scott, Arun Bhaskaran, Xiao Yang, Shane Eum, Boi Quach, and Neha Palegar, and all the members of BioMoDeL who became my lab family. I am grateful for your friendship and bond we formed through this experience and the insightful discussions we've had over the years.

Finally, I would like to acknowledge that the text that appears in Chapter 2 of this dissertation, in full, is a reprint of the material as it appears in Investigative Ophthalmology & Visual Science entitled "Senescence increases choroidal endothelial stiffness and susceptibility to complement injury: Implications for choriocapillaris loss in AMD" published in November 2016 together with the text that appears in the Appendix, in full, which is a reprint of the material as it appears in Molecular Vision entitled "Peptide redesign for inhibition of the complement system: Targeting age-related macular degeneration" published in October 2016. The co-author Kaustabh Ghosh listed in these publications directed and supervised the research, which forms the basis for this dissertation.

DEDICATION

This dissertation is dedicated to my parents and brother, whose selfless love, endless support, and sacrifices have made this possible.

ABSTRACT OF THE DISSERTATION

Role of Endothelial Cell Stiffening in Choroidal Atrophy Associated with Dry Age-Related Macular Degeneration

by

Andrea Paulina Cabrera

Doctor of Philosophy, Graduate Program in Bioengineering
University of California, Riverside, September 2018
Dr. Kaustabh Ghosh, Chairperson

Age-related macular degeneration (AMD) is the leading cause of blindness in the aging population. Recent studies have implicated choriocapillaris (CC) dropout and choroidal thinning in AMD pathogenesis, potentially mediated by hypoxia-induced retinal pigment epithelium dysfunction. However, the precise mechanism underlying choroidal atrophy remains unknown. The goal of this research was to address this vital gap in our mechanistic understanding of choroidal atrophy associated with dry AMD.

Since complement activation, a major risk factor for dry AMD, leads to the deposition of membrane attack complex (MAC; C5b-9n) on choroidal vessels,it may lead to choroidal endothelial cell (EC) atrophy and the observed loss of CC in AMD eyes. Interestingly, MAC deposition also occurs in young non-AMD eyes, thus indicating that specific age-related factors may contribute to MAC-induced choroidal degeneration in AMD eyes. Since aging, a major nonmodifiable risk factor for AMD, has been shown to increase stiffness of retinal vessels and enhance pro-inflamatory cues in non-opthalmic vessels such as aorta and arteries, the central hypothesis of this research was that aging

increases CC stiffening that, in turn, enhances EC susceptibility to MAC injury.

Findings from the current research revealed for the first time that aging leads to choroidal EC stiffening that in turn, contributes significantly to the increased susceptibility to MAC injury. Further, these studies showed that the stiffening of aged choroidal ECs is cytoskeletal-mediated. Remarkably, reducing age-induced EC stiffness prevented MAC injury. Taken together, these novel findings not only elucidate a key role of EC stiffness but also identify potentially new targets (e.g. Rho-mediated cytoskeletal stiffening) for more effective therapies in the future.

Table of Contents

List of Schematics

List of Figures

List of Abbreviations

AMD	Age-related macular degeneration
AFM	Atomic force microscope
BM	Bruch's membrane
C5b-9n	Membrane attack complex pore
CC	Choriocapillaris
EC	Endothelial cell
FBS	Fetal bovine serum
GFP-LAMP1	Green Fluoresence Protein-Lysosome Associated Membrane Protein 1
MAC	Membrane attack complex
PFA	Paraformaldehyde
ROCK	Rho-associated Kinase
VEGF	Vascular endothelial growth factor
VBS	Veronal Buffered Saline

CHAPTER 1

INTRODUCTION

Preface

This Chapter provides a brief background of the pathogenesis of Age-related Macular Degeneration (AMD) and discusses the potential role of age-associated endothelial cell (EC) stiffening in complement-mediated choriocapillaris (CC) degeneration. The global aim of this doctoral research is to understand the link between age-related choroidal EC stiffening, complement activation, and choroidal atrophy associated with dry AMD and to identify new classes of therapeutic targets for superior AMD management in the future.

Background and Significance

Age-related macular degeneration (AMD) is the leading cause of blindness in the elderly population, in which aging is regarded as the major non-modifiable risk factor. This blinding disease affects approximately 11 million people in the US alone with numbers expected to double by the year 2050.[1,2] This eye disease manifests as a loss of central vision (Fig.1A) resulting from blood vessel multiplication and leakiness, as seen by fundus photography (Fig. 1B). Despite the common prevalence of AMD, only 10-15% of individuals with advanced 'wet' stage AMD benefit from current therapies while no therapies exist for the more prevalent early 'dry' form.[3,4] Since dry AMD is a potential risk factor for wet AMD, there is recognition that more effective AMD management can be achieved by tackling the disease at the early stage. Thus, there is a critical need to better understand the mechanisms underlying dry AMD pathophysiology that may aid in the development of treatments for the vast majority of individuals with dry AMD.

Conventional View of AMD Pathophysiology

AMD is an inflammatory disease affecting the macula, the central region of the eye with the highest density of rods and cones, manifesting as a loss of central vision (Fig.1A). This potentially blinding diseases manifest in two forms: the early 'dry' stage and the more advanced 'wet' stage AMD. Dry AMD is clinically diagnosed by the

appearance of drusen deposits, composed predominately of apolipoprotein E and complement factors, between the phagocytic retinal pigment epithelial (RPE) layer and the underlying vasculature called the choriocapillaris (CC; Schematic 1).[3] CC is essential for maintenance of RPE homeostasis,[6] providing the delivery of nutrients and oxygen while the RPE supplies CC with vascular endothelial growth factor (VEGF) that is necessary for the healthy maintenance of blood vessels. As the number and size of drusen deposits increase with AMD progression, molecular diffusion of metabolites and VEGF is impaired, thereby disrupting RPE and choroid homeostatic conditions.[6,7] This, in turn, creates hypoxic conditions in the inner retina, leading to hypoxia-induced VEGF overproduction. Since VEGF simultaneously increases endothelial cell (EC) proliferation and disrupts cell-cell junctions, excessive VEGF secretion leads to uncontrolled vessel multiplication and leakiness, the hallmarks of advanced 'wet' stage of AMD.

Risk Factors Associated with AMD

Several associations have been made from epidemiological studies that link the deficiency of various factors with the incidence of AMD.

Non-modifiable risk factors: Aging is regarded as the major non-modefiable risk factor, with risk increasing from 2% for those aged 50-59, to nearly 30% for those over the age of 75.[14] Several genetic mutations have been identified implicating various pathways such as APOE (apolipoprotein E; chr 19),[15,16] CETP (cholesterylester transfer protein; chr 16),[17] VEGFA (vascular endothelial growth factor A; chr 6),[18,19] TIMP3

(tissue inhibitor of metalloproteinase 3; chr 22)[20] among many more. Further, several complement pathway genes such as complement factor H (CFH) gene on 1q32 and the ARMS2/HTRA1 locus, in addition to C2, CFB, C3 and CFI genes have been identified as potential risk factors.[21-23]

Modifiable risk factors: Cigarette smoking is recognized as a strong risk factor. Specifically, studies have shown that treatment of RPE cultures with nicotine, the most commonly investigated SS toxicant, cause cell thinning/flattening and dissolution of actin cytoskeleton, while nicotine-fed mice exhibited damaged photoreceptor-RPE interface.[24] Additionally, there have been studies reporting an increased risk in relation to sun exposure as well as low dietary intake of vitamins (A, C, and E), zinc, lutein, and omega-3 fatty acids.[25-28] However, the precise underlying mechanisms remain to be determined.

Current Pharmacological Treatments for AMD

Current pharmacological therapies targeting wet AMD are limited to anti-VEGF intravitreal injections, with various forms of anti-VEGF injections available on the market.[29-31]

Limitations: Current pharmacological intervention only targets wet AMD. Despite the success of anti-VEGF therapies in preventing neovascularization, this treatment is invasive, requiring frequent intravitreal injections that could result in infection, increased eye pressure, cataracts, or retinal detachment.[30-33] Further, success of treatment relies on

aggressive, long-term, disease-activity-based therapy. This raises concern for safety with prolonged suppression of systemic VEGF levels and the effect they could have on vascular function in the body.[34]

Due to these limitations and the belief that dry AMD is a potential risk factor for wet stage, there is a growing recognition that AMD can be treated more effectively at the earlier dry stage.[12] Success in this pursuit will, however, depend on our ability to properly dissect the mechanisms underlying the dry stage of this degenerative condition.

Choriocapillaris (CC) Atrophy as a New Target for Dry AMD

AMD has conventionally been regarded as an RPE-centric disease, including my previous studies which shown the contribution of RPE to drusen deposition (Appendix). However, more recent studies have begun to implicate an important role of CC in this condition. Specifically, histological studies of dry AMD eyes have recently shown that drusen deposition at the RPE/CC interface is strongly correlated with loss of choroidal ECs and CC atrophy.[11,12] With the number of drusen deposits increasing as AMD progresses, molecular diffusion of metabolites and VEGF is impaired, disrupting RPE and choroid homeostatic conditions, further exacerbating hypoxic conditions of the inner retina. During the advanced 'wet' stage of AMD, excess production of VEGF by RPE results in the local formation of leaky blood vessels, which if uncontrolled, invade the various tissue layers, resulting in loss of central vision. This potential mechanism points

implicates choroidal vascular atrophy as a key determinant of AMD progression (Schematic 2).

Recent studies have revealed that Dry AMD is associated with subretinal inflammation characterized by excessive complement activation and leukocyte infiltration in the sub-RPE space.[8,9] This sub-retinal inflammatory milieu contributes to membrane attack complex (MAC; C5b-9_n) deposition on the CC.[11,12] Since MAC forms pores in cell membrane and causes cell lysis, it may contribute to choroidal endothelial loss and CC degeneration associated with dry AMD. Indeed, the degenerating CC in old eyes with dry AMD exhibit strong MAC deposition,[11] which is consistent with the hypothesis of MAC-induced CC degeneration. Interestingly, MAC is also abundant on the healthy CC of young eyes.[11] Thus, *specific age-related factors likely contribute to CC degeneration observed in AMD.*

Since dry AMD is more prevalent and a potential risk factor for wet AMD, the potential role of CC degeneration in the pathogenesis of dry AMD necessitates identification of the factors that contribute to the loss of CC in this condition.

Potential Role of Age-associated Endothelial Cell (EC) Stiffening in Complement-mediated CC Degeneration

Vascular stiffening has been implicated in many age-associated pathologies. More specifically, studies have shown that aging is associated with stiffening of various ophthalmic tissues such as retinal vessels and sclera.[35,36] Separate studies with non-

ophthalmic vessels such as aorta and arteries have indicated that age-related vascular stiffening enhances vascular sensitivity to proinflammatory cues.[37,38] Such aberrant stiffness-dependent vascular dysfunction results from altered endothelial cytoskeletal tension (contractility) and mechanotransduction, the process by which mechanical cues get transduced into intracellular biochemical signaling pathways to produce a global cellular response. Importantly, studies by us and others have shown that EC stiffness *alone* can govern EC fate and function.[39-45] Since aging has been associated with stiffening of retinal vessels and the sclera,[35,36] this raises the possibility that choroidal vessels and ECs also become stiffer with aging that, in turn, exacerbates complement-mediated CC degeneration. However, whether aging is associated with increased cytoskeleton-mediated choroidal EC stiffening and enhanced CC sensitivity to complement deposition remains unknown.

My recent findings are the first to identify a possible mechanism by which aging may contribute to CC loss associated with dry AMD.[13] In these studies, cells exhibiting replicative senescence, which recapitulates many features of aging, were used to show that senescence increases choroidal EC stiffness that, in turn, exacerbates complement-induced injury. Remarkably, suppression of cell stiffness via pharmacological inhibition of Rho/ROCK, the key molecular pathway that controls cell stiffness (contractility), prevented these inflammatory effects on senescent ECs. Taken together, these findings indicate that increase in senescent EC stiffness contributes to complement-mediated CC dysfunction. By uncovering the previously unknown role of micromechanical cues in choroidal EC dysfunction, this research has the potential to illuminate a previously

unexplored territory in AMD research that can help identify new therapeutic targets for potentially effective management of dry AMD.

Hypothesis

Based on these findings, **the working hypothesis** of this doctoral dissertation is that aging causes choriocapillaris stiffening, that in turn increases choroidal endothelial cell stiffness, resulting in increased susceptibility to complement injury, culminating in cell lysis and eventual CC degeneration (Schematic 3).

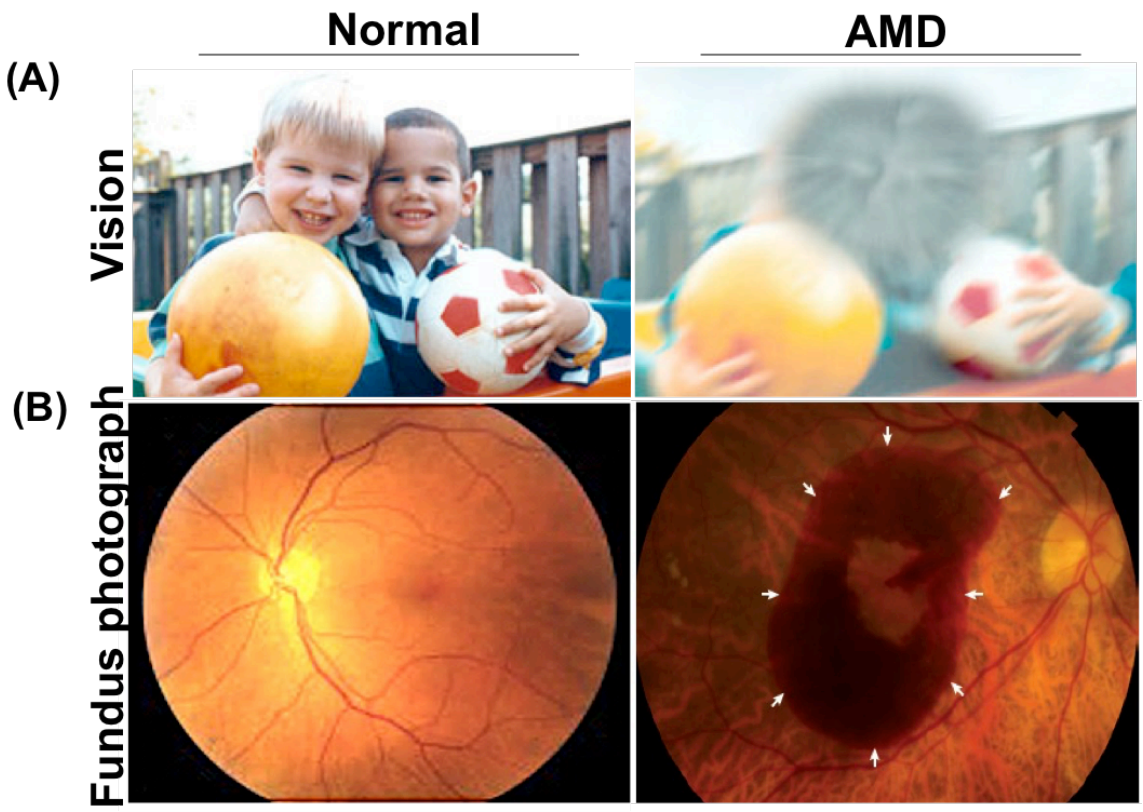

Adapted from:

https://web.archive.org/web/20131022195554/http://www.nei.nih.gov/photo/sims/images/amac_lg.jpg and Bowes Rickman et al. *IOVS* 2013

Figure 1.1: Clinical manifestation of AMD. (A) AMD is an inflammatory disease affecting the macula, the central region of the eye with the highest density of rods and cones, manifesting as a loss of central vision. (B) This loss in central vision is due to the blood vessel multiplication and leakiness.

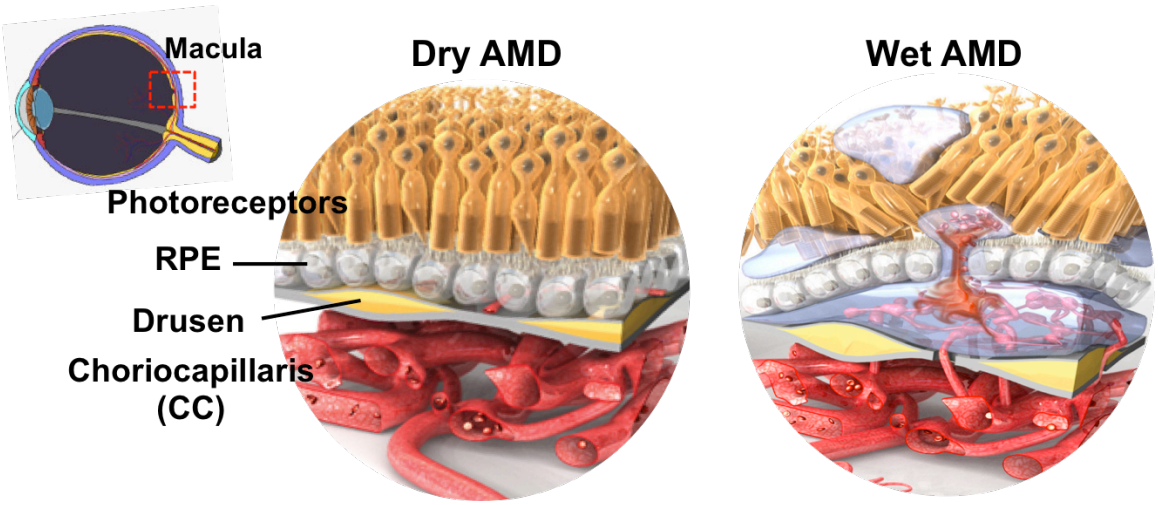

Adapted from: http://www.scienceofamd.org/learn/

Schematic 1.1: Progression of AMD. Dry AMD is clinically diagnosed by the appearance of drusen deposits, composed predominately of apolipoprotein E and complement factors, between the phagocytic retinal pigment epithelial (RPE) layer and the underlying vasculature, the choriocapillaris (CC). As the number and size of drusen deposits increase with AMD progression, molecular diffusion of metabolites and VEGF is impaired, thereby disrupting RPE and choroid homeostatic conditions. This, in turn, creates hypoxic conditions in the inner retina, leading to hypoxia-induced VEGF overproduction. Since VEGF simultaneously increases endothelial cell (EC) proliferation and disrupts cell-cell junctions, excessive VEGF secretion leads to uncontrolled vessel multiplication and leakiness, the hallmarks of advanced 'wet' stage of AMD.

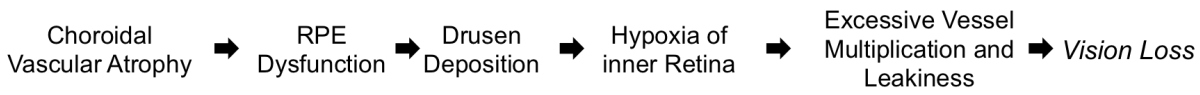

Schematic 1.2. **Potential mechanism of AMD Progression.** Although AMD has conventionally been regarded as an RPE-centric disease, more recent studies have begun to implicate an important role of CC in this condition. Studies of dry AMD eyes have recently shown that drusen deposition at the RPE/CC interface is strongly correlated with loss of choroidal ECs and CC atrophy. With the number of drusen deposits increasing as AMD progresses, molecular diffusion of metabolites and VEGF is impaired, disrupting RPE and choroid homeostatic conditions, further exacerbating hypoxic conditions of the inner retina. During the advanced 'wet' stage of AMD, excess production of VEGF by RPE results in the local formation of leaky blood vessels, which if uncontrolled, invade the various tissue layers, resulting in loss of central vision.

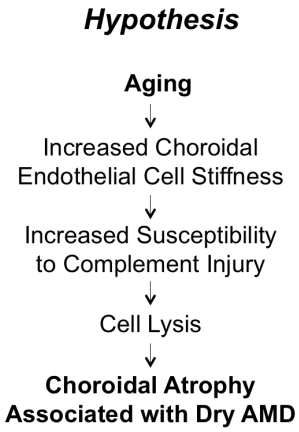

Schematic 1.3. **Working hypothesis** of this doctoral proposal is that aging leads to an increase in Rho-dependent choroidal endothelial EC stiffness that, in turn, exacerbates the degenerative effects of complement activation and causes EC atrophy

References

1. Cook HL, Patel PJ, Tufail A. Age-related macular degeneration: diagnosis and management. *Br Med Bull*. 2008;85:127– 149.

2. Friedman DS, O'Colmain BJ, Munoz B, et al. Prevalence of age-related macular degeneration in the United States. *Arch Ophthalmol*. 2004;122:564–572.

3. Ambati J, Fowler BJ. Mechanisms of age-related macular degeneration. *Neuron*. 2012;75:26–39.

4. Zhang K, Zhang L, Weinreb RN. Ophthalmic drug discovery: novel targets and mechanisms for retinal diseases and glaucoma. *Nat Rev Drug Discov*. 2012;11:541–559.

5. Mullins RF, Johnson MN, Faidley EA, Skeie JM, Huang J. Choriocapillaris vascular dropout related to density of drusen in human eyes with early age-related macular degeneration. *Invest Ophthalmol Vis Sci* 2011;52:1606-1612.

6. McLeod DS, Grebe R, Bhutto I, Merges C, Baba T, Lutty GA. Relationship between RPE and choriocapillaris in age-related macular degeneration. *Invest Ophthalmol Vis Sci*. 2009;50: 4982–4991.

7. McLeod DS, Taomoto M, Otsuji T, Green WR, Sunness JS, Lutty GA. Quantifying changes in RPE and choroidal vasculature in eyes with age-related macular degeneration. Invest *Ophthalmol Vis Sci*. 2002;43:1986–1993.

8. Anderson DH, Mullins RF, Hageman GS, Johnson LV. A role for local inflammation in the formation of drusen in the aging eye. *Am J Ophthalmol* 2002;134:411-431.

9. Parmeggiani F, Romano MR, Costagliola C, et al. Mechanism of inflammation in age-related macular degeneration. *Mediators Inflamm*. 2012;2012:546786.

10. Luo C, Zhao JW, Madden A, Chen M, Xu HP. Complement expression in retinal pigment epithelial cells is modulated by activated macrophages. *Exp Eye Res* 2013;112:93-101.

11. Mullins RF, Schoo DP, Sohn EH, et al. The membrane attack complex in aging human choriocapillaris: relationship to macular degeneration and choroidal thinning. *Am J Pathol* 2014;184:3142-3153.

12. Whitmore SS, Sohn EH, Chirco KR, et al. Complement activation and choriocapillaris loss in early AMD: implications for pathophysiology and therapy. *Prog Retin Eye Res*. 2015;45: 1–29.

13. Cabrera AP, Bhaskaran A, Xu J, Yang X, Scott HA, Mohideen U, Ghosh K; Senescence Increases Choroidal Endothelial Stiffness and Susceptibility to Complement Injury: Implications for Choriocapillaris Loss in AMD. *Invest. Ophthalmol. Vis. Sci.* 2016;57(14):5910-5918.

14. Klein, Ronald, et al. "The epidemiology of age-related macular degeneration." *Am J Ophthalmol* 137.3 (2004): 486-495.

15. McKay GJ, Patterson CC, Chakravarthy U, et al. Evidence of association of APOE with age-related macular degeneration—a pooled analysis of 15 studies. *Hum Mutat* 2011; 32: 1407–16.

16. Reynolds R, Rosner B, Seddon JM. Serum lipid biomarkers and hepatic lipase gene associations with age-related macular degeneration. *Ophthalmology* 2010; 117: 1989–95.

17. Neale BM, Fagerness J, Reynolds R, et al. Genome-wide association study of advanced age-related macular degeneration identifies a role of the hepatic lipase gene (LIPC). *Proc Natl Acad Sci* USA 2010;107: 7395–400.

18. Yu Y, Bhangale TR, Fagerness J, et al. Common variants near FRK/COL10A1 and VEGFA are associated with advanced age-related macular degeneration. *Hum Mol Genet* 2011; 20: 3699–709

19. Rakic JM, Lambert V, Devy L, et al. Placental growth factor, a member of the VEGF family, contributes to the development of choroidal neovascularization. *Invest Ophthalmol Vis Sci* 2003; 44: 3186–93.

20. Chen W, Stambolian D, Edwards AO, et al. Genetic variants near TIMP3 and high-density lipoprotein-associated loci influence susceptibility to age-related macular degeneration.

21. Klein RJ, Zeiss C, Chew EY, et al. Complement factor H polymorphism in age-related macular degeneration. *Science* 2005; 308: 385–89.

22. Maller JB, Fagerness JA, Reynolds RC, Neale BM, Daly MJ, Seddon JM. Variation in complement factor 3 is associated with risk of age-related macular degeneration. *Nat Genet* 2007; 39: 1200–01.

23. Fagerness JA, Maller JB, Neale BM, Reynolds RC, Daly MJ, Seddon JM. Variation near complement factor I is associated with risk of advanced AMD. *Eur J Hum Genet* 2009; 17: 100–04.

24. Yang L, Gong H, Wang Y, Yin H, Chen P, Zhang H. Nicotine alters morphology and function of retinal pigment epithelial cells in mice. *Toxicol Pathol*. 2010;38:560–567.

25. Delcourt C, Carriere I, Cristol JP, Lacroux A, Gerber M. Dietary fat and the risk of age-related maculopathy: the POLANUT study. *Eur J Clin Nutr* 2007; 61: 1341–44.

26. Seddon JM, Ajani UA, Sperduto RD, et al. Dietary carotenoids, vitamins A, C, and E, and advanced age-related macular degeneration. Eye Disease Case-Control Study Group. *JAMA* 1994; 272: 1413–20.

27. SanGiovanni JP, Chew EY, Agron E, et al. The relationship of dietary omega-3 long-chain polyunsaturated fatty acid intake with incident age-related macular degeneration: AREDS report no. 23. *Arch Ophthalmol* 2008; 126: 1274-79.

28. Seddon JM, George S, Rosner B. Cigarette smoking, fish consumption, omega-3 fatty acid intake, and associations with age-related macular degeneration: the US Twin Study of Age-Related Macular Degeneration. *Arch Ophthalmol* 2006; 124: 995–1001.

29. Dixon JA, Oliver SC, Olson JL, Mandava N. VEGF Trap-Eye for the treatment of neovascular age-related macular degeneration. *Expert Opin Investig Drugs* 2009; 18: 1573–80.

30. Do DV. Antiangiogenic approaches to age-related macular degeneration in the future. *Ophthalmology* 2009;116 (10 suppl): S24–S26.

31. Bakri SJ, Snyder MR, Reid JM, Pulido JS, Singh RJ. Pharmacokinetics of intravitreal bevacizumab (Avastin). *Ophthalmology* 2007; 114: 855–59.

32. Schmucker C, Loke YK, Ehlken C, et al. Intravitreal bevacizumab (Avastin) versus ranibizumab (Lucentis) for the treatment of age-related macular degeneration: a safety review. *Br J Ophthalmol* 2011; 95: 308–17.

33. Truong A, Wong TY, Khachigian LM. Emerging therapeutic approaches in the management of retinal angiogenesis and edema. *J Mol Med* 2011; 89: 343–61.

34. Lim LS, Cheung CM, Mitchell P, Wong TY. Emerging evidence concerning systemic safety of anti-VEGF agents—should ophthalmologists be concerned? *Am J Ophthalmol* 2011;152: 329–31.

35. Friedman E, Ivry M, Ebert E, Glynn R, Gragoudas E, Seddon J. Increased scleral rigidity and age-related macular degeneration. *Ophthalmology*. 1989;96:104–108.

36. Kotliar KE, Baumann M, Vilser W, Lanzl IM. Pulse wave velocity in retinal arteries of healthy volunteers. *Br J Ophthalmol*. 2011;95:675–679.

37. Wang M, Monticone RE, Lakatta EG. Proinflammation of aging central arteries: a mini-review. *Gerontology*. 2014;60:519–529.

38. Kothapalli D, Liu SL, Bae YH, et al. Cardiovascular protection by ApoE and ApoE-HDL linked to suppression of ECM gene expression and arterial stiffening. *Cell Rep*. 2012;2:1259–1271.

39. Ghosh K, Thodeti CK, Dudley AC, Mammoto A, Klagsbrun M, Ingber DE. Tumor-derived endothelial cells exhibit aberrant Rho-mediated mechanosensing and abnormal angiogenesis in vitro. *Proc Natl Acad Sci* U S A. 2008;105:11305–11310.

40. Mammoto A, Mammoto T, Kanapathipillai M, et al. Control of lung vascular permeability and endotoxin-induced pulmonary edema by changes in extracellular matrix mechanics. *Nat Commun*. 2013;4:1759.

41. Mammoto A, Mammoto T, Ingber DE. Rho signaling and mechanical control of vascular development. *Curr Opin Hematol*. 2008;15:228–234.

42. Huynh J, Nishimura N, Rana K, et al. Age-related intimal stiffening enhances endothelial permeability and leukocyte transmigration. *Sci Transl Med*. 2011;3:112ra122.

43. Yang X, Scott HA, Ardekani S, Williams M, Talbot P, Ghosh K. Aberrant cell and basement membrane architecture contribute to sidestream smoke-induced choroidal endothelial dysfunction. *Invest Ophthalmol Vis Sci*. 2014;55:3140–3147.

44. Yang X, Scott HA, Monickaraj F, et al. Basement membrane stiffening promotes retinal endothelial activation associated with diabetes. *FASEB J*. 2016;30:601–611.

45. Scott HA, Quach B, Yang X, et al. Matrix stiffness exerts biphasic control over monocyte-endothelial adhesion via Rho-mediated ICAM-1 clustering. *Integr Biol*. 2016;8:869–878.

CHAPTER 2

SENESCENCE INCREASES CHOROIDAL ENDOTHELIAL STIFFNESS AND SUSCEPTIBILITY TO COMPLEMENT INJURY: IMPLICATIONS FOR CHORIOCAPILLARIS LOSS IN AMD

Preface

This chapter explores the role of endothelial cell (EC) stiffening in a replicative senescence model of aging.

The text that appears in this chapter, in full, is a reprint of the material as it appears in Investigative Ophthalmology & Visual Science entitled "Senescence increases choroidal endothelial stiffness and susceptibility to complement injury: Implications for choriocapillaris loss in AMD" published in November 2016.

Introduction

Age-related macular degeneration (AMD), a progressive disease affecting approximately 10 million in the US, is a leading cause of blindness in the aging population.[1,2] It manifests in two forms: the early-stage ‘‘dry’’ AMD that is clinically characterized by retinal pigment epithelium (RPE) atrophy and drusen accumulation between the RPE and underlying choriocapillaris (CC), and the late-stage ‘‘wet’’ AMD marked by abnormal choroidal neovascularization and leakiness.[3] Current therapies approved by the US Food and Drug Administration only target 10% to 15% of all AMD patients who develop the vision-threatening wet stage[3,4] while no therapies exist for the more prevalent dry form. Since dry AMD is a potential risk factor for late-stage wet AMD, there is a recognition that more effective AMD management can be achieved by tackling the disease at the early stage.

Dry AMD is characterized by significant CC degeneration.[5,6] Since the CC is essential for maintenance of RPE homeostasis and viability, CC dropout and associated loss of perfusion have been implicated in RPE hypoxia and atrophy.[3,7,8] This potential role of CC degeneration in the pathogenesis of dry AMD necessitates identification of the factors that contribute to the loss of CC in this condition.

Past studies have revealed that dry AMD is marked by complement activation in the sub-RPE space,[9,10] which leads to the deposition of membrane attack complex (MAC; C5b-9) on the CC.[5,11] Since MAC forms pores in cell membrane and causes cell lysis, it may contribute to choroidal endothelial loss and CC degeneration associated with dry

AMD. Indeed, the degenerating CC in old eyes with dry AMD exhibit strong MAC deposition,[11] which is consistent with the hypothesis of MACinduced CC degeneration. Interestingly, MAC is also abundant on the healthy CC of young eyes.[11] Thus, it is likely that specific age-related factors exacerbate the putative degenerative effects of MAC on the CC.

One potential age-related factor is vascular stiffness. Past studies have shown that aging is associated with stiffening of retinal vessels and the sclera,[12,13] while separate studies in nonophthalmic vessels such as aorta and arteries have indicated that age-related vascular stiffening enhances vascular sensitivity to proinflammatory cues.[14–16] Such aberrant stiffness-dependent vascular dysfunction results from altered endothelial cytoskeletal tension (contractility) and mechanotransduction, the process by which mechanical cues get transduced into intracellular biochemical signaling pathways.[17–23] However, whether aging is associated with increased cytoskeletonmediated choroidal endothelial stiffening and enhanced CC sensitivity to MAC remains unknown.

Using choroidal endothelial senescence as an in vitro model of CC aging, we here show that senescence leads to a significant increase in endothelial cell (EC) stiffness, which correlates with increased complement injury. Notably, the increased stiffness of senescent ECs correlated with greater Rho activity, which is associated with cell tension and stiffness. Finally, we demonstrate that pharmacological modulation of Rho-dependent EC stiffness alone reverses the degenerative effects of complement activation on ECs.

Materials and Methods

EC Culture. Monkey chorioretinal ECs (RF/6A) were purchased from ATCC (Manassas, VA, USA) and grown in Eagle's minimum essential medium (EMEM, ATCC) supplemented with 10% fetal bovine serum (FBS; Thermo Fisher Scientific, Inc., Waltham, MA, USA) and 1x antibiotic-antimycotic mixture (Thermo Fisher Scientific, Inc.). The RF/6A EC culture was maintained at 37^{o}C in a humidified atmosphere with 5% CO^2, with culture medium being replaced every 2 days. For all in vitro studies, culture dishes were coated with 0.1% gelatin (Sigma Aldrich Corp., St Louis, MO, USA) to facilitate robust RF/6A EC adhesion and spreading during the assays.

Detection of EC Senescence. To achieve replicative senescence, lower passage RF/6A ECs were serially expanded by splitting at a 1:3 ratio every 3 days for ≥20 passages. To confirm replicative senescence, low and high passage RF/6A ECs were subjected to X-gal staining, which detects expression of β-galactosidase (β-Gal), a reliable cell senescence marker.[24,25] Specifically, cells were plated at a low density (20,000 cells/cm^2) in starvation medium (EMEM containing 0.5% FBS) for 6 hours. Next, ECs were rinsed twice with ice-cold PBS and fixed with 0.25% glutaraldehyde (Electron Microscopy Sciences, Hatfield, PA, USA) at room temperature (RT) for 10 minutes with gentle rocking. Fixed RF/6A ECs were rinsed twice with ice-cold PBS and incubated in freshly prepared staining solution containing 1 mg/mL X-Gal (Thermo Fisher Scientific, Inc.), 5 mM potassium ferricyanide (Sigma-Aldrich Corp.), 5 mM potassium ferrocyanide

(Sigma-Aldrich Corp.), and 2 mM MgCl2 (Sigma-Aldrich Corp.) for 6 hours at 37 ^{o}C. Brightfield images of stained cells (n ≤18 per condition) were acquired using a microscope (Nikon Eclipse Ti; Nikon Corp., Tokyo, Japan) fitted with a camera (Nikon Digital Sight DSFi1U2; Nikon Corp.) and, following intensity thresholding, the percentage of cells stained by X-gal was quantified using ImageJ (http://imagej.nih.gov/ij/; provided in the public domain by the National Institutes of Health, Bethesda, MD, USA).

Quantitative RT-PCR. Total RNA was isolated from RF/6A EC monolayers (three replicates/condition) using an RNA purification kit (Direct-zol RNA MiniPrep; Zymo Research, Irvine, CA, USA), converted to cDNA with high capacity cDNA reverse transcription (Thermo Fisher Scientific, Inc.), and amplified with the appropriate TaqMan assay for p21 or CD31 primers (Thermo Fisher Scientific, Inc.) on the CFX connect real-time PCR detection system (BioRad, Hercules, CA, USA). Relative mRNA levels were determined by the comparative cycle threshold method with normalization to glyceraldehyde 3-phosphate dehydrogenase (GAPDH; Thermo Fisher Scientific, Inc.).

Complement Activation. To examine the effects of complement activation on RF/6A ECs, cells were plated in starvation medium for 6 hours prior to replacement of medium with veronal buffered saline (VBS; composed of NaCl 145 mM, sodium barbital 1.8 mM, barbituric acid 3 mM, CaCl2 50 uM and 250 uM MgCl2, adjusted to pH 7.4) containing 10% normal human serum (NHS; Complement Technology, Inc., Tyler, TX, USA) for 2

hours at 37°C to promote complement activation. Monkey chorioretinal ECs that were NHS-treated were then either detached for flow cytometry analysis of surface MAC deposition or subjected to trypan blue exclusion assay for determination of cell lysis. To pharmacologically inhibit the senescence-associated effects of cell stiffness, cells were incubated with 1, 2.5, or 5 uM of Y27632 (Rho/ Rho-associated kinase [ROCK] inhibitor; Sigma- Aldrich Corp.) in VBS containing 10% NHS for 2 hours at 37°C. To activate Rho/ROCK–dependent cell stiffness, cells were incubated with 0.025 or 0.05 U/mL Thrombin (Sigma) in VBS containing 10% NHS for 2 hours at 37°C.

Flow Cytometry. Monkey chorioretinal ECs were detached and labeled with PE-labeled mouse anti-human CD146 antibody (BD Biosciences, San Jose, CA, USA) or mouse anti-monkey CD59 antibody (AbCam, Cambridge, UK). Next, RF/6A ECs were fixed with 1% paraformaldehyde (PFA; Electron Microscopy Sciences), detected with a flow cytometer (Cell Lab Quanta SC Beckman Coulter, Brea, CA, USA), and analyzed by single cell analysis software (FlowJo; Treestar, Inc., Ashland, OR, USA). For deposition studies with MAC, RF/6A ECs treated with 10% NHS were detached and labeled with mouse anti-C5b-9 antibody (Abcam), followed by fluorescently labeled anti-mouse IgG (BD Biosciences).

Trypan Blue Exclusion Assay. The RF/6A ECs were plated at a low density in starvation medium for 6 hours before treatment with 10% NHS for 2 hours at 37°C, followed by the addition of 0.1% trypan blue (Thermo Fisher Scientific, Inc.) in PBS for

8 minutes at RT. Next, RF/6A ECs were rinsed twice with PBS twice and fixed with 1% PFA for 10 minutes. Brightfield images of stained cells ($n \leq 18$ per condition) were acquired using a microscope (Nikon Corp.) fitted with a Nikon Digital Sight DS-Fi1U2 camera (Nikon Corp.), and the percentage of cells stained by trypan blue was quantified using ImageJ.

Measurement of EC Stiffness. For measurement of EC stiffness, cells were grown to confluence on sterile 0.1% gelatin-coated cover slips. Next, the confluent EC monolayers were maintained overnight in starvation medium prior to indentation with a biological-grade atomic force microscope (AFM; Veeco Instruments, Plainview, NY, USA). Specifically, cell stiffness was measured in tapping mode using a 5-um spherical glass bead attached to the silicon nitride tip of a 140-um long microcantilever (MLCT, Bruker, Billerica, MA, USA) with bending spring constant of 0.1 N/m. Force curves were obtained and analyzed as per our established protocol.[22] In some measurements, senescent ECs were treated with Y27632 (5 uM; 2 hours at 37^{o}C in starvation media), a pharmacologic inhibitor of Rho/ROCK activity, prior to AFM force indentation.

Rho Activity. Confluent EC monolayers were lysed using RIPA lysis and extraction buffer (G-Biosciences, St. Louis, MO, USA) supplemented with protease and phosphatase inhibitor cocktails (Boston BioProducts, Ashland, MA, USA). RhoA activity was measured from cell lysates using the RhoA G-LISA activation assay kit (Cytoskeleton, Inc, Denver, CO, USA), per the manufacturer's protocol. Results were

obtained by measuring absorbance at 490 nm using a plate reader (Victor2; Perkin Elmer, MA, USA).

Actin Cytoskeleton Staining. The RF/6A ECs were plated at a low density in regular culture medium for 24 hours prior to overnight culture in starvation medium. Next, the cells were fixed in 4% PFA for 15 minutes, rinsed with PBS, and permeabilized using 0.2% Triton X-100 (in 1 mg/mL BSA). To block nonspecific binding, cells were incubated in 2% (wt/vol) BSA for 30 minutes at RT. Next, a 1:200 dilution of AlexaFluor 594 Phalloidin (Thermo Fisher Scientific, Inc.) in 2% BSA was added to cells for 20 minutes in the dark at RT, followed by mounting of the cells on glass slides for fluorescence imaging. For visualization of actin stress fibers, phalloidin-labeled mounted EC cultures were imaged using Nikon Eclipse TI microscope fitted with a Nikon DS-Qi1Mc camera (Nikon Corp.). ImageJ was used to quantify the average number of actin stress fibers per cell from three separate regions along the long axis ($n \geq 20$ cells per condition).

Measurement of Cell Area. To quantify cell area, ECs were plated on plastic culture dishes for 24 hours before being subjected to phase contrast imaging using the aforementioned microscope (Nikon Corp.). Projected cell area (n=250 cells/condition) was measured by tracing the cell perimeter using ImageJ.

Statistics. All data were obtained from multiple cells and multiple replicates/condition

(as indicated in each respective section) and expressed as mean ± standard error or standard deviation, as indicated. Statistical significance was determined using analysis of variance (ANOVA), followed by Tukey's and Bonferroni post-hoc analysis (Instat; GraphPad Software Inc., La Jolla, CA, USA). Results were considered significant if $P < 0.05$.

Results

Senescence Increases Choroidal EC Susceptibility to Complement Injury

Cellular senescence recapitulates many features of aging.[25,26] Thus, to develop an in vitro model of CC aging, RF/6A ECs were cultured to high passages (>P60) to achieve replicative senescence and compared with lower passage (<P40) cells for expression levels of senescence-associated b-galactosidase (SA β- gal), a well-known senescence marker.[24] Staining with X-gal, which yields a blue color when cleaved by SA-b-gal, revealed a 9-fold greater ($P < 0.001$) expression of SA-b-gal in higher passage cells than in the lower passage counterparts (Fig. 1A). To further confirm the senescent phenotype, we compared the expression levels of p21 in the low and high passage cells. p21 is an inhibitor of cyclin-dependent kinase that promotes cell growth arrest and, thereby, senescence.[27] Our qPCR measurements revealed that high passage ECs exhibit 1.7-fold higher levels ($P < 0.01$) of p21 mRNA than low passage ECs (Fig. 1B). Consistent with the typical senescence phenotype, we also observed a markedly greater percentage of ‘‘enlarged’’ cells (projected area >4000 um^2) in the high passage ECs than in the lower passage cells (Supplementary Fig. S1). The low and high passage cells were subsequently termed ‘‘normal’’ and ‘‘senescent’’ ECs, respectively. Notably, the SA-b-gal–expressing senescent ECs did not exhibit any loss of endothelial phenotype, as judged by similar expression levels of classical endothelial-specific markers CD31 (Fig. 1C) and CD146 (Fig. 1D) in normal and senescent ECs.

To test their sensitivity to complement activation associated with dry AMD, we

exposed these cells to complement-competent NHS. By activating the alternative complement pathway, NHS treatment leads to surface MAC deposition similar to that observed in the CC of human dry AMD eyes.[28,29] Flow cytometry analysis of NHS-treated normal and senescent ECs labeled with anti-C5b-9 (anti-MAC) revealed similar degrees of surface MAC deposition in these cells (Fig. 2A). However, when compared with normal ECs, the senescent cells underwent a 3-fold increase ($P < 0.001$) in complement-induced lysis, as judged by greater trypan blue incorporation within the senescent ECs (Fig. 2B, Supplementary Fig. S2). Notably, this increase in complement-induced lysis of senescent ECs did not result from reduced expression of endogenous cell-surface MAC inhibitory factor CD59, whose surface levels were comparable in both normal and senescent ECs (Supplementary Fig. S3). Predictably, the lysed (trypan blue-positive) cells exhibited a rounded morphology (Fig. 2B; inset), which is indicative of impaired cell viability and death.[30,31]

Senescence Is Associated With Increased Choroidal EC Stiffness

Past studies have shown that aging is associated with stiffening of aorta and arteries,[32,33] which also exhibit greater sensitivity to proinflammatory cues.[14,16] Thus, we asked whether the greater sensitivity of senescent RF/6A ECs to complement activation was caused, at least in part, by increased EC stiffness. Multiple force indentation measurements by a biological-grade AFM revealed that, indeed, senescent ECs are ~30% stiffer ($P < 0.01$) than normal ECs (Fig. 3).

Senescent Choroidal ECs Exhibit Higher Rho Activity

Rho is a key mechanotransduction player that regulates actin cytoskeletal tension and, as a consequence, cell stiffness.[19,34] Thus, we looked to see whether the increase in senescent EC stiffness results from a concomitant increase in Rho activity. Measurement of baseline Rho activity in confluent EC monolayers revealed that senescent ECs exhibit 1.4-fold higher ($P < 0.05$) Rho activity than normal ECs (Fig. 4A). Further, since Rho directly regulates actin cytoskeletal tension, its higher activity in senescent ECs predictably correlated with a 35% increase in actin stress fiber density in these cells (Fig. 4B).

Inhibition of Rho Activity Prevents Complement- Induced Lysis of Senescent ECs

To determine whether increased Rho-dependent cell tension (stiffness) exacerbates complement-induced lysis, we cotreated senescent ECs with NHS and a pharmacologic inhibitor (Y27632) of ROCK, the immediate downstream target of Rho that controls myosin-dependent actin tension (cell stiffness). Our AFM measurements confirmed that Y27632 treatment causes a significant ($P < 0.05$) reduction in the stiffness of senescent ECs (Fig. 5A). More importantly, we found that inhibition of Rho/ROCK–dependent cell stiffness alone inhibits complement-induced cell lysis in a dose-dependent manner (IC_{50} ~2.5 uM; Fig. 5B), with the lysis observed at the highest Y27632 dose of 5 uM comparable with that seen in NHS-treated normal ECs.

Increasing Rho Activity in Normal ECs Exacerbates

Complement Injury To confirm the role of cell stiffness in complement injury, normal ECs were cotreated with NHS and thrombin, a Rho agonist that enhances actin cytoskeletal tension and cell stiffness.[35–37] As shown in Figure 6, thrombin treatment of normal ECs produced a dose-dependent increase ($P < 0.001$) in complement-induced cell lysis. That thrombin exacerbates complement injury by increasing Rho/ROCK–mediated cell tension (stiffness) and not via its ability to activate complement38 was confirmed when cotreatment with Rho/ROCK inhibitor Y27632 prevented the increase in cell lysis by thrombin (Fig. 6).

Discussion

Although CC dropout is implicated in RPE atrophy associated with dry AMD, the precise mechanism(s) by which age-related CC degeneration occurs remains elusive. The observation that there is significant MAC deposition on the CC of old AMD eyes has led to the speculation that complement injury contributes to CC loss in dry AMD.[6,39,40] However, MAC is also found on the CC of young healthy eyes. Thus, here we tested the hypothesis that aging increases the susceptibility of choroidal ECs to MAC injury, thereby exacerbating EC lysis and CC degeneration. Using replicative senescence as an in vitro model of aging, we here show that senescent ECs exhibit greater MAC-induced lysis than their normal counterparts. Our studies further reveal that senescence leads to an increase in Rho-mediated cell stiffness that, in turn, contributes significantly to the increased susceptibility of senescent ECs to MAC injury. To our knowledge, this study is the first to identify a possible mechanism by which aging may contribute to CC loss associated with early AMD, thereby providing a rationale for performing detailed studies that examine Rho and EC stiffness as potentially new therapeutic targets for early AMD.

Aging is a major non-modifiable risk factor for AMD. Yet, precisely how it contributes to AMD pathogenesis remains poorly understood. To study the effects of aging on the CC, we established an in vitro model of CC aging by culturing choroidal ECs to high passages, which leads to replicative senescence. Since cellular senescence is implicated in many age-related degenerative phenotypes,[25,41] we reasoned that senescent choroidal ECs will likely recapitulate the phenotype of aging CC in AMD eyes. We

confirmed the induction of cellular senescence by staining for β-gal, measuring p21 mRNA expression and projected cell area, widely used phenotypic markers of cellular senescence. Conceptually, our observation that a cell line (RF/6A) deemed to be immortal exhibits markers of senescence at high passages appears paradoxical. However, in support of our observations, we would like to point out that RF/6A ECs have conventionally been used between passages 18 through 60[42–44] while the studies that used these higher passage cells never assessed the markers of senescence. Thus, to our knowledge, we are the first to use RF/6A ECs past the conventional passage number and measure expression of senescence markers. Consistent with our observations, nonendothelial cell lines transformed with SV40 have been demonstrated to exhibit lack of telomerase activity,[45] an independent marker of senescence.

Dry AMD is associated with subretinal inflammation, which is characterized by complement activation and inflammatory cell infiltration into the sub-RPE space. The infiltrating inflammatory cells are thought to further enhance complement activation either directly by undergoing activation[46,47] or indirectly by stimulating higher expression of complement factors by the RPE.[48] This subretinal inflammatory milieu leads to MAC deposition on the CC. Consistent with these observations, we show that treatment of choroidal ECs with complement-competent serum leads to surface MAC deposition. Intriguingly, however, we found that although MAC deposition was comparable on normal and senescent ECs, the latter underwent significantly greater MAC-induced lysis. In other words, normal cells were found to exhibit lower susceptibility to complement injury. This finding may explain the recent observation that the CC of young eyes remain

healthy despite significant MAC deposition.[11] Furthermore, our observation that cells pre-incubated with lower doses of FBS do not exhibit greater sensitivity to complement attack likely rules out any potential contribution of (FBS starvation-induced) autophagy in complement-mediated cell lysis seen in our assays.

To understand how senescent ECs become more susceptible to complement injury, we looked at the potential role of EC stiffness. This is because (1) aging has been associated with stiffening of retinal vessels and the sclera,[12,13] thus raising the possibility that choroidal ECs/vessels also become stiffer with aging/senescence; (2) nonophthalmic vessels such as aorta and arteries that become stiffer with age[32,33] also exhibit greater sensitivity to proinflammatory cues such as low density lipoporotein[14,16]; and (3) senescence has recently been shown to correlate with increased cytoskeletal tension (a measure of stiffness) in umbilical vein-derived ECs.[49] To determine whether senescence leads to choroidal EC stiffening, we performed force indentation measurements using a biologicalgrade AFM. Atomic force microscope offers a precise, reliable, and analytical technique that we and others have used widely to determine the stiffness of soft biological samples including living cells, extracellular matrices, and soft tissues.[22,50–52] These AFM measurements confirmed our hypothesis that senescent choroidal ECs are significantly stiffer than their normal counterparts.

Mechanistically, cell stiffness is regulated by Rho that, via its downstream target ROCK (Rho-associated Kinase), modulates both actin/myosin-based cytoskeletal tension (contractility) and cortical actin network formation.[19,34] Specifically, past studies by us and others have shown that stiffer, more contractile ECs with dense actin cytoskeletal

filaments exhibit high Rho/ROCK activity while inhibition of Rho/ROCK suppresses these effects.[17,20] Consistent with these findings, we here show that the stiffer senescent choroidal ECs exhibit significantly higher Rho activity, which correlates strongly with a concomitant increase in actin microfilament density. That treatment of senescent ECs with ROCK inhibitor Y27632 significantly inhibited cell stiffness confirms the role of Rho in senescent choroidal EC stiffening.

Importantly, we show that this Rho/ROCK-dependent stiffening of senescent choroidal ECs contributes actively to their increased susceptibility to complement injury because pharmacological inhibition of Rho/ROCK significantly inhibited MAC-induced lysis of these cells. Although these findings are the first to implicate Rho-associated cell stiffness in complement injury, they are generally consistent with the proinflammatory effects of increased Rho/ROCK activity and EC stiffness.[34] Furthermore, if increased cell stiffness indeed plays an important causative role in MAC susceptibility, then increasing the stiffness of normal ECs should increase their MAC-induced lysis. Indeed, we found that pharmacologic activation of Rho/ROCK in normal ECs alone leads to a significant increase in complement injury.

To our knowledge, the current findings are the first to implicate a specific age/senescence-related factor (i.e., Rho-mediated choroidal EC stiffening) in CC atrophy associated with dry AMD.[6] To determine their translational potential, however, these new findings will need to be validated in appropriate animal models of dry AMD, such as the rhesus macaque monkeys that share the same AMD susceptibility genes ARMS2 and HTRA1 with humans, and undergo drusen accumulation as seen in humans.[53,54] Further,

although our findings offer new mechanistic insight into choroidal EC loss and CC degeneration associated with dry AMD, they do not yet explain precisely how cell stiffness increases EC sensitivity to complement injury. In this regard, it must be noted that host tissue cells protect themselves from incessant MAC attack, resulting from the continuously activated alternative complement pathway, by expressing surface inhibitors of MAC pore formation.[55,56] Intriguingly, we show that both normal and senescent ECs express similar levels of surface CD59, an endogenous membrane-bound regulator of the complement system that specifically blocks the assembly and formation of transmembrane MAC pores (C5b-9n) by interacting with the terminal complement proteins C8 and C9, thus preventing C9 polymerization. Given the similarity in CD59 ‘‘expression’’ levels, it is possible that the greater sensitivity of senescent ECs to complement attack results from Rho (tension)-mediated alteration in CD59 conformation, and thereby its ‘‘activity’’; however, this remains to be carefully examined in a separate study.

Conclusion

Using a replicative senescence model of in vitro for aging, my findings reveal that senescent ECs are significantly stiffer than their normal counterparts, which correlates with higher cytoskeletal Rho activity in these cells and their greater susceptibility to complement (MAC) injury. Importantly, inhibition of Rho activity in senescent ECs significantly reduced cell stiffness and MAC-induced lysis. By revealing an important role of senescence-associated choroidal EC stiffening in complement injury, these findings implicate CC stiffening as an important determinant of age-related CC atrophy seen in dry AMD.

AMD is a multifactorial disease that is also regulated by dietary and genetic factors. How these risk factors contribute to the age-related mechanical control of CC susceptibility to complement injury also remains to be determined. A detailed examination of the molecular pathways underlying this mechanical control of choroidal EC dysfunction may lead to the identification of new therapeutic targets for CC atrophy and AMD progression.

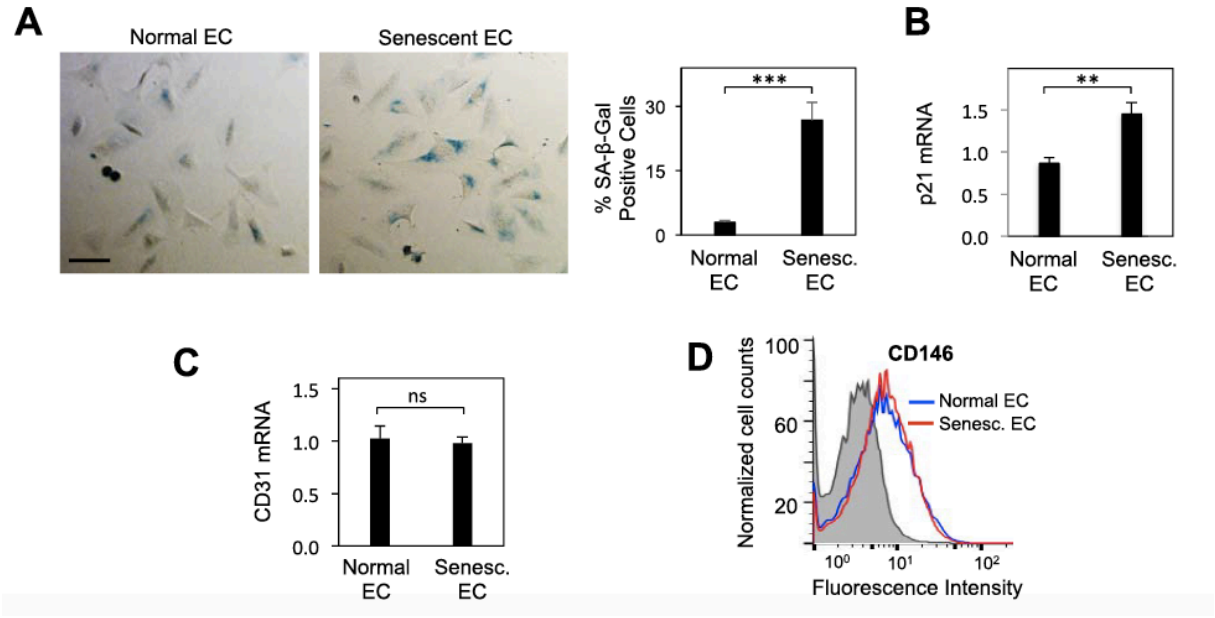

FIGURE 2.1. Senescent ECs exhibit high β-Gal expression. (A) Monkey chorioretinal ECs at low (<P40) and high (>P60) passages were subjected to X-gal staining, which stains β-gal (a senescence marker) blue. Representative brightfield images and net intensity measurements (bar graph) from multiple (n > 1500) cells reveal significantly greater β-gal expression in higher passage (‘‘senescent’’) RF/6A ECs than in lower passage (‘‘normal’’) cells. *** P < 0.001. Bars indicate average ± standard error of mean. Scale bar: 50 um. (B) Quantitative RT-PCR analysis from multiple replicates (n = 3) shows that, when compared with low passage ECs, the high passage cells exhibit significantly higher p21 mRNA expression. ** P < 0.01. Levels of p21 mRNA were normalized with respect to GAPDH. Bars indicate average 6 standard error of mean. (C) Quantitative RT-PCR analysis from multiple replicates (n=3) shows that normal and senescent ECs exhibit similar levels of CD31 mRNA expression. Levels of CD31 mRNA were normalized with respect to GAPDH. Bars indicate average ± standard error of

mean. (D) Normal and senescent ECs were labeled with anti-CD146 or isotype-matched control antibody (solid gray histogram), and subjected to flow cytometry. Histograms of cell counts versus fluorescence indicate that both normal and senescent cells exhibit similar expression levels of cell surface CD146. ns, no significance.

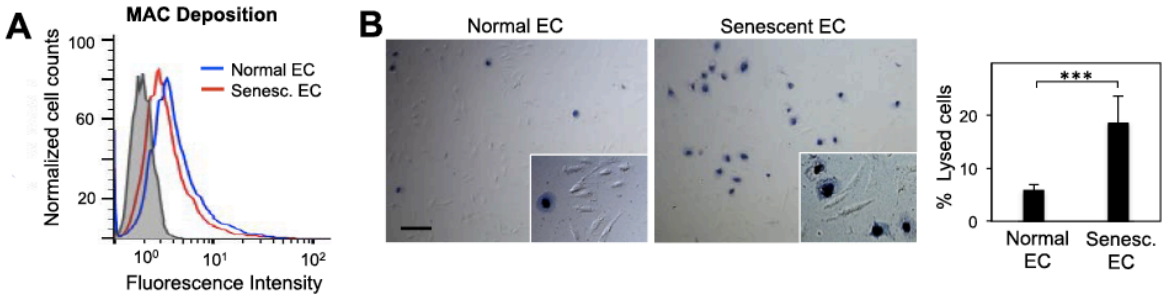

FIGURE 2.2. Senescence increases choroidal EC susceptibility to complement injury. (A) The RF/6A ECs were treated with complement-competent normal human serum (NHS, 10% vol/vol; 2 hours), labeled with anti-MAC (C5b-9) or isotype-matched control antibody (solid gray histogram), and subjected to flow cytometry to detect surface MAC deposition. Histograms of cell counts versus fluorescence indicate that both normal and senescent cells exhibit similar surface MAC deposition. (B) Lysis of NHS treated-cells was detected by trypan blue exclusion assay. Representative brightfield images and counting of trypan blue-loaded cells (bar graph; $n \geq 200$ cells) reveals significantly greater lysis of senescent RF/6A ECs than that of normal cells. *** $P < 0.001$. Bars indicate average ± standard deviation. Scale bar: 100 um.

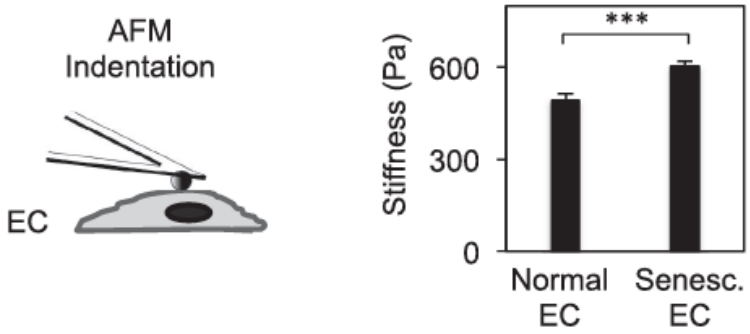

FIGURE 2.3. Senescent ECs exhibit increased stiffness. Schematic: EC stiffness was measured by indentation with a biological-grade AFM fitted with a silicon nitride cantilever tip containing a ~5 um-diameter glass bead. Bar graph: Quantitative analysis of multiple ($n \geq 30$) force indentation measurements reveal a ~30% increase in the stiffness of senescent RF/6A ECs when compared with that of normal cells. *** $P < 0.001$. Bars indicate average ± standard error of mean.

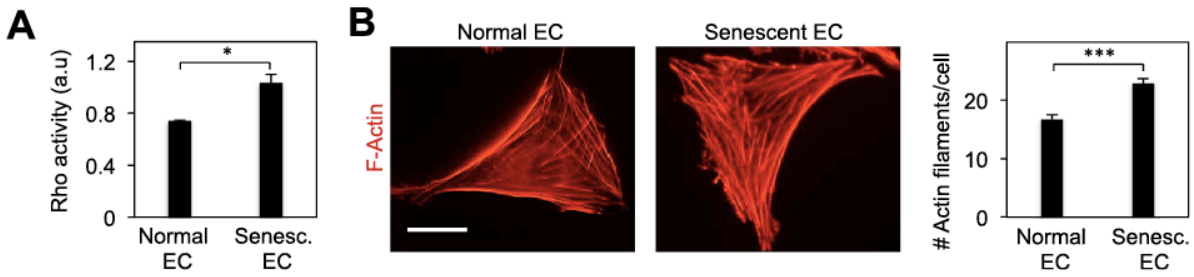

FIGURE 2.4. Rho activity is higher in senescent ECs. (A) Baseline RhoA activity in normal and senescent RF/6A ECs was measured using RhoA G-LISA activation assay. Absorbance measurements show a ~40% increase in Rho activity in senescent RF/6A ECs when compared with normal cells. * $P < 0.05$. Bars indicate average ± standard error of mean. (B) We stained RF/6A ECs with fluorescently labeled phalloidin to visualize actin cytoskeletal filaments. Representative fluorescent images and quantitative analysis of actin filament density (bar graph; n ‡ 30) revealed a 35% increase in actin filament density in senescent cells. *** $P < 0.001$. Bars indicate average ± standard error of mean. Scale bar: 50 um.

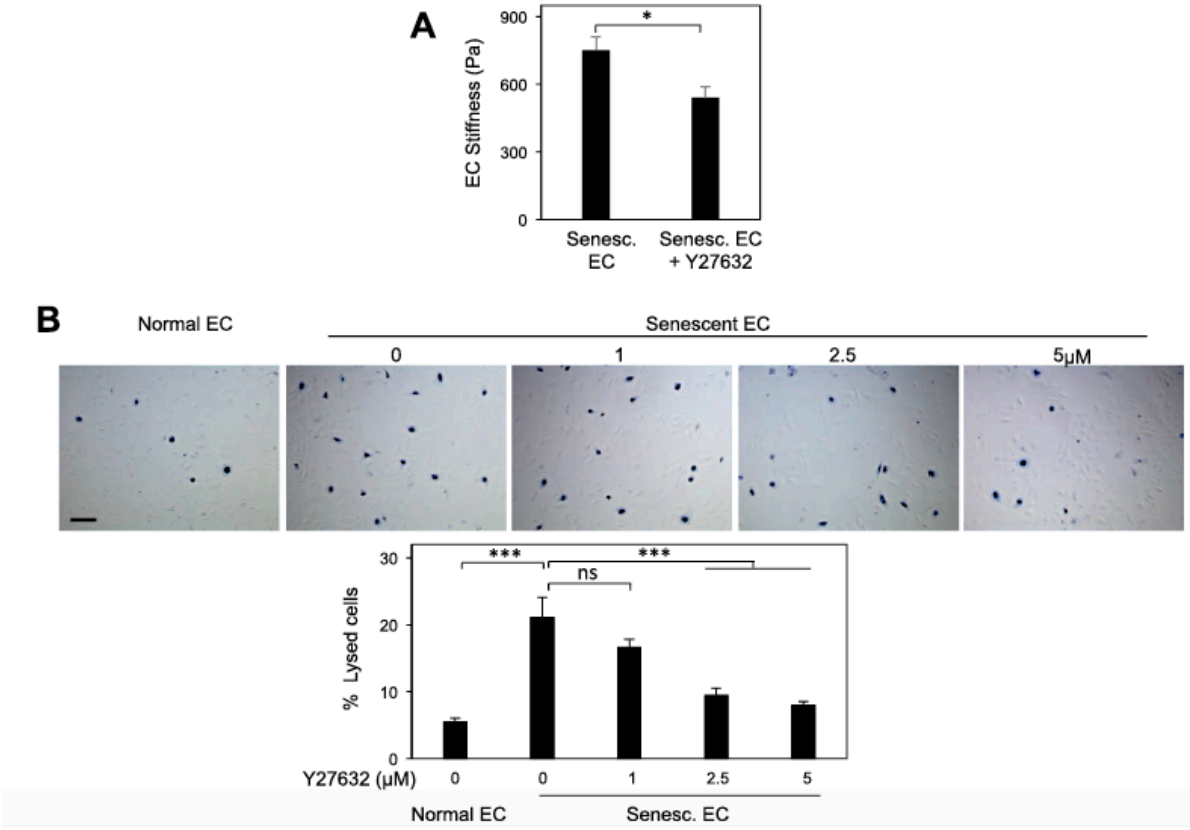

FIGURE 2.5. Inhibition of Rho activity prevents MAC-induced lysis of senescent ECs. (A) Stiffness of ECs was measured by AFM. Quantitative analysis of multiple ($n \geq 30$) force indentation measurements revealed a ~30% decrease in the stiffness of senescent ECs treated with Y27632 (5 uM), a pharmacological Rho/ROCK inhibitor. * $P < 0.05$. Bars indicate average ± standard error of mean. (B) Senescent RF/6A ECs were cotreated with NHS and different doses of Y27632 prior to addition of trypan blue. Representative brightfield images and counting of trypan blue-loaded cells (bar graph; $n \geq 200$ cells) indicate a progressive decrease in complement-induced lysis of senescent cells with increasing dose of Y27632. *** $P < 0.001$. Bars indicate average ± standard error of mean. Scale bar: 100 um.

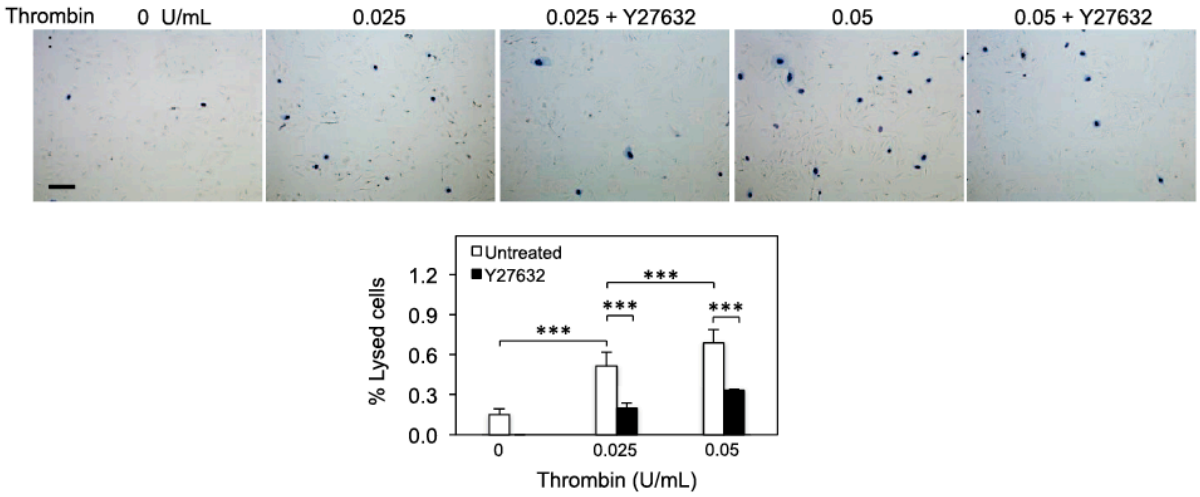

FIGURE 2.6. Increasing Rho-mediated tension promotes complement-induced EC lysis. Normal RF/6A ECs were cotreated with NHS and different doses of thrombin, a Rho agonist, prior to addition of trypan blue. Representative images and counting of trypan blue–loaded cells (bar graph; n ≥ 150 cells) indicate a progressive increase in complement-induced lysis of normal RF/6A ECs with increasing thrombin dose. However, cotreatment of thrombin with pharmacologic Rho/ROCK inhibitor Y27632 (5 uM) significantly prevented cell lysis. *** $P < 0.001$. Bars indicate average ± standard deviation. Scale bar: 100 um.

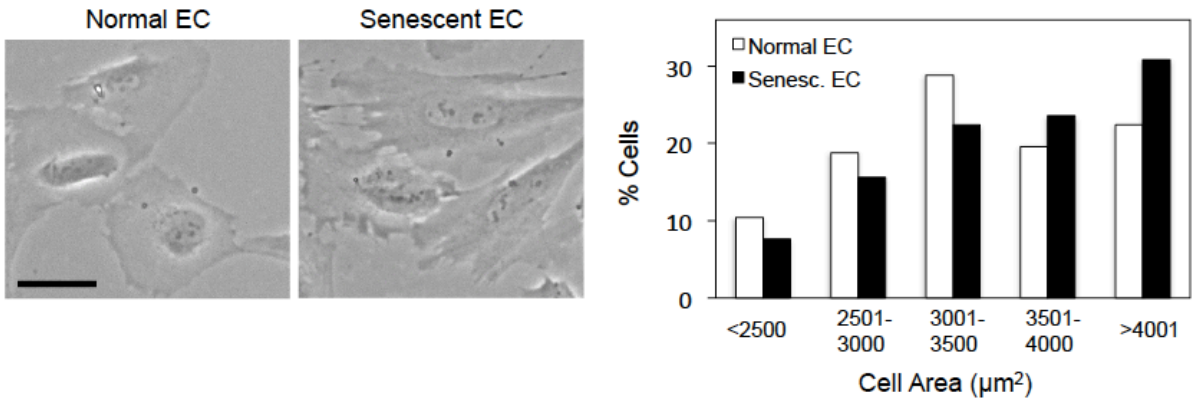

SUPPLEMENTAL FIGURE S2.1. **Senescence leads to an increase in cell area.** Representative phase contrast images and measurement of projected cell area (histogram; n=250 cells) together indicate that senescent ECs are markedly larger than their normal counterparts. Scale bar: 50 um.

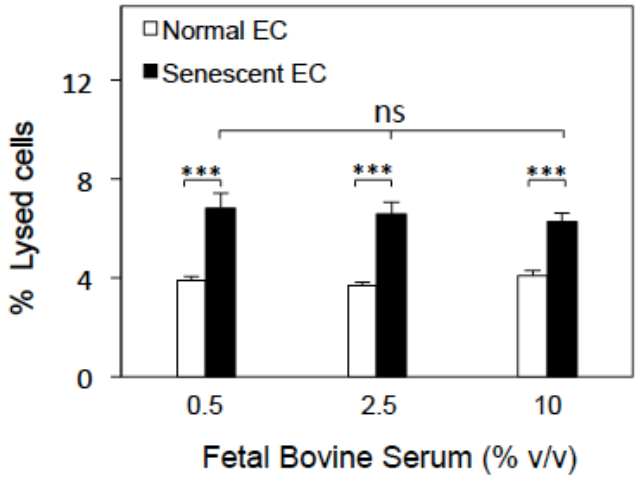

SUPPLEMENTAL FIGURE S2.2. Effect of FBS pre-incubation on susceptibility to complement injury. RF/6A ECs were plated in medium containing different concentrations of FBS (0.5, 2.5, and 10% v/v) for 6h prior to NHS treatment. Lysis of NHS treated-cells was detected by trypan blue exclusion assay. Counting of trypan blue-loaded cells (bar graph; n≥200 cells) reveals that there is no difference in the degree of lysis between ECs preincubated with the three FBS doses (ns, no significance). Bars indicate average ± standard error of mean.

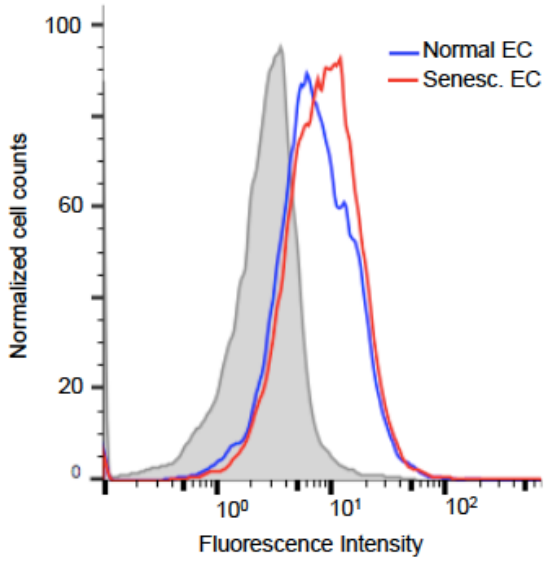

SUPPLEMENTAL FIGURE S2.3. CD59 expression. Normal and senescent ECs were labeled with anti-CD59 or isotype-matched control antibody (solid gray histogram), and subjected to flow cytometry. Histograms of cell counts vs fluorescence indicate that both normal and senescent cells exhibit similar expression levels of cell surface CD59.

References

1. Cook HL, Patel PJ, Tufail A. Age-related macular degeneration: diagnosis and management. Br Med Bull. 2008;85:127–149.

2. Friedman DS, O'Colmain BJ, Munoz B, et al. Prevalence of agerelated macular degeneration in the United States. Arch Ophthalmol. 2004;122:564–572.

3. Ambati J, Fowler BJ. Mechanisms of age-related macular degeneration. Neuron. 2012;75:26–39.

4. Zhang K, Zhang L, Weinreb RN. Ophthalmic drug discovery: novel targets and mechanisms for retinal diseases and glaucoma. Nat Rev Drug Discov. 2012;11:541–559.

5. Whitmore SS, Sohn EH, Chirco KR, et al. Complement activation and choriocapillaris loss in early AMD: implications for pathophysiology and therapy. Prog Retin Eye Res. 2015;45: 1–29.

6. Mullins RF, Johnson MN, Faidley EA, Skeie JM, Huang J. Choriocapillaris vascular dropout related to density of drusen in human eyes with early age-related macular degeneration. Invest Ophthalmol Vis Sci. 2011;52:1606–1612.

7. McLeod DS, Grebe R, Bhutto I, Merges C, Baba T, Lutty GA. Relationship between RPE and choriocapillaris in age-related macular degeneration. Invest Ophthalmol Vis Sci. 2009;50: 4982–4991.

8. McLeod DS, Taomoto M, Otsuji T, Green WR, Sunness JS, Lutty GA. Quantifying changes in RPE and choroidal vasculature in eyes with age-related macular degeneration. Invest Ophthalmol Vis Sci. 2002;43:1986–1993.

9. Parmeggiani F, Romano MR, Costagliola C, et al. Mechanism of inflammation in age-related macular degeneration. Mediators Inflamm. 2012;2012:546786.

10. Anderson DH, Mullins RF, Hageman GS, Johnson LV. A role for local inflammation in the formation of drusen in the aging eye. Am J Ophthalmol. 2002;134:411–431.

11. Mullins RF, Schoo DP, Sohn EH, et al. The membrane attack complex in aging human choriocapillaris: relationship to macular degeneration and choroidal thinning. Am J Pathol. 2014;184:3142–3153.

12. Friedman E, Ivry M, Ebert E, Glynn R, Gragoudas E, Seddon J. Increased scleral rigidity and age-related macular degeneration. Ophthalmology. 1989;96:104–108.

13. Kotliar KE, Baumann M, Vilser W, Lanzl IM. Pulse wave velocity in retinal arteries of healthy volunteers. Br J Ophthalmol. 2011;95:675–679.

14. Wang M, Monticone RE, Lakatta EG. Proinflammation of aging central arteries: a mini-review. Gerontology. 2014;60:519–529.

15. Laurent S. Defining vascular aging and cardiovascular risk. J Hypertens. 2012;(suppl 30):S3–S8.

16. Kothapalli D, Liu SL, Bae YH, et al. Cardiovascular protection by ApoE and ApoE-HDL linked to suppression of ECM gene expression and arterial stiffening. Cell Rep. 2012;2:1259–1271.

17. Ghosh K, Thodeti CK, Dudley AC, Mammoto A, Klagsbrun M, Ingber DE. Tumor-derived endothelial cells exhibit aberrant Rho-mediated mechanosensing and abnormal angiogenesis in vitro. Proc Natl Acad Sci U S A. 2008;105:11305–11310.

18. Mammoto A, Mammoto T, Kanapathipillai M, et al. Control of lung vascular permeability and endotoxin-induced pulmonary oedema by changes in extracellular matrix mechanics. Nat Commun. 2013;4:1759.

19. Mammoto A, Mammoto T, Ingber DE. Rho signaling and mechanical control of vascular development. Curr Opin Hematol. 2008;15:228–234.

20. Huynh J, Nishimura N, Rana K, et al. Age-related intimal stiffening enhances endothelial permeability and leukocyte transmigration. Sci Transl Med. 2011;3:112ra122.

21. Yang X, Scott HA, Ardekani S, Williams M, Talbot P, Ghosh K. Aberrant cell and basement membrane architecture contribute to sidestream smoke-induced choroidal endothelial dysfunction. Invest Ophthalmol Vis Sci. 2014;55:3140–3147.

22. Yang X, Scott HA, Monickaraj F, et al. Basement membrane stiffening promotes retinal endothelial activation associated with diabetes. FASEB J. 2016;30:601–611.

23. Scott HA, Quach B, Yang X, et al. Matrix stiffness exerts biphasic control over monocyte-endothelial adhesion via Rhomediated ICAM-1 clustering. Integr Biol (Camb). 2016;8:869– 878.

24. Debacq-Chainiaux F, Erusalimsky JD, Campisi J, Toussaint O. Protocols to detect senescence-associated beta-galactosidase (SA-betagal) activity, a biomarker of senescent cells in culture and in vivo. Nat Protoc. 2009;4:1798–1806.

25. Campisi J, Robert L. Cell senescence: role in aging and agerelated diseases. Interdiscip Top Gerontol. 2014;39:45–61.

26. Campisi J. Aging cellular senescence, and cancer. Annu Rev Physiol. 2013;75:685–705.

27. Campisi J, d'Adda di Fagagna F. Cellular senescence: when bad things happen to good cells. Nat Rev Mol Cell Biol. 2007;8: 729–740.

28. Johnson LV, Forest DL, Banna CD, et al. Cell culture model that mimics drusen formation and triggers complement activation associated with age-related macular degeneration. Proc Natl Acad Sci U S A. 2011;108:18277–18282.

29. Gorham RD Jr, Forest DL, Tamamis P, et al. Novel compstatin family peptides inhibit complement activation by drusen-like deposits in human retinal pigmented epithelial cell cultures. Exp Eye Res. 2013;116:96–108.

30. Chen CS, Mrksich M, Huang S, Whitesides GM, Ingber DE. Geometric control of cell life and death. Science. 1997;276: 1425–1428.

31. Ghosh K, Ingber DE. Micromechanical control of cell and tissue development: implications for tissue engineering. Adv Drug Deliv Rev. 2007;59:1306–1318.

32. Kovacic JC, Moreno P, Nabel EG, Hachinski V, Fuster V. Cellular senescence vascular disease, and aging: part 2 of a 2-part review: clinical vascular disease in the elderly. Circulation. 2011;123:1900–1910.

33. Kovacic JC, Moreno P, Hachinski V, Nabel EG, Fuster V. Cellular senescence, vascular disease, and aging: part 1 of a 2-part review. Circulation. 2011;123:1650–1660.

34. Huveneers S, Daemen MJ, Hordijk PL. Between Rho(k) and a hard place: the relation between vessel wall stiffness endothelial contractility, and cardiovascular disease. Circ Res. 2015;116:895–908.

35. Cuerrier CM, Gagner A, Lebel R, Gobeil F Jr, Grandbois M. Effect of thrombin and bradykinin on endothelial cell mechanical properties monitored through membrane deformation. J Mol Recognit. 2009;22:389–396.

36. Birukova AA, Smurova K, Birukov KG, Kaibuchi K, Garcia JG, Verin AD. Role of Rho GTPases in thrombin-induced lung vascular endothelial cells barrier dysfunction. Microvasc Res. 2004;67:64–77.

37. Birukova AA, Tian X, Cokic I, Beckham Y, Gardel ML, Birukov KG. Endothelial barrier disruption and recovery is controlled by substrate stiffness. Microvasc Res. 2013;87:50–57.

38. Krisinger MJ, Goebeler V, Lu Z, et al. Thrombin generates previously unidentified C5 products that support the terminal complement activation pathway. Blood. 2012;120:1717– 1725.

39. Sennlaub F, Auvynet C, Calippe B, et al. CCR2 monocytes infiltrate atrophic lesions in age-related macular disease and mediate photoreceptor degeneration in experimental subretinal inflammation in Cx3cr1 deficient mice. EMBO Mol Med. 2013;5:1775–1793.

40. Skeie JM, Mullins RF. Macrophages in neovascular age-related macular degeneration: friends or foes? Eye (Lond). 2009;23: 747–755.

41. Baker DJ, Wijshake T, Tchkonia T, et al. Clearance of p16Ink4apositive senescent cells delays ageing-associated disorders. Nature. 2011;479:232–236.

42. Lou D, Hu F. Co-distribution of von Willebrand factor and fibronectin in cultured rhesus endothelial cells. Histochem J. 1987;19:431–438.

43. Ottino P, Finley J, Rojo E, et al. Hypoxia activates matrix metalloproteinase expression and the VEGF system in monkey choroid-retinal endothelial cells: involvement of cytosolic phospholipase A2 activity. Mol Vis. 2004;10:341–350.

44. Amrite AC, Kompella UB. Celecoxib inhibits proliferation of retinal pigment epithelial and choroid-retinal endothelial cells by a cyclooxygenase-2-independent mechanism. J Pharmacol Exp Ther. 2008;324:749–758.

45. Kim NW, Piatyszek MA, Prowse KR, et al. Specific association of human telomerase activity with immortal cells and cancer. Science. 1994;266:2011–2015.

46. Camous L, Roumenina L, Bigot S, et al. Complement alternative pathway acts as a positive feedback amplification of neutrophil activation. Blood. 2011;117:1340–1349.

47. Rutar M, Valter K, Natoli R, Provis JM. Synthesis and propagation of complement C3 by microglia/monocytes in the aging retina. PLoS One. 2014;9:e93343.

48. Luo C, Zhao J, Madden A, Chen M, Xu H. Complement expression in retinal pigment epithelial cells is modulated by activated macrophages. Exp Eye Res. 2013;112:93–101.

49. Cheung TM, Yan JB, Fu JJ, Huang J, Yuan F, Truskey GA. Endothelial cell senescence increases traction forces due to age-associated changes in the glycocalyx and SIRT1. Cell Mol Bioeng. 2014;8:63–75.

50. Lehenkari PP, Charras GT, Nykanen A, Horton MA. Adapting atomic force microscopy for cell biology. Ultramicroscopy. 2000;82:289–295.

51. Adams WJ, O'Grady ML, Ghosh K, Gibbs AD, Geisse NA, Ingber DE, Parker KK. Viscoelastic indentation of extremely soft biological samples. Biophysical J. 2009;96:398a.

52. Ghosh K, Pan Z, Guan E, et al. Cell adaptation to a physiologically relevant ECM mimic with different viscoelastic properties. Biomaterials. 2007;28:671–679.

53. Pennesi ME, Neuringer M, Courtney RJ. Animal models of age related macular degeneration. Mol Aspects Med. 2012;33:487– 509.

54. Francis PJ, Appukuttan B, Simmons E, et al. Rhesus monkeys and humans share common susceptibility genes for age-related macular disease. Hum Mol Genet. 2008;17:2673–2680.

55. Acosta J, Hettinga J, Fluckiger R, et al. Molecular basis for a link between complement and the vascular complications of diabetes. Proc Natl Acad Sci U S A. 2000;97:5450–5455.

56. Lee MS, Jones T, Song DY, Jang JH, Jung JU, Gao SJ. Exploitation of the complement system by oncogenic Kaposi's sarcoma-associated herpesvirus for cell survival and persistent infection. PLoS Pathog. 2014;10:e1004412.

57. Koo E, Neuringer M, SanGiovanni JP. Macular xanthophylls lipoprotein-related genes, and age-related macular degeneration. Am J Clin Nutr. 2014;(100 suppl 1):336S–346S.

58. Barker FM II, Snodderly DM, Johnson EJ, et al. Nutritional manipulation of primate retinas, V: effects of lutein, zeaxanthin, and n-3 fatty acids on retinal sensitivity to blue-lightinduced damage. Invest Ophthalmol Vis Sci. 2011;52:3934–3942.

CHAPTER 3

AGE-RELATED ENDOTHELIAL CELL STIFFENING CONTRIBUTES TO COMPLEMENT-MEDIATED CHOROIDAL ATROPHY ASSOCIATED WITH DRY AMD

Preface

Using a unique in vitro model derived from a non-human primate pre-clinical model of dry AMD, this chapter shows for the first time that aging increases the susceptibility to complement injury and offers a possible mechanism by which aging may contribute choroidal degeneration.

Introduction

Age-related macular degeneration (AMD) is the leading cause of vision loss in the elderly population, affecting approximately 11 million people in the US.[1, 2] AMD manifests in two forms: the early-stage ‘‘dry’’ AMD, clinically characterized by retinal pigment epithelium (RPE) atrophy and drusen accumulation between the RPE and underlying choriocapillaris (CC), and the late-stage ‘‘wet’’ AMD marked by abnormal choroidal neovascularization and leakiness.[3] Despite the common prevalence of this potentially blinding disease, only 10-15% of individuals with advanced wet stage AMD benefit from current therapies while no therapies exist for the more prevalent early dry form.[3,4] Since dry AMD is a potential risk factor for wet AMD, there is recognition that more effective AMD management can be achieved by treating the disease at the early stage. With prevalence projected to double by the year 2050, there is a critical need to understand the mechanisms underlying dry AMD pathophysiology that can aid in the development of treatments for the vast majority of individuals with this disease.

There is substantial evidence of RPE degeneration to play a key role in early AMD, with research focusing on the underlying mechanisms of RPE atrophy.[5-7] However, more recent studies have begun to implicate an important role of the underlying vasculature (CC and larger choroidal vessels) in this condition.[8-13] Importantly, histological studies of dry AMD eyes have shown that drusen deposition at the RPE/CC interface is strongly correlated with loss of choroidal endothelial cells (EC) and CC atrophy.[9] Further, studies have also shown that choroidal thinning is associated

with dry AMD.[10, 12] Indeed, many studies have shown that the loss of vascular support leads to hypoxia-induced RPE dysfunction.[14,15] During the advanced 'wet' stage of AMD, excess production of VEGF by hypoxic RPE results in the local formation of leaky blood vessels, which if uncontrolled, invade the various tissue layers, resulting in loss of central vision. This potential mechanism implicates choroidal vascular atrophy as an early determinant of AMD progression. However, how choroidal vessels undergo atrophy is poorly understood.

Dry AMD is associated with complement activation in the sub-RPE space, with the membrane attack complex (MAC; C5b-9n) specifically localizing on the CC.[8-10] Since MAC can lead to pore formation on the cell membrane,[18] it is possible that choroidal ECs are a direct target of MAC. ECs incapable of combating pore formation could potentially result in cell lysis, contributing to choroidal degeneration associated with dry AMD. Indeed, studies have shown that the degenerating CC in old eyes with dry AMD exhibit strong MAC deposition,[10] which is consistent with the hypothesis of MAC-induced choroidal degeneration. Interestingly, MAC is also abundant on the healthy CC of young eyes. Thus, specific age-related factors likely contribute to CC degeneration and choroidal thinning observed in AMD.

Indeed, our earlier studies showed that senescence, a hallmark of aging, causes increased susceptibility to complement injury.[19] However, whether this phenomena, which was shown using an in vitro replicative senescence model to mimic aging, also occurs in a pre-clinical model of biological aging and dry AMD remains unknown. Further, separate studies with non-ophthalmic vessels such as aorta and arteries have

indicated that age-related vascular stiffening enhances vascular sensitivity to proinflammatory cues.[20, 21] Such aberrant stiffness-dependent vascular dysfunction results from altered endothelial cytoskeletal tension (contractility) and mechanotransduction, the process by which mechanical cues get transduced into intracellular biochemical signaling pathways to produce a global cellular response.[22-24] Importantly, studies by us and others have shown that EC stiffness alone can govern EC fate and function.[25-28] Since aging has been associated with stiffening of retinal vessels and the sclera,[29,30] this raises the possibility that choroidal vessels and ECs also become stiffer with aging that, in turn, exacerbates complement-mediated CC degeneration. However, whether aging is associated with increased cytoskeleton-mediated choroidal EC stiffening and enhanced choroidal sensitivity to complement deposition remains unknown.

As more studies emerge and the role of choroidal atrophy associated with dry AMD is implicated, the need for clinically relevant models is imperative. Thus, to further explore the role of age-induced mechanical cues in complement-mediated EC atrophy associated with AMD, we have isolated choroidal endothelial cells from the macular region of rhesus macaques (*Macaca mulatta*) with and without dry AMD. Rhesus monkeys provide a robust model for dry AMD because their retina is anatomically similar to that of humans, they share the same AMD susceptibility genes ARMS2 and HTRA1 with humans, and undergo macular drusen accumulation as seen in humans.[31,32] Further, this monkey model undergoes MAC localization at the level of the CC, also observed in humans.

Using this novel in vitro model of dry AMD we show for the first time that aging

is associated with choroidal endothelial cell stiffening. Importantly, this age-associated EC stiffening correlates with increased susceptibility to complement-induced injury. Further, by decreasing cell stiffness alone via pharmacological inhibition of Rho, the key molecular pathway that controls cytoskeletal tension and contractility and thereby cell stiffness, these complement-induced effects on stiffer ECs can be prevented. By uncovering the previously unknown role of micromechanical cues in choroidal EC dysfunction, this research has the potential to illuminate a previously unexplored territory in AMD research that can help identify new therapeutic targets for early management of dry AMD.

Materials and Methods

Cell Isolation. Rhesus monkey endothelial cells from the macular region of the choroid were isolated from three different young normal, old normal, and old monkeys with severe drusen. For this study, one young normal (6 years old; YN), old normal (20 years old; ON) and old monkey with severe drusen (19 years old; OD) was selected for this study. Specifically, choroidal vessels from inner choroid and choriocapillaris / Bruch's membrane complex obtained from 8mm biopsy punches. Any adherent tissue was brushed off and intact vessels were cut into 1mm pieces and washed three times with isolation buffer (MCDB131 basal medium containing 30 mM HEPES, 1x antibiotic-antimycotic). Tissue was incubated in 0.1% collagenase I in MCDB131 medium for 2h at 37^{o}C with frequent agitation followed by neutralization of collagenase with MCDB131 medium containing 10% FBS. The mixture was then filtered through a sterile 70um mesh prior to centrifugation and washing three times in isolation buffer. Cells were then resuspended in enriched endothelial growth medium composed of MCDB131 medium supplemented with 15% FBS, 1x Glutamax, VEGF (1 ng/ml), EGF (5 ng/ml), bFGF (8 ng/ml), Heparin (100 μg/ml), Ascorbic acid (50 μg/ml), 1x Antibiotic-Antimycotic prior to seeding onto fibronectin-coated (1 μg/cm^2) dishes. Four hours after cell plating, cells were rinsed with PBS to remove all non-adherent cells and supplemented with fresh enriched endothelial growth medium. Cells were grown on fibronectin-coated dishes and supplemented with enriched medium for the first two passages with medium replaced every two days until cultured reached 70-80% confluence.

Rhesus monkey fibroblasts from an abdomen skin biopsy were isolated from young (15 years old). Specifically, tissue was cut into 1mm pieces and washed three times with isolation buffer (DMEM basal medium containing 30 mM HEPES, 1x antibiotic-antimycotic). Tissue was incubated in 0.1% collagenase I in DMEM medium for 2h at 37^{o}C with frequent agitation followed by neutralization of collagenase with DMEM medium containing 10% FBS. The mixture was then filtered through a sterile 70um mesh prior to centrifugation and washing three times in isolation buffer. Cells were then resuspended in fibroblast growth medium composed of DMEM containing 10% FBS, 1x Glutamax, sodium pyruvate, and 1x Pen-Strep.

Rhesus RPE cells were isolated from a young normal monkey. Specifically, RPE was scraped off and immediately stored in RNAlater storage reagent (Applied Biosytems) to stabilize and protect RNA for later use.

Cell Culture. Rhesus monkey ECs were grown on 0.5% gelatin coated dishes in MCDB 131 basal medium (Corning) supplemented with 10% fetal bovine serum (FBS; HyClone GE), 10 mM L-glutamine (Life Technologies), 10 ng/mL epidermal growth factor (Sigma), 4 ng/mL basic fibroblast growth factor (Life Technologies), 1 mg/mL hydrocortisone (Sigma), and 1x antibiotic/antimycotic supplement (Life Technologies). EC culture was maintained at 37^{o}C in a humidified atmosphere with 5% CO_2, with cells being seeded at 10,000 cells/cm-sq and passaged every two days. For all in vitro studies, cells were seeded at 40,000 cells/cm-sq. in starvation medium (MCDB 131 basal medium supplemented with 2.5% FBS and 1x antibiotic-antimycotic) for six hours prior to assays.

Fibroblast culture were grown on tissue culture plastic in DMEM containing 10% FBS, 1x Glutamax, sodium pyruvate, and 1x Pen-Strep. Fibroblast culture was maintained at 37^{o}C in a humidified atmosphere with 5% CO_2, with cells being seeded at 20,000 cells/cm-sq and passaged every four days after reaching 85% confluence.

Rhesus monkey iPSC-derived RPE was used as previously reported.[33, 34] Briefly, RPE were grown on tissue culture plastic in Miller medium[35] supplemented with 5% fetal bovine serum (FBS; HyClone, Logan, UT) at 37 °C and 5% CO_2 in a humidified incubator. After culturing for 10 days, the cells acquired pigmentation.

Complement Activation. To examine the effects of complement activation on rhesus monkey choroidal ECs, cells were treated with 5% normal human serum (NHS; Complement Technology, Inc., Tyler, TX, USA) in veronal buffered saline (VBS; NaCl [145 mM], sodium barbital [1.8 mM], barbituric acid [3 mM], CaCl2 [50 uM], and MgCl2 [25uM], adjusted to pH 7.4) for 3 hours at 37^{o}C to promote complement protein deposition on the cell surface. To confirm the role of complement deposition and subsequent injury, cells were co-treated with complement inhibitor as previously reported.[36] Briefly, complement inhibitor (RSI-compstatin-PEG analog; 2uM) was pre-mixed with 5% NHS on a rocker for 30 min at room temperature prior to addition to EC cultures for 3 hours at 37^{o}C.

To prevent the effects of age-associated cell stiffening, cells were co-treated with NSC23776, a pharmacological Rac1 inhibitor (1000uM) or Y27632, a pharmacological inhibitor of Rho/ Rho-associated kinase (ROCK; 100uM) in 5% NHS for 3 hours at 37^{o}C.

Quantitative RT-PCR. Total RNA was isolated from cell monolayers using an RNA purification kit (Direct-zol RNA MiniPrep; Zymo Research, Irvine, CA, USA). All samples were treated with DNAse to ensure no contaminant DNA was present. RNA was converted to cDNA with high capacity cDNA reverse transcription kit (Applied Biosystems), and amplified with the appropriate TaqMan PCR primers for VE-cadherin, VEGFR2, or RPE65 (Thermo Fisher Scientific, Inc.) on the CFX connect real-time PCR detection system (BioRad, Hercules, CA, USA). Amplification was performed so that there was linear accumulation of PCR products. Relative mRNA levels were determined by the comparative cycle threshold method with normalization to glyceraldehyde 3-phosphate dehydrogenase (GAPDH; Thermo Fisher Scientific, Inc.).

Flow Cytometry. Monkey choroidal ECs were cultured for 48h prior to detachment with accutase. ECs were labeled with PE-conjugated anti-CD146 antibody (BD Biosciences, San Jose, CA, USA) for 20 min at 4°C in FACS buffer (0.5% BSA and 2mM EDTA). R-Phycoerythrin IgG was used as Isotype control. Acquisition of >25,000 events were performed on an NovoCyte flow cytometer (ACEA Biosciences, San Diego, CA) followed by single cell analysis (FlowJo; Treestar, Inc., Ashland, OR, USA).

Immunofluorescence Labeling. Monkey choroidal ECs were plated onto gluteraldehyde-crosslinked gelatin cover slips. Upon completion of assay, cells were fixed in 4% PFA for 15 minutes and rinsed with PBS. Next, cells were incubated with BSA (2% wt/vol, 30 minutes, RT following) to prevent non-specific binging prior to

primary antibody incubation with anti-C5b-9 (2 hours, RT). ECs were rinsed and labeled with secondary antibody (1 hour, RT). For visualization of actin cytoskeleton, ECs were permeabilized (0.2% Triton X-100 in 1 mg/mL BSA) prior to incubation with AlexaFluor 594 Phalloidin (20 minutes, RT), followed by mounting of the cells on glass slides for fluorescence imaging with Zeiss 880 Airyscan confocal or Nikon Eclipse TI epifluorescent microscope. ImageJ was used to quantify the fluoerescence intensity signal and percent cells with damaged actin stress fibers ($n \geq 60$ cells per condition).

Atomic Force Microscopy. For measurement of EC stiffness, cells were grown to confluence on gluteraldehyde-crosslinked gelatin cover slips. EC monolayers in calcium buffer (NaCl [136 mM], KCl [4.6 mM], MgSO4[1.2 mM], CaCl2 [1.1 mM] KHPO4 [1.2 mM], NaHCO3 [5 mM], Glucose [5.5 mM], and HEPES [20 mM]) were indented using a biological-grade atomic force microscope (AFM; Asylum Research). Specifically, cell stiffness was measured in contact mode using a silicon nitride cantilever (0.1 N/m spring constant) modified with a 5μm spherical borosilicate glass bead (Novascan). EC monolayers were indented on a minimum of 20 different spots, each indented a three times using a 2.5 nN indentation force. In some measurements, OD ECs were treated with Y27632 (100 uM; 1 hour, 37^{o}C) prior to indentation.

Rho Activity. RhoA activity was measured from cell lysates using the RhoA G-LISA activation assay kit (Cytoskeleton, Inc, Denver, CO, USA), per the manufacturer's protocol. Briefly, Confluent EC monolayers were lysed over ice. Supernatant was

collected and maintained. Equal amounts of protein was loaded into assay wells. Results were obtained by measuring absorbance at 490 nm using a plate reader (Victor2; Perkin Elmer, MA, USA).

Western Blot. Expression of endothelial phosphorylated and total myosin light chain (MLC) were determined by Western blot. Briefly, confluent EC monolayers were lysed in RIPA buffer containing protease and phosphatase inhibitors, and the lysates were centrifuged to obtain protein supernatant. An equal amount of protein was loaded in 10% SDS-polyacrylamide gel and the separated proteins transferred onto a nitrocellulose membrane for detection with polyclonal rabbit anti-Phospho-Myosin Light Chain 2 (Ser19) antibody (Cell Signaling Technologies) or monoclonal rabbit anti- Myosin Light Chain 2 (D18E2) antibody (Cell Signaling Technologies) followed by detection with goat Anti-rabbit IgG horseradish peroxidase (HRP)-conjugated secondary antibody (Cell Signaling Technologies). GAPDH (Sigma) was used as the loading control. Protein bands were visualized using a chemiluminescent detection kit (Thermo Scientific) coupled with a camera-based imaging system (Biospectrum AC ImagingSystem) while the densitometric analysis was performed by ImageJ software.

Measurement of Cell Area. To quantify cell area, ECs were plated on plastic culture dishes for 6 hours before being subjected to phase contrast imaging using the aforementioned microscope (Nikon Corp.). Projected cell area (n = 50 cells/condition) was measured by tracing the cell perimeter using ImageJ.

Statistics. All data were obtained from multiple cells and multiple replicates/condition (as indicated in each respective section) and expressed as mean ± standard error or standard deviation, as indicated. Statistical significance was determined using analysis of variance (ANOVA), followed by Tukey's and Bonferroni post-hoc analysis (Instat; GraphPad Software Inc., La Jolla, CA, USA). Results were considered significant if $P < 0.05$.

Results

Rhesus Monkey Model of Dry AMD

To study the mechanisms underlying CC atrophy associated with dry AMD, choroidal endothelial cells (ECs) were isolated from the macular region of young normal (6 years old; YN), old normal (20 years old; ON) and old monkeys with severe drusen (19 years old; OD). Monkeys were selected based on AMD diagnosis made by identification of drusen deposits in corresponding fundus photographs (Figure 3.1A). Monkey retinal sections immunolabeled for anti-C5b-9 revealed MAC deposition localized to the CC, similar to the pattern seen in humans (Fig 3.1B).[10] Thus, we rationalized that this model was ideal for in vitro study of CC aging atrophy associated with dry AMD.

Phenotypic Characterization of Monkey Choroidal ECs

To confirm the viability of these isolated cells, we first seeded and confirmed that the cells grew well in culture. Isolated ECs were grown in endothelial-selective culture medium where cobblestone colonies (Fig. 3.2A), characteristic of endothelial cells, emerged soon after seeding and at confluence became contact-inhibited, a characteristic of ECs. To confirm endothelial phenotype, we looked for positive VE-Cadherin mRNA expression, using fibroblasts as a negative control (Fig 3.2B). To further validate EC phenotype, we looked for mRNA expression of endothelial-specific VEGFR2 and CD146 surface protein expression by flow cytomery (Fig 3.2C, 2D). Using RPE65 as a marker

for retinal pigment epithelial cells (RPE) together with pigmentation and cell morphology, we show that our cultures do not contain any RPE contaminants (Suppl. Fig. S3.1).

Choroidal ECs From Drusen Eyes Exhibit Increased Susceptibility To Complement Injury

To determine whether there is any difference in sensitivity to complement activation associated with dry AMD, ECs were treated with NHS to activate the complement pathway. Our measurements of phalloidin-labeled actin cytoskeleton revealed that old ECs isolated from AMD eyes, exhibit significantly greater susceptibility ($P<0.001$) to complement injury, as measured by the damage to actin cytoskeleton (Fig 3.3A). Interestingly, this preferential complement injury, was not due to differential levels of complement deposition across the three different cells as confirmed by similar fluorescence intensity of C5b-9-immunoreactivity (Fig 3.3B). Further, co-treatment with complement-inhibitory peptide revealed that susceptibility to complement injury of OD ECs could be prevented; thereby confirming complement-induced injury did indeed result from complement deposition (Suppl. Fig. S3.2).

Choroidal ECs from Drusen Eyes have Increased Stiffness

Our previous studies using replicative senescence to mimic biological aging have shown that senescence increases chorioretinal EC stiffness,[19] which is consistent with the role of vascular stiffening in many aging models of aorta and

arteries.[21] Further, studies have shown that aging is associated with stiffening of both retinal and non-retinal vessels.[20,30] Thus to determine whether the increased in complement injury susceptibility was caused by this age-induced EC stiffening, force indentation measurements were obtained using a biological-grade AFM. Our measurements revealed that cells from old drusen-laden eyes are significantly stiffer ($P<0.05$) than their young counterparts (Fig 3.4).

Choroidal ECs from Drusen Eyes Exhibit Decreased Rho Activity

Rho is a key mechanotransduction player that regulates actin cytoskeletal tension and, as a consequence, cell stiffness.[24,37] Thus, we looked to see whether the increase in OD EC stiffness is a direct result from an increase in Rho activity. Measurement of baseline Rho activity in confluent EC monolayers revealed that OD ECs exhibit lower ($P < 0.05$) Rho activity than YN ECs (Fig. 3.5A). Since activated Rho kinase inhibits myosin light chain (MLC) phosphatase by phosphorylating its myosin binding subunit, we confirmed this counterintuitive finding by looking at MLC phosphorylation (pMLC). Consistent with studies showing that Rho regulates MLC phosphorylation,[38,39] our findings revealed that stiffer OD ECs with low Rho activity also have lower ($P< 0.001$) MLC phosphorylation (Fig. 3.5B). Thus, to understand how OD ECs are becoming stiffer, we looked at the actin cytoskeleton because previous studies by us and others have shown that stiffer, more contractile ECs have dense actin cytoskeletal filaments. Interestingly, our findings reveal that stiffer OD ECs exhibit a robust cortical actin arrangement while YN and ON ECs have a cytoskeleton composed of stress actin fibers

(Fig. 3.5C).

Decreasing Rho-mediated Cell Stiffening Prevents Complement Injury In Choroidal ECs From Drusen Eyes

To confirm whether cell stiffness alone contributes to greater susceptibility to complement-induced injury, we used the pharmacological Rac1 inhibitor (NSC23776) to mediate cell stiffness. Rac1 is a member of the Rho family that that regulates cortical actin cytoskeletal arrangement, which has been shown to contribute to cell stiffness.[40,41] Thus, we depolymerized Rac-mediated cortical actin in OD ECs (Supp. Fig. S3.3). Our AFM measurements confirm that that Rac inhibition decreases cell stiffness (Fig. 3.6A). Importantly, reducing cell stiffness alone significantly prevented complement-induced injury in OD ECs as measured by damage to actin cytoskeleton (Fig 6B). To further confirm cytoskeletal contribution to cell stiffness, ROCK inhibitor (Y27632) was used to depolymerizing actin fibers. ROCK is a downstream effector of Rho, a key mechanotransduction player that regulates cell stiffness by increasing myosin light chain phosphorylation. Thus, Y27632 also caused depolymerization of cortical actin in OD ECs (Supp. Fig. S3.4). Our AFM measurements confirm that that ROCK inhibition decreases cell stiffness (Fig. 7A). Importantly, reducing cell stiffness alone significantly prevented complement-induced injury in OD ECs as measured by damage to actin cytoskeleton (Fig 3.7B).

Rho-Mediated Cytoskeletal Retraction Prevents Complement Injury In Young ECs

Cytoskeletal structure plays a role in cell response to various mechanical and biochemical cues. Thus, to determine whether stress fiber cytoskeletal arrangement observed in YN ECs may contribute to prevention of complement injury, we looked at the effect of complement activation on cell morphology. Interestingly, YN ECs undergo significant retraction while OD ECs remain fixed as judged by cell area and aspect ratio measurements (Fig. 3.8). Rho-mediated stress fibers are known to generate a centripetal (inward) tension and could thus play a role in the retraction observed.[42] Thus, to confirm the role of actin stress fiber-mediated retraction in complement injury, YN ECs were treated with Y27632, a pharmacological Rho/ROCK inhibitor that depolymerizes actin (Supp. Fig. S3.5). As shown in Figure 3.8, stress fiber depolymerization exacerbated ($P < 0.001$) complement injury of YN ECs (Fig. 9). Our observations that Rac inhibition prevented complement injury may be a result of increased cell retraction because decreasing Rac activity indeed caused OD EC retraction (Suppl. Fig. S3.3).

Discussion

Although aging is considered the major risk factor for AMD, its precise role in disease initiation and progression remains poorly understood. To explain the mechanistic basis of the clinical observation of RPE degeneration, new studies are beginning to implicate a potential role of CC and choroidal atrophy that correlates remarkably with drusen density.[9] However, the mechanisms underlying choroidal degeneration have yet to be elucidated. Interestingly, C5b-9 deposition is found around the CC of both AMD (old) and non-AMD (young) eyes, yet only old eyes develop this potentially blinding disease.[10] This observation led us to consider that aging is increasing the susceptibility of ECs to complement-mediated injury and subsequent lysis, which could explain choroidal atrophy associated with dry AMD. Using a unique in vitro model derived from a non-human primate pre-clinical model of dry AMD, we confirmed this hypothesis while further showing that age-associated EC stiffening is a key contributor to complement-mediated injury. To our knowledge, this study is the first to identify a possible mechanism by which aging may contribute choroidal degeneration.

Aging is a major nonmodifiable risk factor for AMD. However, precisely how it contributes to AMD pathogenesis remains poorly understood. To study the effects of aging on choroidal atrophy associated with dry AMD, choroidal ECs were isolated from the macular region of young, old, and old drusen-laden rhesus monkey eyes. Currently there is a lack of in vivo and in vitro models for the study of choroidal atrophy associated with dry AMD. While there are in vivo models of induced choroidal atrophy, the majority

of studies focus on the role of choroidal neovascularization (CNV) in wet AMD. These models have been essential in providing means to test new therapies. However, since dry AMD is a risk factor for wet AMD, the need to have models specifically for the study of dry AMD is imperative. Current in vitro models of dry AMD have been limited to use of transformed cell lines.[43] Our previous work using a replicative senescence model to mimic biological aging was useful in identifying a potential role of age-associated CC degeneration in the pathogenesis of dry AMD.[19] However, these findings remained to be validated in an appropriate aging model. Thus, here we aimed to establish a clinically relevant in vitro model to study the effects of aging on choroidal atrophy associated with dry AMD.

This in vitro model derived from rhesus monkeys is distinct because unlike other animal models, these monkeys recapitulate many of the features of human dry AMD. Importantly, rhesus monkeys have been found to share the same genetic polymorphisms in ARMS2 (LOC387715) and HTRA1 associated with human AMD,[32] though this was not independently verified for the monkeys used in this study. Further, unlike other animal models such as the Ccl2-/-, and double knockout Ccl2-/- Ccr2-/-, and Ccl2-/- Cx3cr1-/- mice which exhibit several hallmarks of AMD such as subretinal drusen-like accumulations (composed of accumulations of subretinal lipid laden microglia), thickening of Bruch's membrane, increase in autofluorescence and lipofuscin granules, photoreceptor malfunction, and the occurrence of CNV, rhesus monkeys share the unique structure of the human macula and spontaneously develop macular drusen, the clinical hallmark of dry AMD.[44-46] Further, consistent with past observations from human retinal

sections of dry AMD eyes,[10] monkey retinal sections revealed strong immunoreactivity for anti-C5b-9 (MAC) around the CC. Thus, the use of macular choroidal ECs derived from this monkey model of dry AMD greatly strengthens the clinical implications of our findings.

Previous studies have shown that drusen density correlates with CC dropout.[9] However, the mechanisms underlying CC atrophy still remain poorly understood. The observations of increased C5b-9 (MAC) deposition around the CC points towards a potential role of complement activation in CC degeneration. Indeed, treatment of choroidal ECs with complement-competent serum revealed that OD ECs isolated from drusen-laden eyes undergo significantly greater complement-induced atrophy. Interestingly, this preferential complement injury was not due to differential levels of complement deposition across the three different ECs as confirmed by similar levels of C5b-9-immunoreactivity on the cell surface. Consistent with human eye sections that show increased C5b-9 deposition in AMD eyes,[11] our findings in monkey retinal sections of increased C5b-9 deposition on the CC increasing with age may appear paradoxical. However, in support of our observations, we would like to emphasize that the effects we see in differences in complement injury response in vitro is not due to the rate of MAC deposition. In vivo, CC of aged monkeys has been exposed to complement activation for a longer length of time due to old age of monkeys compared to their young counterparts and thus could explain the differences in C5b-9 deposition observed in tissue. Additionally, by using a complement-inhibiting peptide we confirmed this atrophic effect was indeed a result from complement injury.

To understand how ECs from aging eyes become more susceptible to complement injury, we examined the potential role of EC stiffness. This is because previous studies by us and others have shown that increased EC stiffening increases sensitivity to proinflamatory cues. [19-21] Our AFM indentation measurements reveal for the first time that aged choroidal ECs are significantly stiffer than their younger counterparts. Mechanistically, cell stiffness is regulated by Rho that, via its downstream target ROCK (Rho-associated Kinase), modulates both actin/myosin-based cytoskeletal tension and contractility.[24] Remarkably, stiffer choroidal OD ECs exhibit significantly lower Rho activity than YN ECs, which was consistent with lower myosin light chain phosphorylation. To understand this counterintuitive trend, we looked at the actin cytoskeleton because previous studies by us and others have shown that stiffer, more contractile ECs have dense actin cytoskeletal filaments. [19,22,25] Interestingly, our findings revealed that stiffer OD ECs exhibit a robust cortical actin arrangement in contrast to YN and ON ECs, which have stress actin fibers. This observation is consistent with past studies that have demonstrated an active role of cortical actin in aortic EC stiffening.

To elucidate the mechanism underlying the distinct organization of actin cytoskeleton and assess the role of cortical actin in age-associated OD EC stiffening, we focused on Rac, a member of the Rho family of proteins that is known to stabilize cortical actin.[40] Pharmacological inhibition of Rac in OD ECs resulted in marked disruption of cortical actin, which correlated with significant reduction of cell stiffness and increased protection against complement injury. Precisely how cortical actin-dependent cell stiffness alters susceptibility to complement injury is not clear. It is

possible that the activity of surface-bound transmembrane complement regulators that prevent MAC pore formation (e.g. factor H, CD59, and decay accelerating factor), may be altered by cell/membrane stiffness imparted by cortical actin. This idea is supported by studies that have revealed an important role of cortical actin arrangement/activity in the dynamics and spatial organization of cell membrane proteins. [47-49] Whether this mechanism is applicable in choroidal ECs is yet to be investigated.

Previous studies have shown that the establishment of actin cytoskeleton and associated mechanotransduction and cell behavior relies greatly on two key members of the Rho family of GTPases viz. Rac RhoA and Rac.[50,51,55] Since each protein has a distinct role, a fine balance in their activities is essential for proper regulation of cell function. Rac in particular has been shown to participate in cortical actin polymerization known to play a key role in forming cell-matrix adhesion while Rho induces formation of stress fibers and generation of inward-directed contractile forces (cytoskeletal tension).[40,42] Thus, it is intuitive that in response to membrane-disrupting conditions, cells with high Rho and stress fiber density will undergo greater retraction to minimize membrane damage than those with robust cortical actin. Indeed, the lower susceptibility of YN ECs to complement activation, which results in the membrane deposition of cytolytic MAC pores, correlated with its higher Rho-associated stress fiber density and greater retraction. In contrast, the robust cortical actin and reduced stress fiber density of OD ECs impaired their ability to retract and minimize membrane damage. Together, these findings indicate that Rho-associated stress fibers protect YN ECs from the detrimental effects of complement activation. If so, then decreasing Rho-mediated

contractility should increase complement injury. Indeed, we found that pharmacological Rho/ROCK inhibition in YN ECs alone leads to a significant increase in complement injury.

To our knowledge, these findings are the first to implicate a specific age-associated factor in CC atrophy associated with dry AMD. Although our findings offer new mechanistic insight into choroidal EC loss and CC degeneration associated with dry AMD, they do not yet explain precisely how age-induced cell stiffness increases EC sensitivity to complement injury. In this regard, it must be noted that cells are armed with a host of protective mechanisms to survive complement attack. This study does not look at the role of complement regulatory factors on the EC surface such as MAC-inhibitory protein (MAC-IP; CD59), Decay accelerating factor (DAF), membrane cofactor protein (MCP; CD46), and complement receptor type 1 (CR1; CD35). Further, whether activity of these proteins regulated by cell stiffness remains to be studied. Additionally, how Rac inhibition prevents complement injury in OD ECs remains to be further elucidated. It is possible that cortical actin disassembly is necessary for lysosomal-dependant spontaneous repair of damaged cell membranes, thus it is possible that greater sensitivity of stiffer OD ECs to complement injury results from impaired Rho-mediated lysosomal trafficking. However, this remains to be carefully examined in a separate study.

Further, AMD is a multifactorial disease that is also regulated by dietary and genetic factors.[31,32,53,54] How these risk factors contribute to the age-related mechanical control of choroidal susceptibility to complement injury also remains to be determined. Additionally, it should be pointed out that though we have isolated choroidal cells from

three monkeys corresponding to young normal, old nomal, and old with drusen, our study is limited by the use of only one monkey per group. Further studies examining the phenomenon of EC stiffness leading to increased susceptibility are necessary with a larger cohort. Although our novel findings present a paradigm shift in the mechanistic understanding of dry AMD pathogenesis, many questions still remained to be addressed. For example, the present study does not explain whether and how choroidal atrophy can lead to RPE atrophy, the clinical manifestation of AMD. Further, can choroidal atrophy contribute to drusen formation through RPE loss? Additionally, we show that EC stiffening alone is a key determinant of increased susceptibility complement injury. Interestingly, Bruchs membrane stiffening has also been shown to occur in aging eyes. Could this mechanical alteration in contribute to altered RPE VEGF expression that could then affect choroidal viability? One potential way of addressing these questions can be the use of co-culture assays that could be set-up to study the crosstalk between the RPE and choroid.

Conclusion

In summary, in the present study we performed in vitro characterization of a unique model for the study of choroidal atrophy associated with dry AMD. Previous studies have shown that MAC deposition alone is *not sufficient* for choroidal dropout. However, our findings demonstrate that age-induced EC stiffening alone exacerbates complement injury necessary for disease progression. Importantly, this model will help further examine the link between age-associated choroidal EC stiffening, complement activation, and choroidal atrophy associated with dry AMD. By uncovering the previously unknown role of micromechanical cues in choroidal EC dysfunction, this research has the potential to illuminate a previously unexplored territory in AMD research that can help identify new therapeutic targets for potentially effective management of dry AMD.

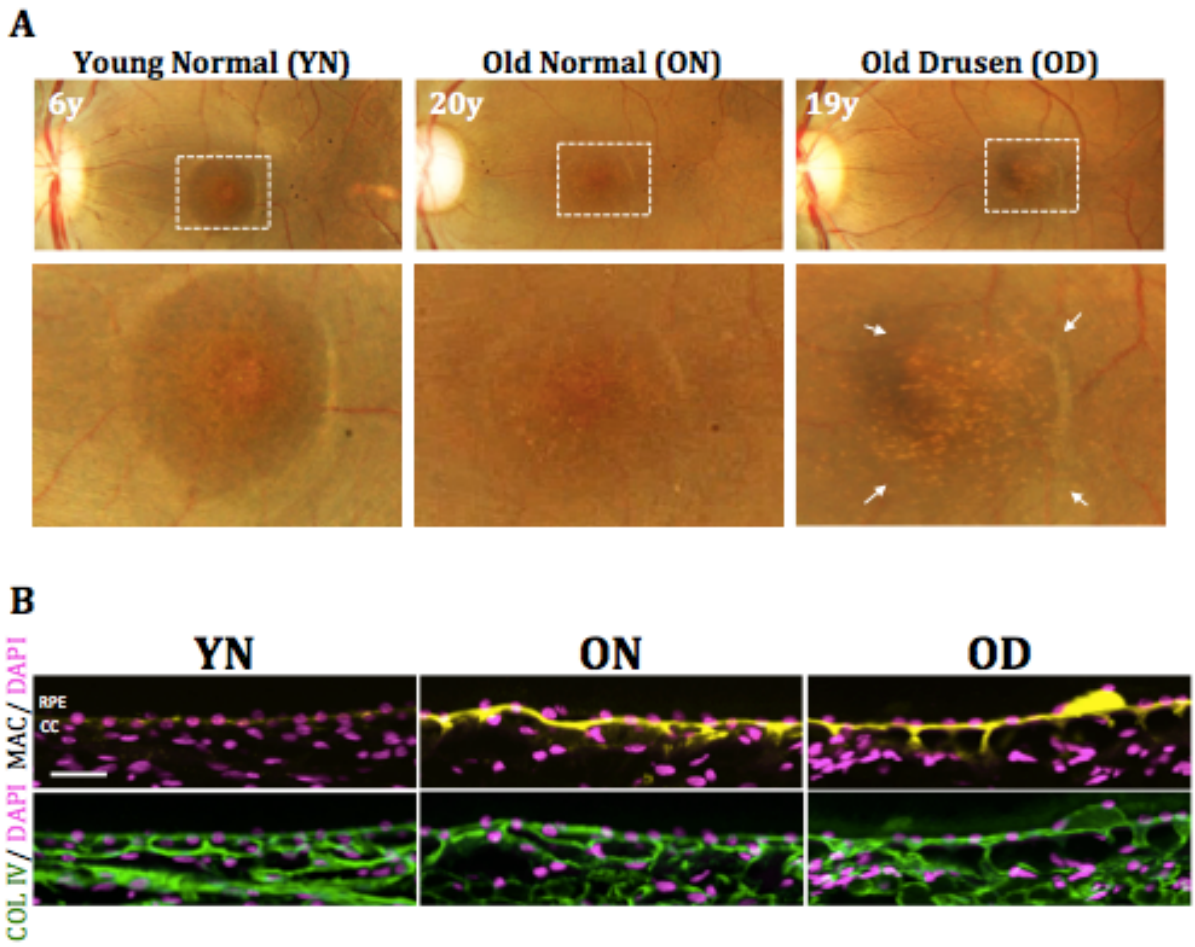

FIGURE 3.1: **Isolation of Choroidal ECs From Macular Region of Rhesus Monkey Eyes.** (A) Choroidal endothelial cells were selectively isolated from the macular region of rhesus monkey eyes based on fundus photograph screening for dry AMD. Images show fundus of of young normal (6 years old; YN), old normal (20 years old; ON) and old eyes with severe drusen (19 years old; OD). Bottom panel shows magnified macular region identifying drusen deposits, indicated by arrows. (B) Eye sections of young normal (7 years old; YN), old normal (21 years old; ON) and old monkeys with severe drusen (30 years old; OD) were dual-labeled with anti-C5b-9 MAC antibody (yellow)

and anti-Collagen IV (green) antibodies. C5b-9 immunoreactivity was specific to Bruch's membrane and choriocapillaris. Notably, C5b-9 labeling was not found on RPE or outer choroid. C5b-9 was present on all sections with highest intensity of labeling in CC of old eyes with severe drusen. Scale bar 50um. RPE, Retinal pigment epitheliuml; CC, choriocapillaris.

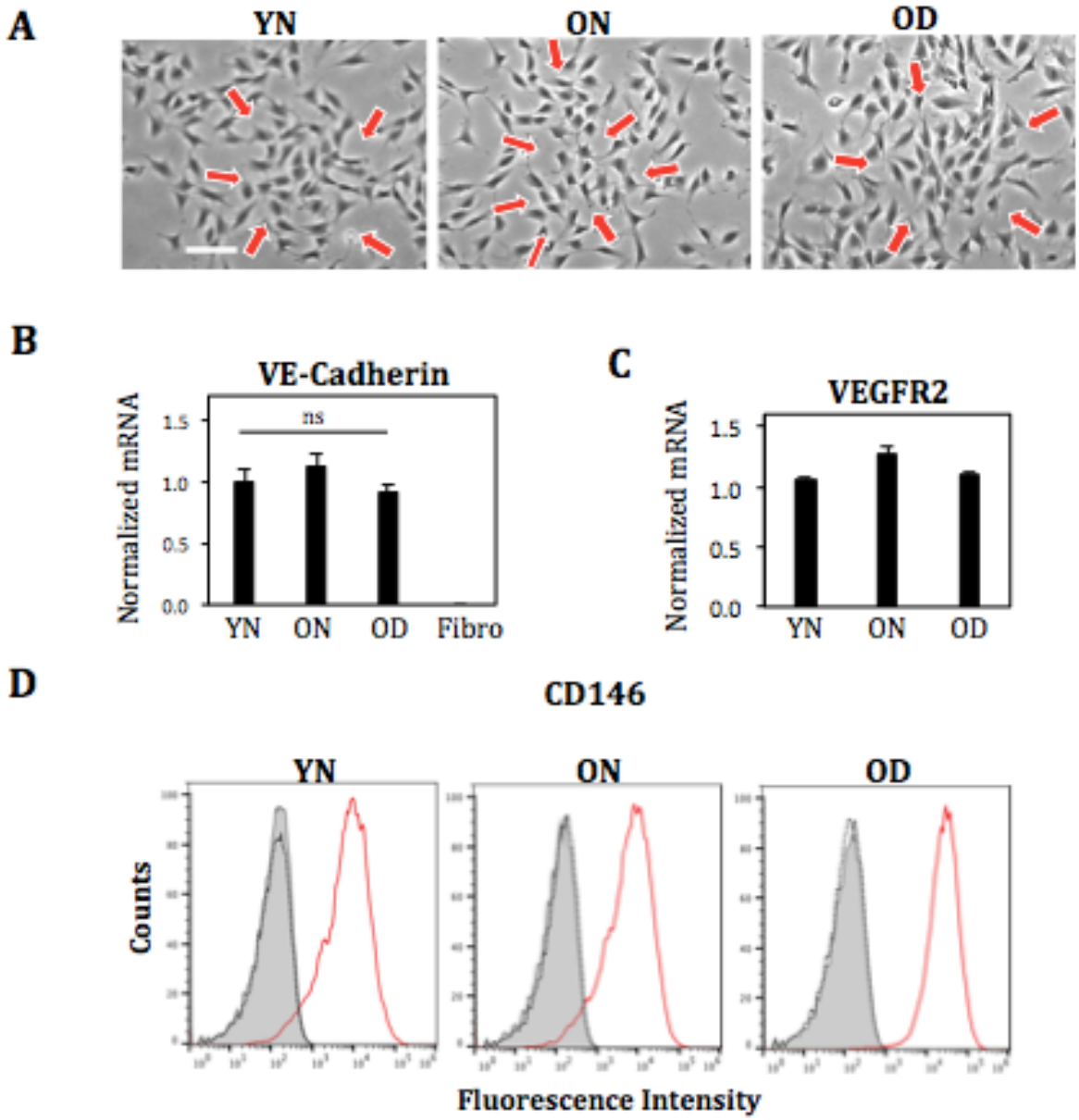

FIGURE 3.2: Phenotypic Characterization of Monkey Choroidal ECs. (A) Monkey choroidal ECs isolated from the macular region young normal (6 years old; YN), old normal (20 years old; ON) and old monkeys with severe drusen (19 years old; OD) form cobblestone colonies characteristic of endothelial cells, indicated by arrows. Scale bar:

100 um. (B) Quantitative PCR analysis from multiple replicates (n=3) shows positive VE-cadherin mRNA expression. Monkey fibroblasts were used as a negative control. Levels of VE-Cadherin mRNA were normalized with respect to GAPDH. Bars indicate average ± standard error of mean. (C) Quantitative RT-PCR analysis from multiple replicates (n=3) shows that isolated monkey choroidal cells exhibit similar levels of VEGFR2 mRNA expression. Levels of VEGFR2 mRNA were normalized with respect to GAPDH. Bars indicate average ± standard error of mean. (D) Monkey choroidal cells were labeled with anti-CD146 or isotype-matched control antibody (solid gray histogram), and subjected to flow cytometry analysis. Histograms of cell counts versus fluorescence indicate that cells exhibit similar expression levels of cell surface CD146.

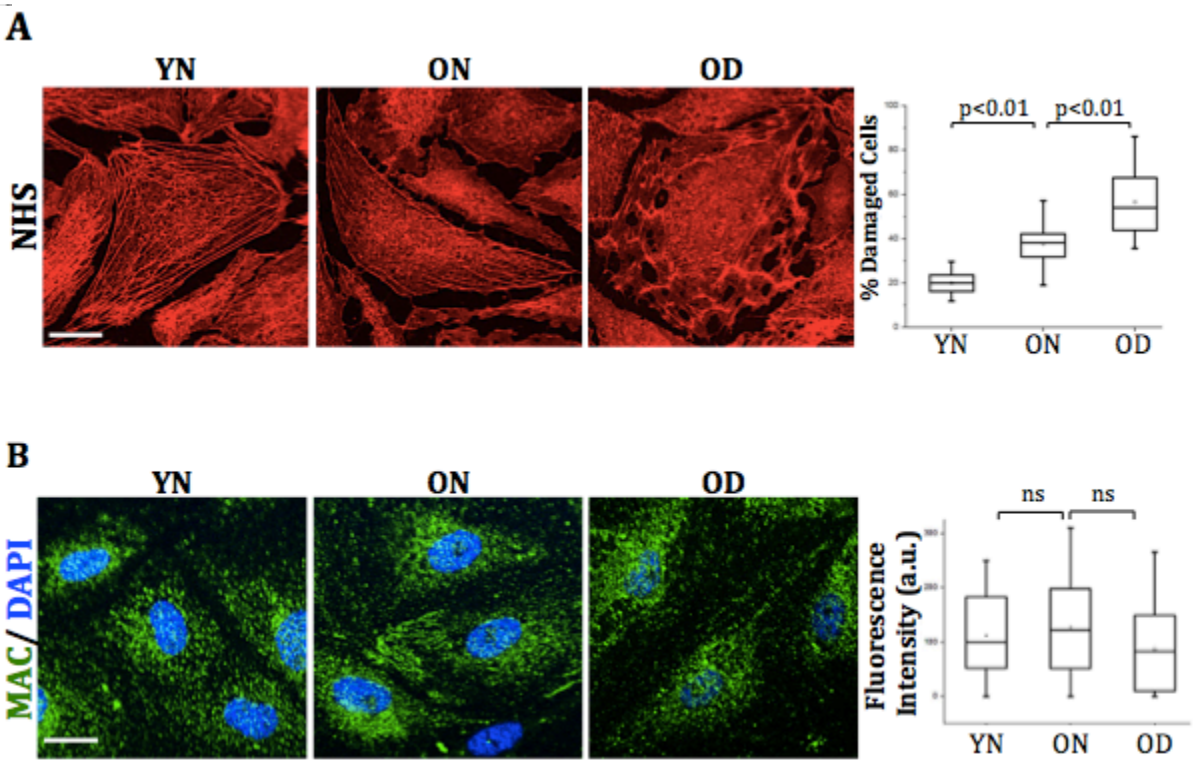

FIGURE 3.3: Choroidal ECs from Drusen Eyes Exhibit Increased Susceptibility to Complement injury. (A) Choroidal ECs were treated with complement-competent normal human serum (NHS, 5% vol/vol; 3h, 37^{o}C). Phalloidin-labeled F-actin fibers reveal significantly greater damage to cytoskeleton in OD ECs compared to YN and ON ECs ($P < 0.001$). Scale bar: 25 um. (B) Immunolabeling of anti-MAC (C5b-9) was used to detect surface MAC deposition. Representative images and fluorescence intensity measurements (bar graph; $n \geq 75$ cells) reveal that YN, ON, and OD ECs exhibit similar surface MAC deposition.

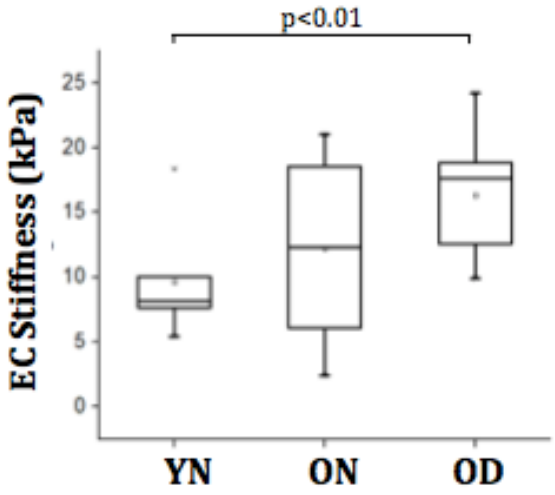

FIGURE 3.4: Choroidal ECs from Drusen Eyes Have Increased Stiffness. EC stiffness was measured using a biological-grade AFM fitted with a silicon nitride cantilever tip modified with a 5 μm-diameter glass bead. Quantitative analysis of multiple ($n \geq 45$) force indentation measurements revealed that mean stiffness of ECs isolated from old drusen-laden eyes was 2-fold higher compared to ECs isolated from young normal eyes ($P < 0.05$).

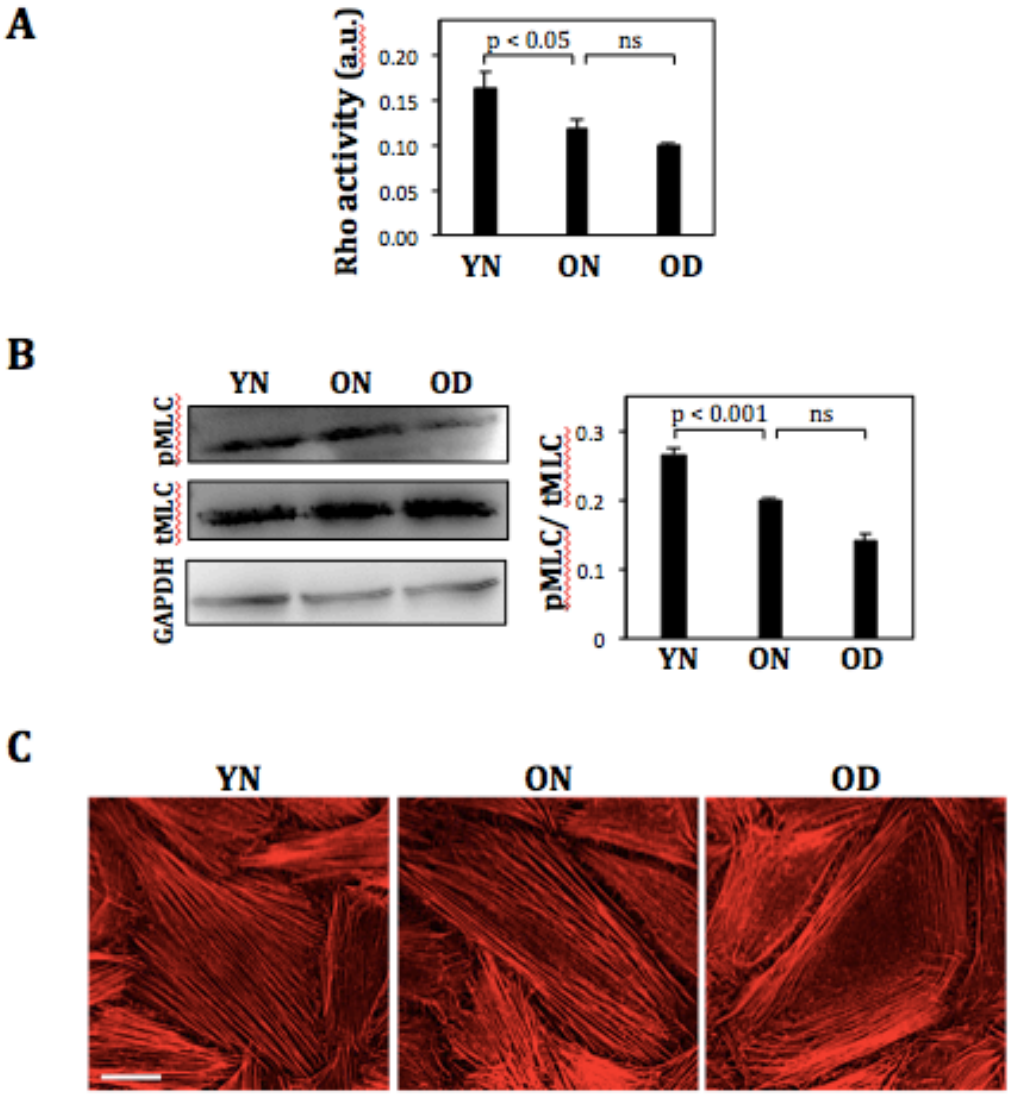

FIGURE 3.5: Choroidal ECs from Drusen Eyes Have Low Rho Activity. (A) Baseline RhoA activity of choroidal ECs was measured using RhoA G-LISA activation assay. Absorbance measurements show a ~60% decrease in Rho activity in OD ECs when compared with YN ECs ($P < 0.05$). Bars indicate average ± standard error of mean. (B) ECs monolayers were subjected to Western blotting for detection of phosphorylated

myosin light chain (MLC) expression. Representative protein bands (18 kDa) and their densitometric analysis (mean ± std. dev.) normalized to total MLC (loading control) shows that MLC phosphorylation is decreased in OD ECs ($P < 0.001$). (C) Choroidal ECs were stained with fluorescently labeled phalloidin to visualize actin cytoskeletal filaments. Representative fluorescent image revealed robust stress actin fiber in YN and ON ECs and a cortical actin cytoskeletal arrangement in OD ECs. Scale bar: 50 um.

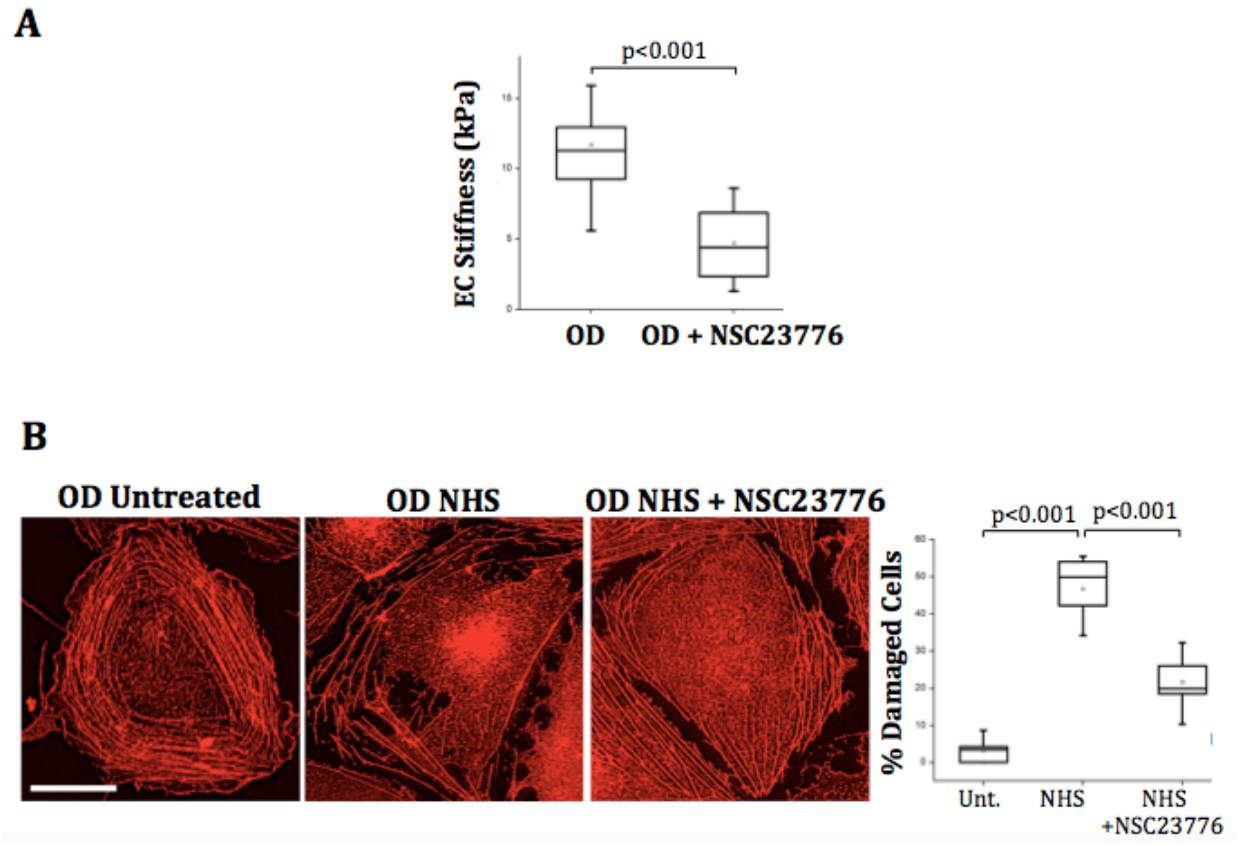

FIGURE 3.6: Decreasing Rac-Mediated Cell Stiffening Prevents Complement Injury In Choroidal ECs From Drusen Eyes. (A) EC stiffness was measured by AFM. Average force indentation measurements (n > 50) of OD ECs treated with pharmacological Rac1 inhibitor (NSC23776; 1000uM) revealed a ~2-fold decrease in stiffness (P> 0.001). (B) OD ECs were co-treated with NHS and NSC23776. Representative images and counting of damaged phalloidin-labeled actin cytoskeleton fibers (box plot; n > 100) reveal an average ~2.5-fold decrease of complement-induced injury in OD ECs (P < 0.001). Scale bar: 25 um.

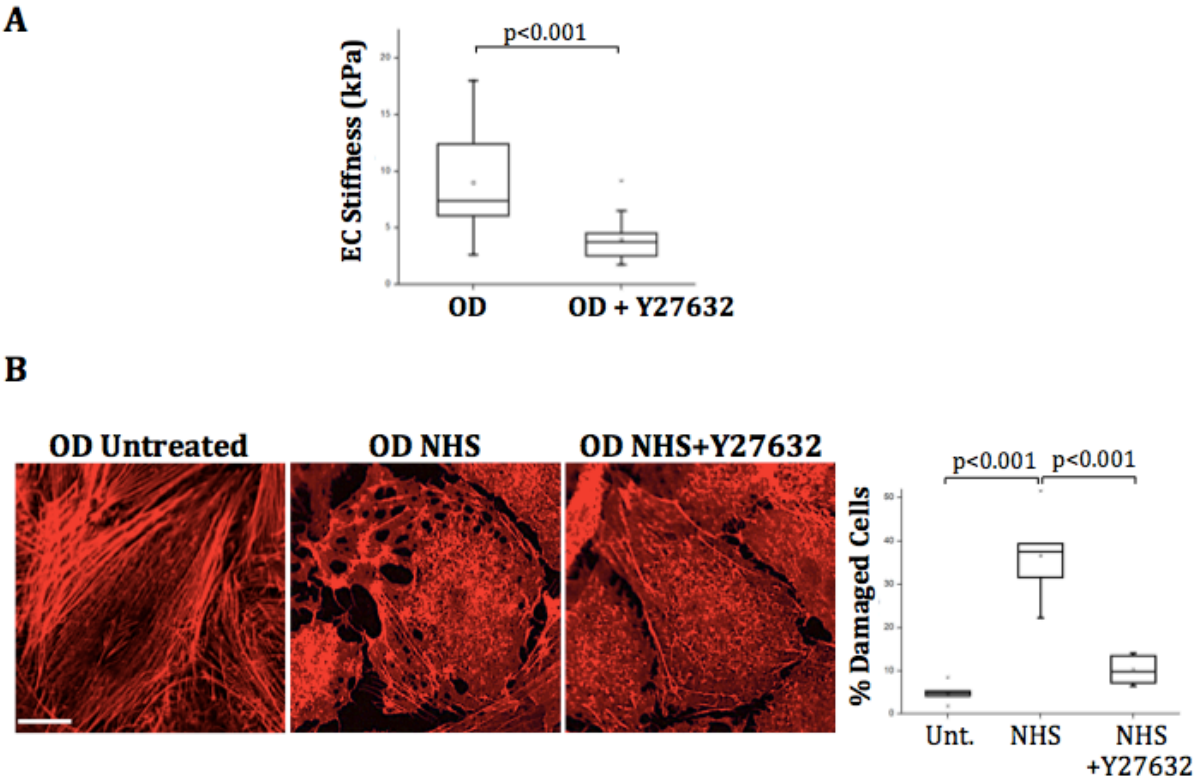

FIGURE 3.7: Decreasing Rho/ROCK Mediated Cell Stiffening Prevents Complement Injury In Choroidal Ecs From Drusen Eyes. (A) EC stiffness was measured by AFM. Average force indentation measurements (n > 40) of OD ECs treated with pharmacological ROCK inhibitor (Y27632; 100uM) revealed a ~1.9-fold decrease in stiffness (P> 0.001). (B) OD ECs were co-treated with NHS and Y27632. Representative images and counting of damaged phalloidin-labeled actin cytoskeleton fibers (box plot; n > 100) reveal an average ~3.5-fold decrease of complement-induced injury in OD ECs (P < 0.001). Scale bar: 25 um.

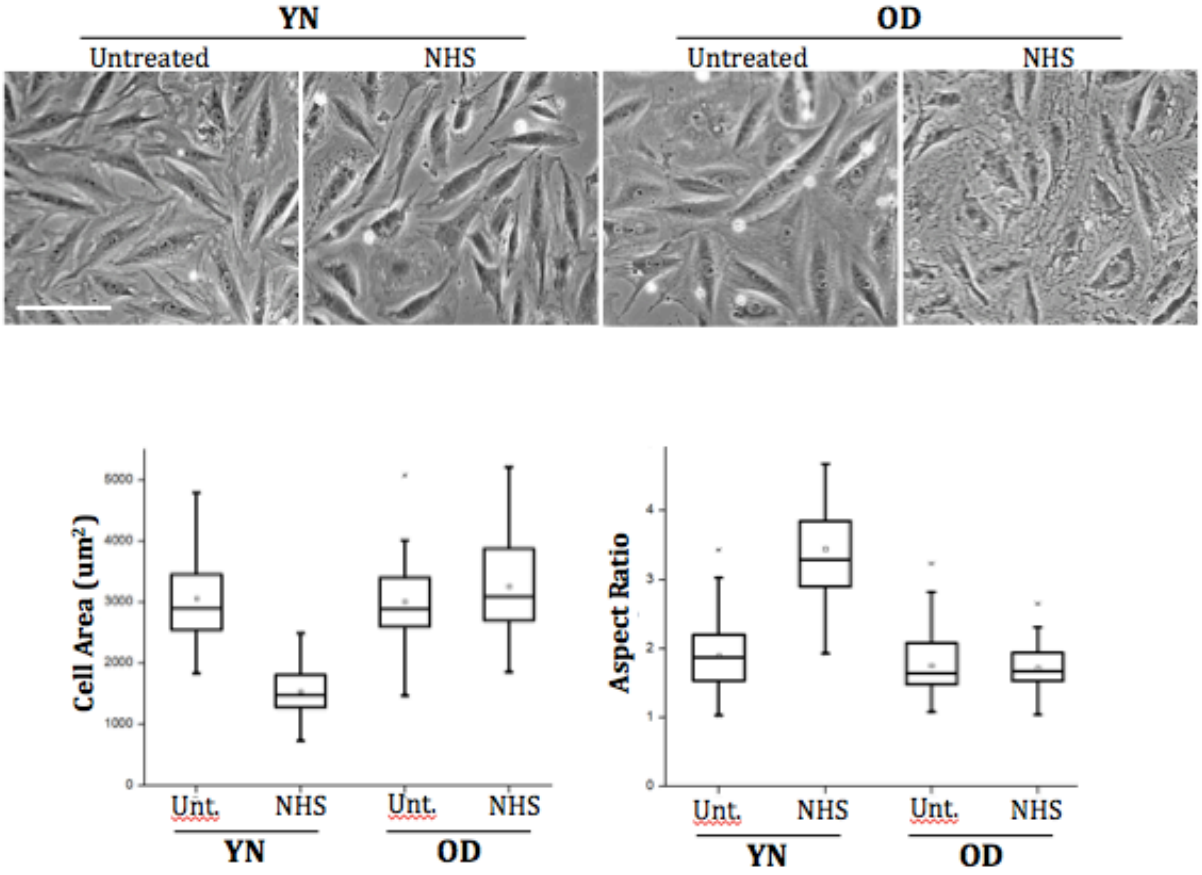

FIGURE 3.8: Complement Injury Causes YN EC Retraction. Representative phase contrast images and measurement of projected cell area together with aspect ratio (box plot; n=250 cells) indicate that only YN ECs undergo significant retraction compared to OD ECs. Scale bar: 10 μm.

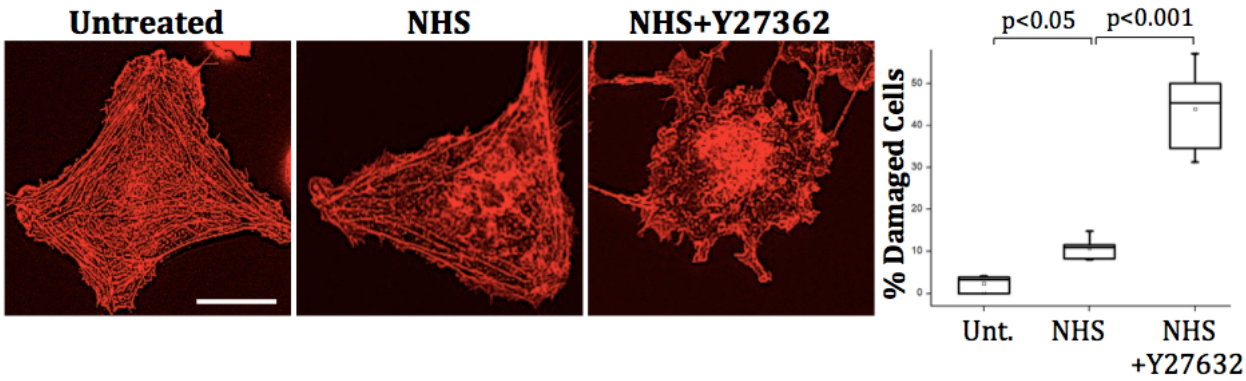

FIGURE 3.9: Inhibition Of Rho-Mediated Retraction Exacerbates Complement Injury In YN ECs. YN ECs were co-treated with NHS and Y27632. Representative images and counting of damaged phalloidin-labeled actin cytoskeleton fibers (box plot; n>100) reveal an average ~40% increases of complement-induced injury in YN ECs (P<0.001). Scale bar: 25 um.

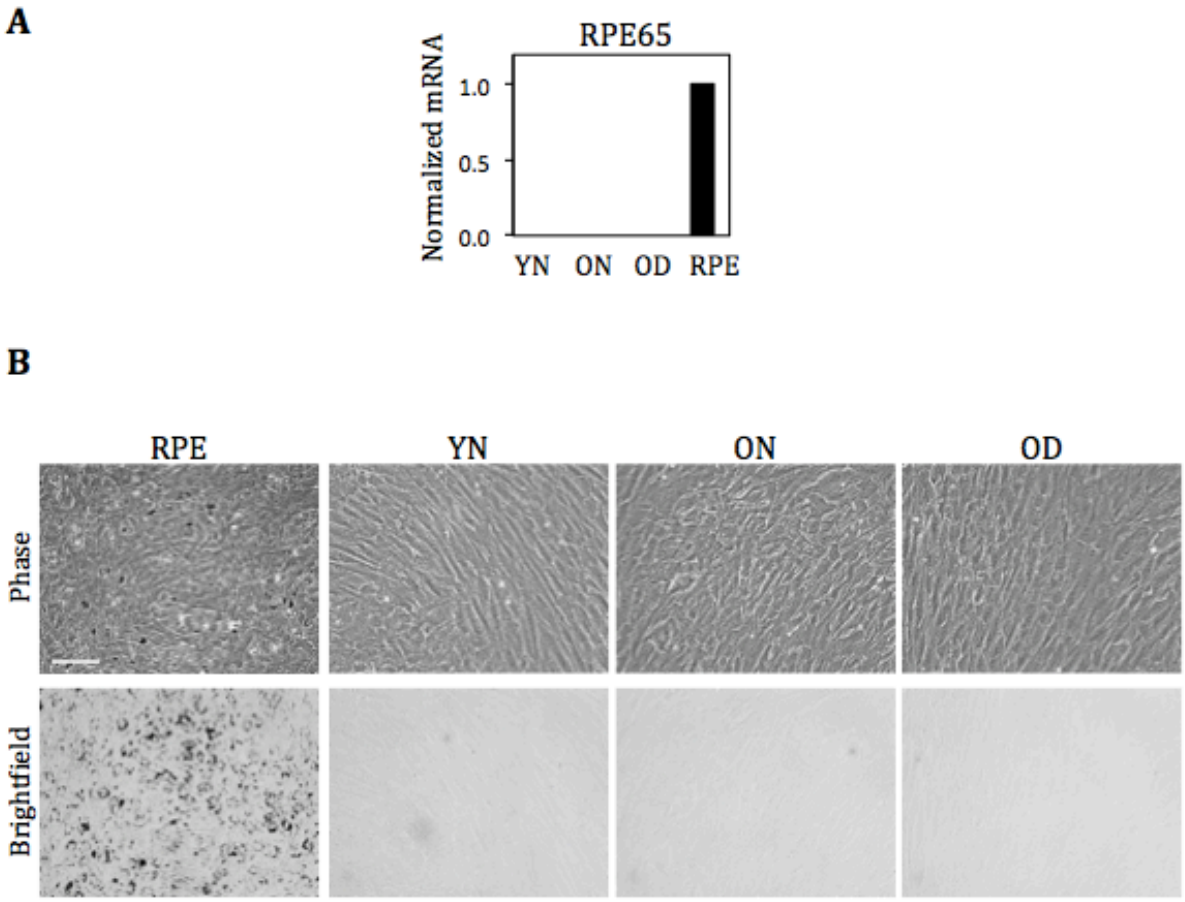

SUPPLEMENTAL FIGURE S3.1. **ECs do not express RPE65.** (A) Quantitative RT-PCR analysis from multiple replicates (n=3) shows that isolated monkey choroidal endothelial cells do not express RPE65 mRNA expression, a RPE phenotypic marker. Levels of RPE65 mRNA were normalized with respect to GAPDH. Representative phase contrast and brightfield images of 10 day RPE and ECs cultures show that ECs lack pigmentation, a characteristic of RPE. Scale bar: 10 um

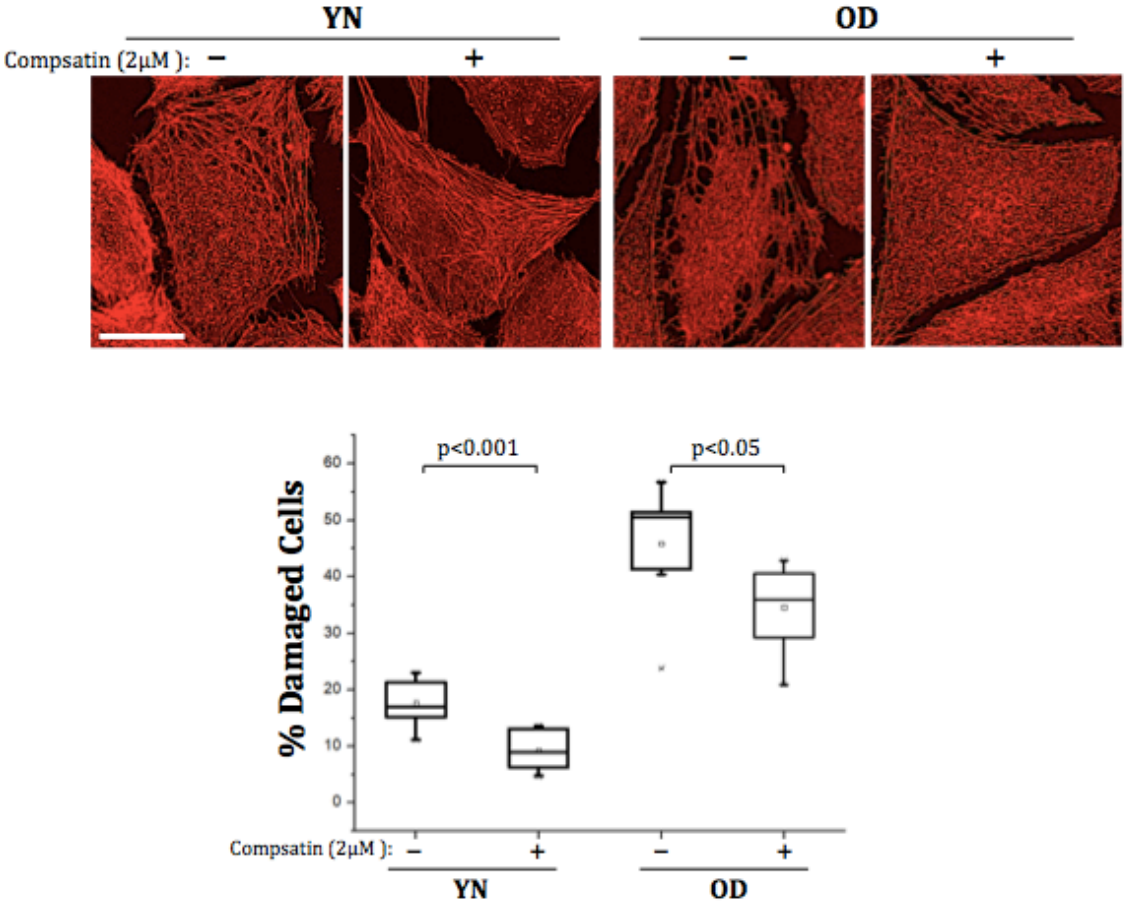

SUPPLEMENTAL FIGURE S3.2. **Compstatin prevents complement injury.** To confirm the role of complement deposition and subsequent injury, cells were co-treated with complement inhibitor (RSI-compstatin-PEG analog; 2uM) and 5% NHS. Analysis of representative images of phalloidin labeled actin cytoskeleton revealed that ECs treated with complement inhibitor underwent significantly less complement-induced damaged as judged by the disruption of the actin cytoskeleton. Scale bar: 25 um.

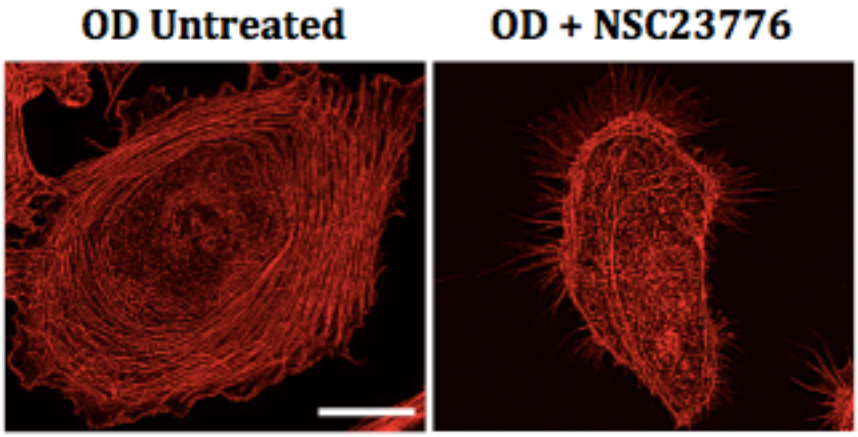

SUPPLEMENTAL FIGURE S3.3. **Pharmacological Rac inhibition disrupts cortical actin in OD ECs.** OD ECs were treated with Rac inhibitor NSC23776. Representative images of phalloidin-labeled cytoskeleton revealed disruption of the cortical actin together with cell retraction. Scale bar: 25 um

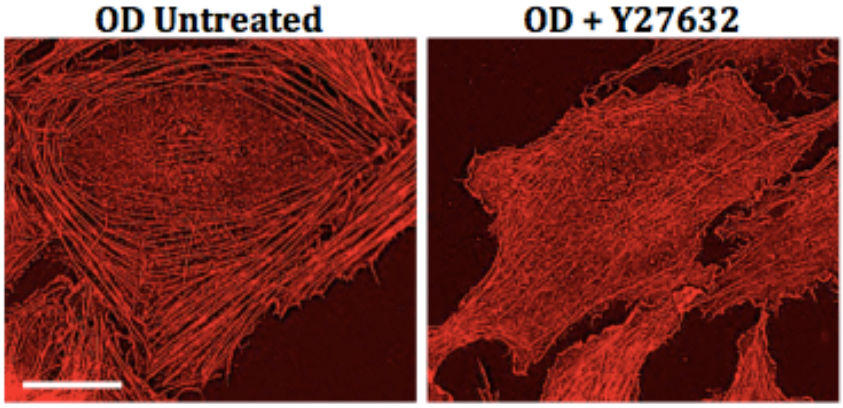

SUPPLEMENTAL FIGURE S3.4. **Pharmacological Rho/ROCK inhibition disrupts cortical actin in OD ECs.** OD ECs were treated with Y27632. Representative images of phalloidin-labeled cytoskeleton revealed disruption of the robust cortical actin arrangement. Scale bar: 25 um.

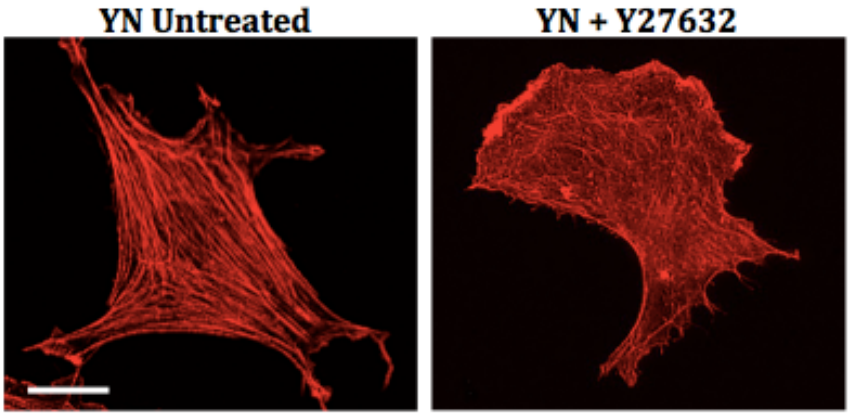

SUPPLEMENTAL FIGURE S3.5. **Pharmacological Rho/ROCK inhibition disrupts actin stress fibers in YN ECs.** YN ECs were treated with Y27632. Representative images of phalloidin-labeled cytoskeleton revealed disruption of the actin stress fibers. Scale bar: 25 um

References

1. Cook HL, Patel PJ, Tufail A. Age-related macular degeneration: diagnosis and management. *Br Med Bull*. 2008;85:127– 149.

2. Friedman DS, O'Colmain BJ, Munoz B, et al. Prevalence of age-related macular degeneration in the United States. *Arch Ophthalmol*. 2004;122:564–572.

3. Ambati J, Fowler BJ. Mechanisms of age-related macular degeneration. *Neuron*. 2012;75:26–39.

4. Zhang K, Zhang L, Weinreb RN. Ophthalmic drug discovery: novel targets and mechanisms for retinal diseases and glaucoma. *Nat Rev Drug Discov*. 2012;11:541–559.

5. Liang, F. Q., & Godley, B. F. (2003). Oxidative stress-induced mitochondrial DNA damage in human retinal pigment epithelial cells: a possible mechanism for RPE aging and age-related macular degeneration. *Experimental eye research*, *76*(4), 397-403.

6. Kaarniranta, K., Sinha, D., Blasiak, J., Kauppinen, A., Veréb, Z., Salminen, A., Petrovski, G. (2013). Autophagy and heterophagy dysregulation leads to retinal pigment epithelium dysfunction and development of age-related macular degeneration. *Autophagy*, *9*(7), 973-984.

7. Young, R. W. (1987). Pathophysiology of age-related macular degeneration. *Survey of ophthalmology*, *31*(5), 291-306.

8. Whitmore SS, Sohn EH, Chirco KR, et al. Complement activation and choriocapillaris loss in early AMD: implications for pathophysiology and therapy. *Prog Retin Eye Res*. 2015;45: 1–29.

9. Mullins RF, Johnson MN, Faidley EA, Skeie JM, Huang J. Choriocapillaris vascular dropout related to density of drusen in human eyes with early age-related macular degeneration. *Invest Ophthalmol Vis Sci* 2011;52:1606-1612.

10. Mullins RF, Schoo DP, Sohn EH, et al. The membrane attack complex in aging human choriocapillaris: relationship to macular degeneration and choroidal thinning. *Am J Pathol* 2014;184:3142-3153.

11. Bhutto, I., & Lutty, G. (2012). Understanding age-related macular degeneration (AMD): relationships between the photoreceptor/retinal pigment epithelium/Bruch's membrane/choriocapillaris complex. *Molecular aspects of medicine*, *33*(4), 295-317.

12. McLeod, D. S., Taomoto, M., Otsuji, T., Green, W. R., Sunness, J. S., & Lutty, G. A. (2002). Quantifying changes in RPE and choroidal vasculature in eyes with age-

related macular degeneration. *Investigative ophthalmology & visual science*, *43*(6), 1986-1993.

13. "Choroidal thickness in healthy Chinese subjects." *Investigative ophthalmology & visual science* 52, no. 13 (2011): 9555-9560.

14. Blasiak, Janusz, Goran Petrovski, Zoltán Veréb, Andrea Facskó, and Kai Kaarniranta. "Oxidative stress, hypoxia, and autophagy in the neovascular processes of age-related macular degeneration." *BioMed research international* 2014 (2014).

15. Kinnunen, Kati, Goran Petrovski, Morten C. Moe, András Berta, and Kai Kaarniranta. "Molecular mechanisms of retinal pigment epithelium damage and development of age‐related macular degeneration." *Acta ophthalmologica* 90, no. 4 (2012): 299-309.

16. Anderson DH, Mullins RF, Hageman GS, Johnson LV. A role for local inflammation in the formation of drusen in the aging eye. *Am J Ophthalmol* 2002;134:411-431.

17. Parmeggiani F, Romano MR, Costagliola C, et al. Mechanism of inflammation in age-related macular degeneration. *Mediators Inflamm*. 2012;2012:546786.

18. Bayly-Jones, C., Bubeck, D., & Dunstone, M. A. (2017). The mystery behind membrane insertion: a review of the complement membrane attack complex. *Phil. Trans. R. Soc. B*, *372*(1726), 20160221.

19. Cabrera AP, Bhaskaran A, Xu J, Yang X, Scott HA, Mohideen U, Ghosh K; Senescence Increases Choroidal Endothelial Stiffness and Susceptibility to Complement Injury: Implications for Choriocapillaris Loss in AMD. *Invest. Ophthalmol. Vis. Sci.* 2016;57(14):5910-5918.

20. Wang M, Monticone RE, Lakatta EG. Proinflammation of aging central arteries: a mini-review. *Gerontology*. 2014;60:519–529.

21. Kothapalli D, Liu SL, Bae YH, et al. Cardiovascular protection by ApoE and ApoE-HDL linked to suppression of ECM gene expression and arterial stiffening. *Cell Rep*. 2012;2:1259–1271.

22. Ghosh K, Thodeti CK, Dudley AC, Mammoto A, Klagsbrun M, Ingber DE. Tumor-derived endothelial cells exhibit aberrant Rho-mediated mechanosensing and abnormal angiogenesis in vitro. Proc Natl Acad Sci U S A. 2008;105:11305–11310.

23. Mammoto A, Mammoto T, Kanapathipillai M, et al. Control of lung vascular permeability and endotoxin-induced pulmonary oedema by changes in extracellular matrix mechanics. Nat Commun. 2013;4:1759.

24. Mammoto A, Mammoto T, Ingber DE. Rho signaling and mechanical control of vascular development. Curr Opin Hematol. 2008;15:228–234.

25. Huynh J, Nishimura N, Rana K, et al. Age-related intimal stiffening enhances endothelial permeability and leukocyte transmigration. Sci Transl Med. 2011;3:112ra122.

26. Yang X, Scott HA, Ardekani S, Williams M, Talbot P, Ghosh K. Aberrant cell and basement membrane architecture contribute to sidestream smoke-induced choroidal endothelial dysfunction. Invest Ophthalmol Vis Sci. 2014;55:3140–3147.

27. Yang X, Scott HA, Monickaraj F, et al. Basement membrane stiffening promotes retinal endothelial activation associated with diabetes. FASEB J. 2016;30:601–611.

28. Scott HA, Quach B, Yang X, et al. Matrix stiffness exerts biphasic control over monocyte-endothelial adhesion via Rhomediated ICAM-1 clustering. Integr Biol (Camb). 2016;8:869– 878.

29. Friedman E, Ivry M, Ebert E, Glynn R, Gragoudas E, Seddon J. Increased scleral rigidity and age-related macular degeneration. *Ophthalmology*. 1989;96:104–108.

30. Kotliar KE, Baumann M, Vilser W, Lanzl IM. Pulse wave velocity in retinal arteries of healthy volunteers. *Br J Ophthalmol*. 2011;95:675–679.

31. Pennesi ME, Neuringer M, Courtney RJ. Animal models of age related macular degeneration. *Mol Aspects Med*. 2012;33:487–509.

32. Francis PJ, Appukuttan B, Simmons E, et al. Rhesus monkeys and humans share common susceptibility genes for age-related macular disease. *Hum Mol Genet*. 2008;17:2673–2680.

33. Tachibana M, Ma H, Sparman ML, et al. X-chromosome inactivation in monkey embryos and pluripotent stem cells. *Dev Biol*. 2012; 371: 146–155.

34. McGill, T. J., Stoddard, J., Renner, L. M., Messaoudi, I., Bharti, K., Mitalipov, S., Neuringer, M. (2018). Allogeneic iPSC-Derived RPE Cell Graft Failure Following Transplantation Into the Subretinal Space in Nonhuman Primates. *Investigative ophthalmology & visual science*, *59*(3), 1374-1383.

35. Maminishkis A, et al. (2006) Confluent monolayers of cultured human fetal retinal pigment epithelium exhibit morphology and physiology of native tissue. Invest Ophthalmol Vis Sci 47:3612–3624.

36. Mohan, R. R., Cabrera, A. P., Harrison, R. E., Gorham Jr, R. D., Johnson, L. V., Ghosh, K., & Morikis, D. (2016). Peptide redesign for inhibition of the complement system: Targeting age-related macular degeneration. *Molecular vision*, *22*, 1280.

37. Huveneers S, Daemen MJ, Hordijk PL. Between Rho(k) and a hard place: the relation between vessel wall stiffness endothelial contractility, and cardiovascular disease. Circ Res. 2015;116:895–908.

38. Essler M, Amano M, Kruse HJ, Kaibuchi K, Weber PC, Aepfelbacher M. Thrombin inactivates myosin light chain phosphatase via Rho and its target Rho kinase in human endothelial cells. J Biol Chem. 1998;273:21867–21874.

39. Zeng L, Xu H, Chew TL, Eng E, Sadeghi MM, Adler S, Kanwar YS, Danesh FR. HMG CoA reductase inhibition modulates VEGF-induced endothelial cell hyperpermeability by preventing RhoA activation and myosin regulatory light chain phosphorylation. FASEB J. 2005;19:1845–1847.

40. Vouret-Craviari, V., Boquet, P., Pouysségur, J., & Van Obberghen-Schilling, E. (1998). Regulation of the actin cytoskeleton by thrombin in human endothelial cells: role of Rho proteins in endothelial barrier function. *Molecular biology of the cell*, *9*(9), 2639-2653.

41. Fels, J., Jeggle, P., Kusche-Vihrog, K., & Oberleithner, H. (2012). Cortical actin nanodynamics determines nitric oxide release in vascular endothelium. *PLoS One*, *7*(7), e41520.

42. Chrzanowska-Wodnicka M, Burridge K. Rho-stimulated contractility drives the formation of stress fibers and focal adhesions. J Cell Biol. 1996;133:1403–1415.

43. Zeng, S., Whitmore, S. S., Sohn, E. H., Riker, M. J., Wiley, L. A., Scheetz, T. E., Mullins, R. F. (2016). Molecular response of chorioretinal endothelial cells to complement injury: implications for macular degeneration. *The Journal of pathology*, *238*(3), 446-456.

44. Ambati, J., Anand, A., Fernandez, S., Sakurai, E., Lynn, B.C., Kuziel, W.A., Rollins, B.J., Ambati, B.K., 2003. An animal model of age-related macular degeneration in senescent Ccl-2- or Ccr-2-deficient mice. Nat. Med. 9 (11), 1390–1397.

45. Combadiere, C., Sennlaub, F., at al. (2007). CX3CR1-dependent subretinal microglia cell accumulation is associated with cardinal features of age-related macular degeneration. J. Clin. Investig. 117 (10), 2920–2928.

46. Ross, R.J., Zhou, M., Shen, D., Fariss, R.N., Ding, X., Bojanowski, C.M., Tuo, J., Chan, C.C., 2008. Immunological protein expression profile in Ccl2/Cx3cr1 deficient mice with lesions similar to age-related macular degeneration. Exp. Eye Res. 86 (4), 675–683

47. Sechi, A. S., & Wehland, J. (2000). The actin cytoskeleton and plasma membrane connection: PtdIns (4, 5) P (2) influences cytoskeletal protein activity at the plasma membrane. *Journal of cell science*, *113*(21), 3685-3695.

48. Weed, S. A., & Parsons, J. T. (2001). Cortactin: coupling membrane dynamics to cortical actin assembly. *Oncogene*, *20*(44), 6418.

49. Goswami, D., Gowrishankar, K., Bilgrami, S., Ghosh, S., Raghupathy, R., Chadda, R. & Mayor, S. (2008). Nanoclusters of GPI-anchored proteins are formed by cortical actin-driven activity. *Cell*, *135*(6), 1085-1097.

50. van Nieuw Amerongen, G. P., Beckers, C. M. L., Achekar, I. D., Zeeman, S., Musters, R. J. P., & Van Hinsbergh, V. W. M. (2007). Involvement of Rho kinase in endothelial barrier maintenance. *Arteriosclerosis, thrombosis, and vascular biology*, *27*(11), 2332-2339.

51. Rolli-Derkinderen, M., Toumaniantz, G., Pacaud, P., & Loirand, G. (2010). RhoA phosphorylation induces Rac1 release from guanine dissociation inhibitor α and stimulation of vascular smooth muscle cell migration. *Molecular and cellular biology*, *30*(20), 4786-4796.

52. Prasain, N., & Stevens, T. (2009). The actin cytoskeleton in endothelial cell phenotypes. *Microvascular research*, *77*(1), 53-63.

53. Koo E, Neuringer M, SanGiovanni JP. Macular xanthophylls lipoprotein-related genes, and age-related macular degeneration. Am J Clin Nutr. 2014;(100 suppl 1):336S–346S.

54. Barker FM II, Snodderly DM, Johnson EJ, et al. Nutritional manipulation of primate retinas, V: effects of lutein, zeaxanthin, and n-3 fatty acids on retinal sensitivity to blue-lightinduced damage. Invest Ophthalmol Vis Sci. 2011;52:3934–3942.

55. Burridge, K., & Wennerberg, K. (2004). Rho and Rac take center stage. *Cell*, *116*(2), 167-179.

CHAPTER 4

ROLE OF RHO-MEDIATED LYSOSOME TRAFFICKING IN COMPLEMENT-INDUCED INJURY ASSOCIATED WITH DRY AMD

Preface

Studies performed in Chapter 3 demonstrated that aging increases choroidal EC stiffening that contributes to increased susceptibility to complement mediated injury. These findings are the first to identify a possible mechanism by which aging may contribute to choroidal atrophy associated with dry AMD. However, they do not yet explain precisely how age-associated cell stiffness increases EC sensitivity to complement injury. Thus, this chapter aims to understand how age-associated cell stiffness increases EC sensitivity to complement injury by examining the role of rho-mediated lysosome trafficking for the repair of damaged cell membranes.

Figures 4.1-4.3 were obtained in collaboration with Prof. Hyle Park, University of California, Riverside.

Introduction

Dry AMD is characterized by choroidal atrophy, observed as CC dropout and choroidal thinning.[1-6] Importantly, the severity of CC dropout increases with the density of drusen deposits.[2] Despite these important findings, the mechanisms underlying choroidal atrophy still remain poorly understood. Abundant evidence implicates complement activation in the pathogenesis dry AMD.[7-9] Further, studies have shown that the terminal factor of the compliment activation pathway, membrane attack complex (MAC; C5b-9n), specifically localizes on the CC.[3] Interestingly, MAC is found on the CC of both young and old eyes yet only old eyes develop dry AMD. Since assembly of MAC on the cell membrane can lead to pore formation,[10] it is possible that this can lead to cell lysis and contribute to choroidal atrophy associated with dry AMD. Using an in vitro pre-clinical model of dry AMD, studies performed in Chapter 3 demonstrated that (a) aging increases in susceptibility to complement-induced injury, (b) aging increases choroidal EC stiffness, and (c) decreasing cell stiffness prevents complement-induced injury. These findings offer new mechanistic insight into choroidal EC loss and CC degeneration associated with dry AMD. However, they do not yet explain precisely how cell stiffness increases EC susceptibility to complement injury.

There are several mechanisms in place to eliminate MAC from the cell membrane and restore membrane integrity.[11-13] Exocytosis by lysosomes is known to play an important role in membrane resealing after injury.[14-19] Specifically, lysosomes move bidirectionally along microtubules (propelled by dynein and kinesins), and eventually

fuse and integrate with the cell membane.[20,21] Since vesicle fusion kinetics is strongly dependent on membrane bending properties,[22] it is possible that age-induced choroidal EC stiffening, which results, at least in part, from cytoskeletal tension, alters the efficiency of lysosomal exocytosis. Indeed, many studies implicate the actin cytoskeleton as a key player in regulating exocytosis. Specifically, studies have shown that the cytoskeleton plays various roles during exocytosis. For instance, the cytoskeleton has been shown to create a physical/functional barrier whose removal is necessary during exocytosis to allow secretory vesicles to access the cell membrane.[24-26] Conversely, others have shown that the cytoskeleton plays a more active role by directing lysosomal vesicles to the membrane fusion sites and providing the driving force to complete fusion.[27-29] Thus, it is plausible that EC stiffening, which is mediated by the tension in the cytoskeleton, can affect lysosomal exocytosis. However, whether lysosome trafficking is impaired in stiffer choroidal ECs and whether it contributes complement injury associated with dry AMD remains unknown. Together, findings from our and others studies' have led us to hypothesize that the greater degree of complement-mediated injury in stiffer OD ECs results from impaired lysosomal trafficking.

Material and Methods

Cell Culture. Rhesus monkey ECs from the macular region of the choroid isolated from young normal (6 years old; YN) and old monkeys with severe drusen (19 years old; OD) were grown on 0.5% gelatin coated dishes in MCDB 131 basal medium (Corning) supplemented with 10% fetal bovine serum (FBS; HyClone GE), 10 mM L-glutamine (Life Technologies), 10 ng/mL epidermal growth factor (Sigma), 4 ng/mL basic fibroblast growth factor (Life Technologies), 1 mg/mL hydrocortisone (Sigma), and 1x antibiotic/antimycotic supplement (Life Technologies). EC culture was maintained at 37^{o}C in a humidified atmosphere with 5% CO_2, with cells being seeded at 10,000 cells/cm-sq and passaged every two days.

GFP-LAMP1 Transfection. YN and OD ECs were plated at 6k cells/cm^2 in complete medium for six hours to ensure maximal spreading. ECs were then transfected with Cell Light Lysosomes-GFP-LAMP1 (Lysosome Associated Membrane Protein 1, a key lysosomal protein found of the lysosome membrane) BacMam 2.0 transfection reagent as per manufacturer's protocol (100 ppm; ThermoFisher). GFP-LAMP1 labeled ECs remained in transfection reagent-containing complete culture medium for 72h, to ensure maximum GFP-LAMP1 transfection.

Complement Activation. To examine the effects of complement activation on rhesus monkey choroidal ECs, cells were treated with 5% normal human serum (NHS;

Complement Technology, Inc., Tyler, TX, USA) in veronal buffered saline (VBS; NaCl [145 mM], sodium barbital [1.8 mM], barbituric acid [3 mM], CaCl2 [50 uM], and MgCl2 [25uM], adjusted to pH 7.4) for 30 minutes at 37^{o}C to promote complement protein deposition on the cell surface.

To inhibit the effects of age-associated cell stiffening, cells were co-treated with Y27632, a pharmacological inhibitor of Rho/ Rho-associated kinase (ROCK; 100uM) in 5% NHS for 3 hours at 37^{o}C.

Imaging of Lysosome Trafficking. YN and OD ECs were plated at 40k cells/cm^2 onto gluteraldehyde-crosslinked gelatin coated glass-bottom dishes in phenol-red free starvation medium (MCDB 131 basal medium supplemented with 2.5% FBS and 1x antibiotic-antimycotic). Cells were in culture for six hours to ensure maximal spreading prior to time-lapse imaging with Keyence BZ-710 epifluorescent microscope. Images were captured at 15-second intervals for duration of 10 minutes.

Analysis of Lysosome Trafficking. Images were aligned using Matlab to ensure proper alignment of field of view. Images were then converted to gray scale and background was subtracted from each frame leaving only GFP-labeled lysosomes in field of view. Using the image processing toolbox in Matlab, images were binarized based on thresholding to select particles that could easily be identified for analysis. Coordinates of particle

centroids were obtained and analyzed frame by frame to obtain particle trajectories. Coordinates were then traced and lysosome velocity was determined.

Results

Decreased rate of lysosome trafficking correlates with aging

To determine the effect of aging on lysosome trafficking in choroidal ECs, we first measured the baseline lysosome trafficking rates in YN and stiffer OD ECs. Time-lapse images revealed that YN ECs exhibit higher lysosome trafficking rates compared to stiffer OD ECs (Fig 4.1).

Complement activation impairs lysosome trafficking in choroidal ECs

To determine whether lysosomal trafficking contributes to increased susceptibility to complement injury associated with dry AMD, lysosome trafficking rates in complement activated YN and OD ECs were observed. Time-lapse imaging revealed that complement activation significantly decreases lysosomal trafficking in YN and OD ECs (Fig 4.2).

Increased cell stiffening inhibits lysosome trafficking

Studies have shown that actin cytoskeleton has many roles in lysosomal exocytosis. Thus, to determine whether my previous findings showing age-induced EC stiffening can contribute to the increased susceptibility to complement injury, we pharmacologically inhibited Rho/ROCK. Time-lapse images confirmed that pharmacological inhibition of Rho/ROCK causes a significant increase of lysosomal trafficking of choroidal OD ECs (Fig 4.3).

Discussion

Previous studies (Chapters 2 and 3) revealed that aging increases the susceptibility to complement injury of choroidal ECs. To understand how stiffer ECs from aging eyes become more susceptible to complement injury, I explored the potential role of lysosomal exocytosis. Time-lapse images of GFP-LAMP1-transfetcted ECs revealed that aged choroidal ECs have a significantly slower rate of lysosome trafficking when compared with their younger counterparts. Since my previous studies show that complement deposition occurs at the same rate in young (YN) and old (OD) choroidal ECs, this observation of slower baseline trafficking rates may explain why OD ECs undergo a greater degree of complement injury. Interestingly, we further show that complement activation severely decreases lysosome trafficking in choroidal ECs. Thus, it is likely that the already slow baseline trafficking rates in OD ECs simply cannot meet membrane resealing rate required for the maintenance of the membrane integrity and become extensively damaged by the simultaneous and compounding effect of ongoing complement injury.

Since studies in Chapter 3 revealed that the actin cytoskeleton contributes to EC stiffening and the cytoskeleton has been shown to contribute in various ways to lysosomal exocytosis, here the role of cytoskeleton in lysosomal trafficking was explored. Our time-lapse images revealed that decreasing cell stiffness with a pharmacological Rho/ROCK inhibitor causes an increase in baseline lysosomal trafficking in OD ECs. However, whether this increase in baseline lysosomal trafficking in aged choroidal ECs

can indeed contribute to membrane repair and thus prevent the extensive damage of complement deposition remains to be carefully examined in the future.

Chapter 4 shows, for the first time, that there is a decrease in the velocity of Rho-mediated lysosome trafficking in OD ECs. Further, this decrease in velocity of lysosome trafficking is associated with aging. Remarkably, inhibiting EC stiffening reverses the effect of reduced lysosome trafficking. Importantly, these studies are the first to show that (i) aging decreases lysosome trafficking in choroidal ECs, (ii) complement injury contributes to impaired lysosome trafficking, and (iii) modulation of EC stiffening can reverse impaired rho-mediated lysosome trafficking of stiffer ECs. Together, these findings identify a crucial role of impaired Rho-mediated lysosome trafficking and its contributions to complement injury and further implicate EC stiffness, as a novel therapeutic target for choroidal atrophy associated with dry AMD.

Conclusion

Studies performed using an in vitro pre-clinical model of dry AMD revealed that aging lead to choroidal EC stiffening that correlates with an increase in susceptibility to complement injury. To determine the role of EC stiffening in increased susceptibility to complement injury, the role of lysosomal was explored. Our studies revealed that age-associated cell stiffening leads to significant decrease in lysosome trafficking in choroidal ECs. Further, by activating the complement system we revealed that lysosomal trafficking is inhibited in the stiffer OD ECs. Finally, we show that pharmacological modulation of Rho/ROCK activity reverses the effects of EC stiffness on lysosome trafficking. Collectively, these findings reveal a novel and crucial role of rho-mediated lysosomal trafficking in membrane resealing and its contribution to complement-mediated choroidal atrophy associated with dry AMD.

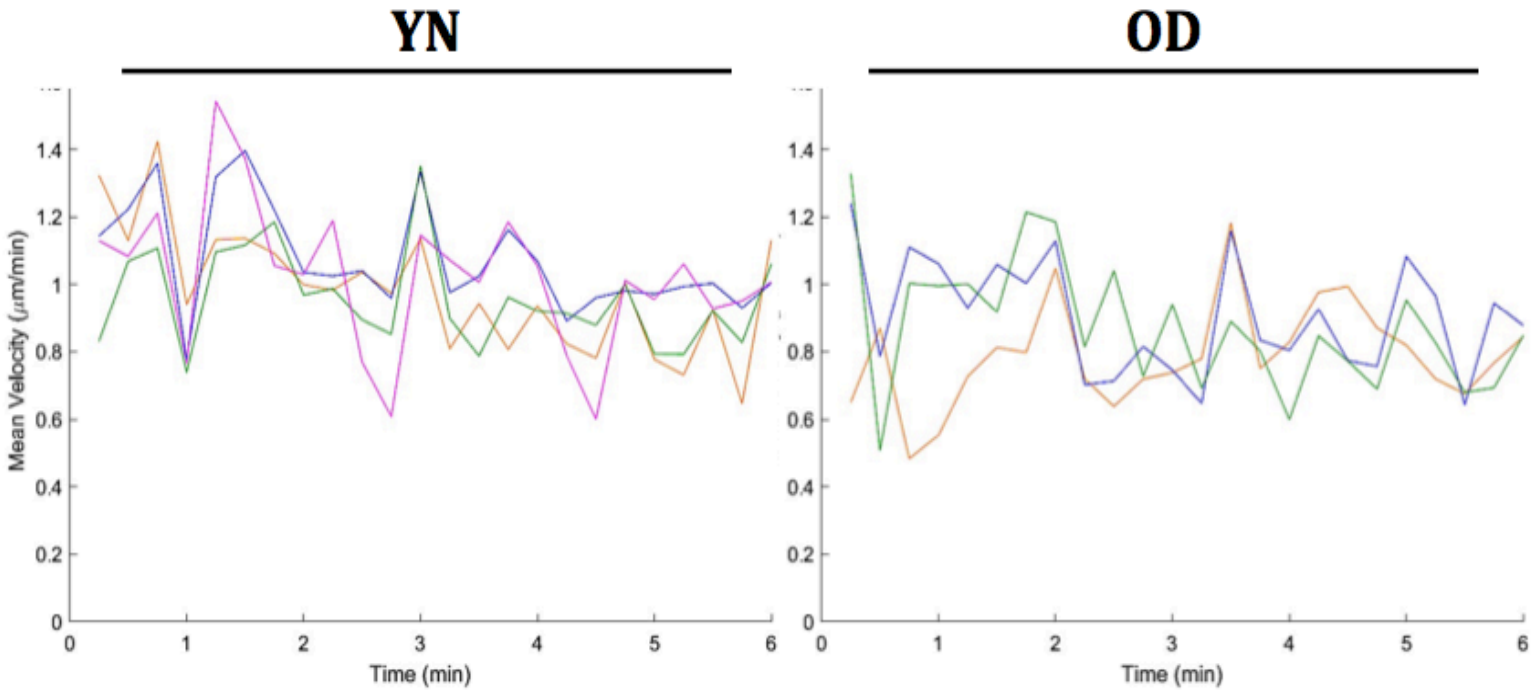
YN
OD
Mean Velocity (μm/min)
Time (min)
Time (min)
0
0.2
0.4
0.6
0.8
1
1.2
1.4
0
1
2
3
4
5
6

Fig. 4.1. Aging causes decreased lysosome trafficking rates. Mean velocity vs. time plots reveal that OD cells on average have decreased velocity compared to their YN counterparts. Each line graph indicates the average velocities of lysosomes within one cell.

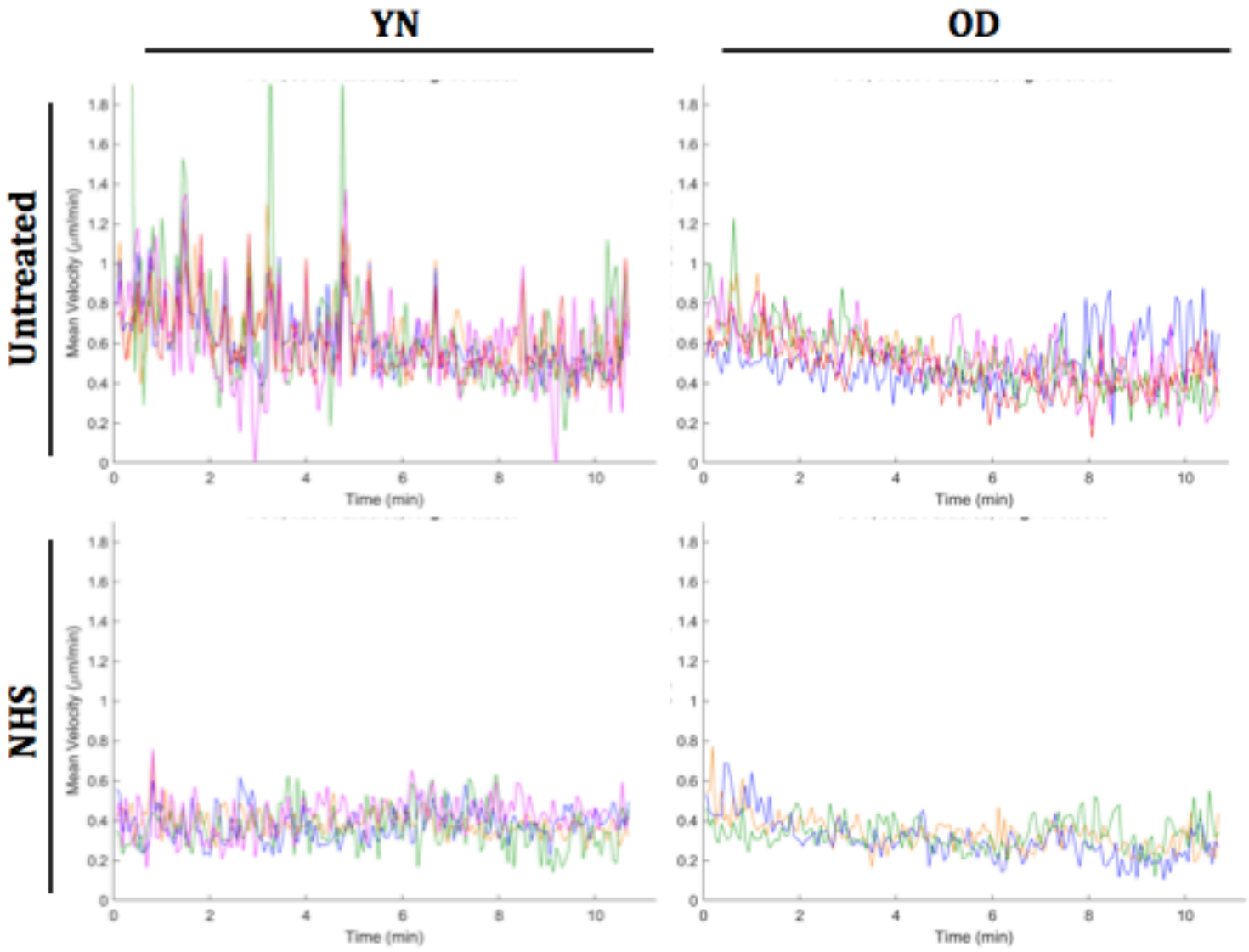
YN
OD
Untreated
NHS
Mean Velocity (μm/min)
Time (min)

Fig. 4.2. Complement injury decreases lysosome trafficking rate. Mean velocity vs. time plots reveal that treatment with complement-competent serum (5% NHS; 30 min) significantly decreases lysosome trafficking rates. Further, the trafficking rates in OD cells on average are slower than their YN counterparts. Each line graph indicates the average velocities of lysosomes within one cell.

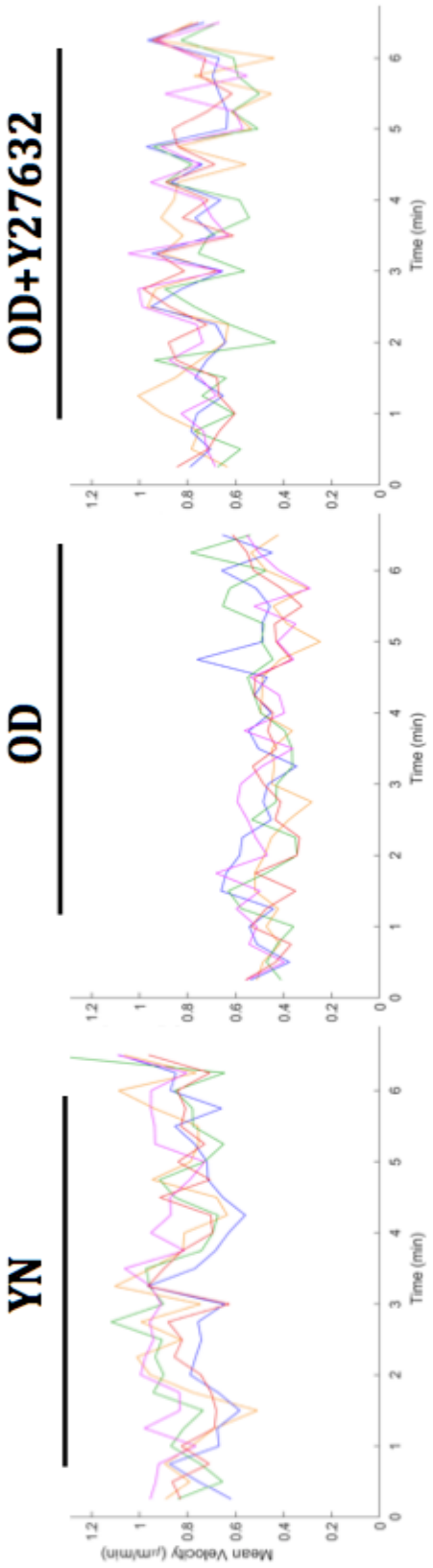
YN
OD
OD+Y27632
Mean Velocity (μm/min)
Time (min)
0
0.2
0.4
0.6
0.8
1
1.2
0
1
2
3
4
5
6

Fig. 4.3. Increased EC stiffening correlates with decreased lysosome trafficking rate. Mean velocity vs. time plots reveal that treatment with pharmacological Rho/ROCK inhibitor (Y23632; 100uM, 30 min) significantly increases lysosome trafficking rates of stiffer ECs. Each line graph indicates the average velocities of lysosomes within one cell.

References

1. Whitmore SS, Sohn EH, Chirco KR, et al. Complement activation and choriocapillaris loss in early AMD: implications for pathophysiology and therapy. *Prog Retin Eye Res*. 2015;45: 1–29.

2. Mullins RF, Johnson MN, Faidley EA, Skeie JM, Huang J. Choriocapillaris vascular dropout related to density of drusen in human eyes with early age-related macular degeneration. *Invest Ophthalmol Vis Sci* 2011;52:1606-1612.

3. Mullins RF, Schoo DP, Sohn EH, et al. The membrane attack complex in aging human choriocapillaris: relationship to macular degeneration and choroidal thinning. *Am J Pathol* 2014;184:3142-3153.

4. Bhutto, I., & Lutty, G. (2012). Understanding age-related macular degeneration (AMD): relationships between the photoreceptor/retinal pigment epithelium/Bruch's membrane/choriocapillaris complex. *Molecular aspects of medicine*, *33*(4), 295-317.

5. McLeod, D. S., Taomoto, M., Otsuji, T., Green, W. R., Sunness, J. S., & Lutty, G. A. (2002). Quantifying changes in RPE and choroidal vasculature in eyes with age-related macular degeneration. *Investigative ophthalmology & visual science*, *43*(6), 1986-1993.

6. "Choroidal thickness in healthy Chinese subjects." *Investigative ophthalmology & visual science* 52, no. 13 (2011): 9555-9560.

7. Parmeggiani F, Romano MR, Costagliola C, et al. Mechanism of inflammation in age-related macular degeneration. Mediators Inflamm. 2012;2012:546786

8. Anderson DH, Mullins RF, Hageman GS, Johnson LV. A role for local inflammation in the formation of drusen in the aging eye. Am J Ophthalmol. 2002;134:411–431.

9. Mullins RF, Schoo DP, Sohn EH, et al. The membrane attack complex in aging human choriocapillaris: relationship to macular degeneration

10. Bayly-Jones, C., Bubeck, D., & Dunstone, M. A. (2017). The mystery behind membrane insertion: a review of the complement membrane attack complex. *Phil. Trans. R. Soc. B*, *372*(1726), 20160221.

11. Rus, H. G., Niculescu, F. I., & Shin, M. L. (2001). Role of the C5b‐9 complement complex in cell cycle and apoptosis. *Immunological reviews*, *180*(1), 49-55.

12. Sims, P. J., Faioni, E. M., Wiedmer, T., & Shattil, S. J. (1988). Complement proteins C5b-9 cause release of membrane vesicles from the platelet surface that are enriched in the membrane receptor for coagulation factor Va and express prothrombinase activity. *Journal of Biological Chemistry*, *263*(34), 18205-18212.

13. Nicholson-Weller, A., & Halperin, J. A. (1993). Membrane signaling by complement C5b-9, the membrane attack complex. *Immunologic research*, *12*(3), 244-257.

14. Reddy, A., Caler, E. V., & Andrews, N. W. (2001). Plasma membrane repair is mediated by Ca2+-regulated exocytosis of lysosomes. *Cell*, *106*(2), 157-169.

15. McNeil, P. L., & Kirchhausen, T. (2005). An emergency response team for membrane repair. *Nature Reviews Molecular Cell Biology*, *6*(6), 499.

16. Togo, T., Alderton, J. M., Bi, G. Q., & Steinhardt, R. A. The mechanism of facilitated cell membrane resealing. *Journal of Cell Science*. 1999; *112*(5), 719-731.

17. McNeil, P. L., & Kirchhausen, T. An emergency response team for membrane repair. *Nature Reviews Molecular Cell Biology*. 2005;*6*(6), 499-505.

18. Gerasimenko, J. V., Gerasimenko, O. V., & Petersen, O. H. (2001). Membrane repair: Ca2+-elicited lysosomal exocytosis. *Current Biology*, *11*(23), R971-R974.

19. Idone, V., Tam, C., & Andrews, N. W. (2008). Two-way traffic on the road to plasma membrane repair. *Trends in cell biology*, *18*(11), 552-559.

20. Lanzetti, L. Actin in membrane trafficking. *Current opinion in cell biology*. 2007; *19*(4), 453-458.

21. Dai, J., & Sheetz, M. P. Regulation of endocytosis, exocytosis, and shape by membrane tension. In *Cold Spring Harbor symposia on quantitative biology*. 1995; 60, 567-571. Cold Spring Harbor Laboratory Press.

22. Zanin, M. P., Phillips, L., Mackenzie, K. D., & Keating, D. J. Aging differentially affects multiple aspects of vesicle fusion kinetics. *PloS one*. 2011;*6*(11), e27820.

23. Porat-Shliom, N., Milberg, O., Masedunskas, A., & Weigert, R. (2013). Multiple roles for the actin cytoskeleton during regulated exocytosis. *Cellular and Molecular Life Sciences*, *70*(12), 2099-2121.

24. Gutierrez LM (2012) New insights into the role of the cortical cytoskeleton in exocytosis from neuroendocrine cells. Int Rev Cell Mol Biol 295:109–137

25. Malacombe M, Bader MF, Gasman S (2006) Exocytosis in neuroendocrine cells: new tasks for actin. Biochim Biophys Acta 1763(11):1175–1183

26. Eitzen G (2003) Actin remodeling to facilitate membrane fusion. Biochim Biophys Acta 1641(2–3):175–181

27. Nightingale TD, Cutler DF, Cramer LP (2012) Actin coats and rings promote regulated exocytosis. Trends Cell Biol (6):329–337

28. Sokac AM, Bement WM (2006) Kiss-and-coat and compartment mixing: coupling exocytosis to signal generation and local actin assembly. Mol Biol Cell 17(4):1495–1502

29. Masedunskas A, Porat-Shliom N, Weigert R (2012) Regulated exocytosis: novel insights from intravital microscopy. Traffic 13(5):627–634

CHAPTER 5

CONCLUSION

The goal of this research was to understand the role of age-related EC stiffening in choroidal atrophy associated with Dry AMD and to identify new therapeutic targets for the slowdown or prevention of AMD progression. Studies in Chapter 2 show that senescence, a hallmark of aging, increases the susceptibility of choroidal ECs to complement injury and subsequent EC lysis. This increase in susceptibility to complement injury correlates with increased rho-mediated EC stiffness. Importantly, pharmacological inhibition of Rho/ROCK activity reduced EC stiffness and prevented the effect of EC lysis. These findings were the first to implicate Rho-mediated choroidal EC stiffening as a specific age/senescence-related factor in choroidal atrophy associated with dry AMD. However, the phenomenon observed here needed to be validated in an appropriate animal model of dry AMD.

In Chapter 3, we establish a unique in vitro model derived from a non-human primate pre-clinical model of dry AMD. Using this model, we show for the first time that aging causes choroidal EC stiffening. This age-associated EC stiffening correlates with increased susceptibility to complement-induced injury. Remarkably, by decreasing cell stiffness alone via pharmacological inhibition of Rho, these complement-induced effects on stiffer ECs can be prevented. Importantly, we show the protective effect of rho-mediated EC contractility in preventing complement injury.

Finally, Chapter 4 aims to explain a possible mechanism by which age-induced cell stiffness increases EC susceptibility to complement injury by exploring the role of lysosome trafficking for the repair of MAC-induced cell membrane injury. Collectively, these findings reveal a novel and crucial role of Rho-mediated cytoskeletal EC stiffening in choroidal atrophy associated with dry AMD.

Working Model

The findings from my studies indicate a key and crucial role of age-induced cell stiffening in choroidal atrophy associated with dry AMD (Schematic 5.1). Specifically, I show that aging leads to increased susceptibility to complement injury. This increase in susceptibility to complement injury correlates with EC stiffening. Counterintuitively, Rho activity, which is associated with cell tension and stiffness, decreases in stiffer choroidal ECs, which correlates with a reduction in actin stress fiber density. Instead, the OD ECs exhibit a robust cortical actin arrangement that contributes to its higher stiffness and greater susceptibility to complement injury. Notably, the stiffer choroidal ECs fail to retract during complement activation while their younger counterparts, which have a higher density of Rho-associated actin stress fibers, undergo significant retraction in response to membrane-damaging complement activation. These findings indicate that Rho-associated stress fibers impart cells with the ability to retract in response to membrane MAC deposition, thus serving as a protective mechanism against complement injury.

Future Directions

Though these findings offer new mechanistic insight into choroidal EC atrophy and choroidal degeneration associated with dry AMD, they do not yet explain precisely how age-induced cell stiffness increases EC sensitivity to complement injury. AMD is a multifactorial disease that is also regulated by dietary, genetic, biochemical, and molecular factors.[1-4] Thus, to begin to fully understand AMD pathogenesis, different aspects of this disease will need to be explored.

Complement activation is a hallmark of AMD with C5b-9 deposition localizing on the CC.[5-7] Since host ECs are equipped with an array of protective mechanisms to survive complement attack,[8-10] the expression levels of various surface-bound complement regulators should be assessed. Further, since cytoskeletal organization has been shown to play a key role in the dynamics and spatial assembly of proteins on the cell membrane,[11-13] it is possible that cytoskeleton-mediated EC stiffening alters the activity of transmembrane complement regulators, especially CD46 that is physically anchored to the cytoskeleton.[14] This is another aspect that should be further examined in aging and AMD CC and choroid.

Additionally, the role of endothelial glycocalyx (GCX), a complex network of various proteoglycans and glycoproteins that is physically anchored to the cell membrane, in choroidal complement injury should be carefully investigated.[15-17] This is because heparan sulfate proteoglycan (HSPG), a major GCX component, binds factor H (CFH), a crucial soluble-phase complement regulator that blocks MAC formation.[18]

Indeed, recent studies have implicated age-induced GCX shedding in various pathologies associated with complement activation.[19,20] Thus, it is plausible that the loss of HSPG from CC endothelial membrane reduces surface binding of CFH in aging eyes, thereby increasing the susceptibility for membrane MAC deposition and, ultimately, lysis. Additionally, since GCX is anchored to the membrane via transmembrane proteoglycans,[21] cell stiffness could play a role in GCX spatial organization and/or integrity.

Studies in chapter 3 show the role of cortical actin in cell stiffening. Further, depolymerization of the robust cortical actin ring of stiffer OD ECs prevented complement associated injury. Since cortical actin is physically anchored to the cell membrane by various adaptor proteins such as talin, tensin, filamin and α–actinin,[22] which play a key role in stabilizing the cytoskeleton, these proteins may contribute to the stiffening-dependent EC susceptibility to complement injury. One potential candidate is α–actinin, whose expression is known to correlate directly with the density of cortical actin ring.[23] Since cortical actin creates a physical scaffold underlying the cell membrane,[24-26] it is possible that α-actinin-mediated cortical actin stabilization may prevent the disassembly of cortical actin, which has been shown to be necessary for lysosome-mediated membrane repair.

Further, since cortical actin polymerization is regulated by Rac, the activity levels of this GTPase should be analyzed. If stiffer cells are indeed found to have significantly higher Rac, the GDP-GTP exchange factors (GEFs) and GTPase-activating proteins (GAPs), which regulate Rho and Rac can be investigated. GEFs and GAPs regulate the

nucleotide (GDP or GTP) bound to Rho or Rac, thus determining the activity of Rho and Rac and the interactions of these with their downstream targets.[27,28] Thus, it is possible that if Rac levels are significantly elevated, GEFs and/or GAPs may be dysregulated. Further, studies in chapter 3 revealed that stiffer ECs isolated from AMD eyes have lower Rho activity levels compared to their young counterparts. Since studies have shown that Rac and Rho are antagonistic,[29,30] with the two proteins suppressing each other's activities, Rac and Rho the interplay in choroidal ECs should be examined.

Studies reported in this dissertation demonstrated how age-associated cell stiffening leads to increased complement-mediated choroidal EC atrophy. Since the choroid is essential for maintenance of retinal pigment epithelial (RPE) homeostasis,[31] the crosstalk between these two cell types should be explored. Co-culture studies may provide insight to whether choroidal atrophy leads to RPE degeneration, or visa versa. Additionally, very little is known regarding whether aging ECs secrete factors that can lead to RPE dysfunction.

Successful completion of these follow up studies has the potential to not only implicate Rho-mediated choroidal EC stiffening and mechanotransduction as new therapeutic targets for dry AMD but also identify other previously unknown mechanisms by which aging contributes to choroidal loss and dry AMD progression.

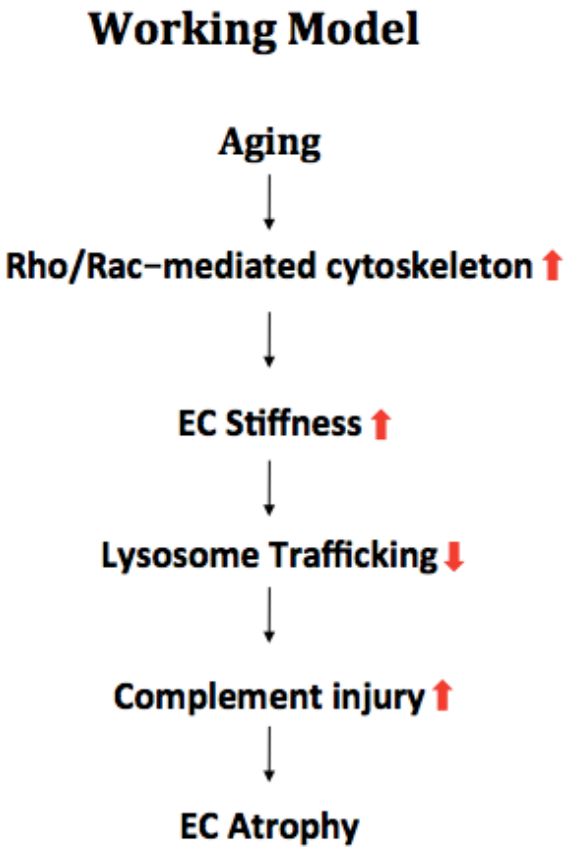

Schematic 5.1: Working model of endothelial mechanotransduction mediating the effect of endothelial cell (EC) stiffness on EC atrophy.

References

1. Pennesi ME, Neuringer M, Courtney RJ. Animal models of age related macular degeneration. *Mol Aspects Med*. 2012;33:487–509.

2. Francis PJ, Appukuttan B, Simmons E, et al. Rhesus monkeys and humans share common susceptibility genes for age-related macular disease. *Hum Mol Genet*. 2008;17:2673–2680.

3. Koo E, Neuringer M, SanGiovanni JP. Macular xanthophylls lipoprotein-related genes, and age-related macular degeneration. Am J Clin Nutr. 2014;(100 suppl 1):336S–346S.

4. Barker FM II, Snodderly DM, Johnson EJ, et al. Nutritional manipulation of primate retinas, V: effects of lutein, zeaxanthin, and n-3 fatty acids on retinal sensitivity to blue-lightinduced damage. Invest Ophthalmol Vis Sci. 2011;52:3934–3942.

5. Anderson DH, Mullins RF, Hageman GS, Johnson LV. A role for local inflammation in the formation of drusen in the aging eye. *Am J Ophthalmol* 2002;134:411-431.

6. Parmeggiani F, Romano MR, Costagliola C, et al. Mechanism of inflammation in age-related macular degeneration. *Mediators Inflamm*. 2012;2012:546786.

7. Mullins RF, Schoo DP, Sohn EH, et al. The membrane attack complex in aging human choriocapillaris: relationship to macular degeneration and choroidal thinning. *Am J Pathol* 2014;184:3142-3153.

8. Charreau, Béatrice, Armelle Cassard, Laurent Tesson, B. Mauff Le, Jean-Marc Navenot, Dominique Blanchard, Douglas Lublin, Jean-Paul Soulillou, and Ignacio Anegon. "Protection of rat endothelial cells from primate complement-mediated lysis by expression of human CD59 and/or decay-accelerating factor." *Transplantation* 58, no. 11 (1994): 1222-1229.

9. Brooimans, R. A., van Wieringen, P. A., van Es, L. A., & Daha, M. R. (1992). Relative roles of decay‐accelerating factor, membrane cofactor protein, and CD59 in the protection of human endothelial cells against complement‐mediated lysis. *European journal of immunology*, *22*(12), 3135-3140.

10. Heckl-Östreicher, B., Wosnik, A., & Kirschfink, M. (1996). Protection of porcine endothelial cells from complement-mediated cytotoxicity by the human complement regulators CD59, C1 inhibitor, and soluble complement receptor type 1: analysis in a pig-to-human in vitro model relevant to hyperacute xenograft rejection. *Transplantation*, *62*(11), 1693-1696.

11. Sechi, A. S., & Wehland, J. (2000). The actin cytoskeleton and plasma membrane connection: PtdIns (4, 5) P (2) influences cytoskeletal protein activity at the plasma membrane. *Journal of cell science*, *113*(21), 3685-3695.

12. Weed, S. A., & Parsons, J. T. (2001). Cortactin: coupling membrane dynamics to cortical actin assembly. *Oncogene*, *20*(44), 6418.

13. Goswami, D., Gowrishankar, K., Bilgrami, S., Ghosh, S., Raghupathy, R., Chadda, R. & Mayor, S. (2008). Nanoclusters of GPI-anchored proteins are formed by cortical actin-driven activity. *Cell*, *135*(6), 1085-1097.

14. Liszewski, M. Kathryn, Marilyn Leung, Wenying Cui, V. Bala Subramanian, John Parkinson, Paul N. Barlow, Marianne Manchester, and John P. Atkinson. "Dissecting sites important for complement regulatory activity in membrane cofactor protein (MCP; CD46)." *Journal of Biological Chemistry* 275, no. 48 (2000): 37692-37701.

15. Reitsma, S., Slaaf, D. W., Vink, H., Van Zandvoort, M. A., & oude Egbrink, M. G. The endothelial glycocalyx: composition, functions, and visualization. *Pflügers Archiv-European Journal of Physiology*. 2007; *454*(3), 345-359

16. Weinbaum, S., Zhang, X., Han, Y., Vink, H., & Cowin, S. C. Mechanotransduction and flow across the endothelial glycocalyx. *Proceedings of the National Academy of Sciences*; 2003;*100*(13), 7988-7995.

17. Weinbaum, S., Tarbell, J. M., & Damiano, E. R. The structure and function of the endothelial glycocalyx layer. *Annu. Rev. Biomed. Eng.2007; 9*, 121-167

18. Boels, M. G., Lee, D. H., van den Berg, B. M., Dane, M. J., van der Vlag, J., & Rabelink, T. J. The endothelial glycocalyx as a potential modifier of the hemolytic uremic syndrome. *European journal of internal medicine*. 2013; *24*(6), 503-509.

19. Ushiyama, A., Kataoka, H., & Iijima, T. Glycocalyx and its involvement in clinical pathophysiologies. *Journal of intensive care*; 2016, *4*(1), 59.

20. Keenan, T. D., Pickford, C. E., Holley, R. J., Clark, S. J., Lin, W., Dowsey, A. Bishop, P. N. Age-dependent changes in heparan sulfate in human Bruch's membrane: implications for age-related macular degenerationheparan sulfate in human Bruch's membrane. *Investigative ophthalmology & visual science*. 2014;*55*(8), 5370-5379.

21. Reitsma, S., Slaaf, D. W., Vink, H., Van Zandvoort, M. A., & Oude Egbrink, M. G. The endothelial glycocalyx: composition, functions, and visualization. *Pflügers Archiv-European Journal of Physiology*. 2007; *454*(3), 345-359.

22. Zaidel-Bar R, Geiger B. The switchable integrin adhesome. J Cell Sci 2010; 123:1385-8.

23. Gulino-Debrac, D. Mechanotransduction at the basis of endothelial barrier function. *Tissue barriers*. 2013; *1*(2), e24180.

24. Prasain, N., & Stevens, T. (2009). The actin cytoskeleton in endothelial cell phenotypes. *Microvascular research*, *77*(1), 53-63.

25. Köster, D. V., & Mayor, S. (2016). Cortical actin and the plasma membrane: inextricably intertwined. *Current opinion in cell biology*, *38*, 81-89.

26. Dudek, S.M., Garcia, J.G., 2001. Cytoskeletal regulation of pulmonary vascular permeability. J. Appl. Physiol. 91, 1487–1500

27. Machesky, L. M., & Hall, A. Rho: a connection between membrane receptor signalling and the cytoskeleton. *Trends in cell biology*. 1996; *6*(8), 304-310.

28. Burridge, K., & Wennerberg, K. Rho and Rac take center stage. *Cell*. 2004; *116*(2), 167-179.

29. Wildenberg, G. A., Dohn, M. R., Carnahan, R. H., Davis, M. A., Lobdell, N. A., Settleman, J., & Reynolds, A. B. (2006). p120-catenin and p190RhoGAP regulate cell-cell adhesion by coordinating antagonism between Rac and Rho. *Cell*, *127*(5), 1027-1039.

30. Rottner, K., Hall, A., & Small, J. V. (1999). Interplay between Rac and Rho in the control of substrate contact dynamics. *Current Biology*, *9*(12), 640-S1.

31. McLeod DS, Grebe R, Bhutto I, Merges C, Baba T, Lutty GA. Relationship between RPE and choriocapillaris in age-related macular degeneration. *Invest Ophthalmol Vis Sci*. 2009;50: 4982–4991.

APPENDIX

The text of the Appendix, in full, is a reprint of the material as it appears in:

Mohan RR, Cabrera AP, Harrison RES, Gorham RD Jr, Johnson LV, Ghosh K, Morikis D (2016) Peptide Redesign for Inhibition of the complement system: Targeting age-related macular degeneration, Molecular Vision 22:1280-1290.

The co-author contribution is as follows:

Rohith R Mohan, performed molecular-level research and computational modeling

Andrea Cabrera, performed cellular-level research

Ronald D Gorham Jr, designed peptides

Reed ES Harrison and Lincoln V Johnson, provided expertise with molecular-level and cellular-level assays, respectively.

Kaustabh Ghosh, directed and supervised cellular-level research

Dimitrios Morikis, designed peptides and directed and supervised molecular-level and computational modeling research.

PEPTIDE REDESIGN FOR INHIBITION OF THE COMPLEMENT SYSTEM: TARGETING AGE-RELATED MACULAR DEGENERATION

The complement system has been implicated as a major factor in the development and progression of age-related macular degeneration (AMD) [1,2]. Genome-wide associated studies (GWASs) have shown that single nucleotide polymorphisms (SNPs) in complement regulators Factor H and Factor I and complement proteins C3, C2, and Factor B are genetic risk factors for AMD [2-4]. An important GWAS finding is the Y402H SNP of Factor H, in which a tyrosine in position 402 is replaced by a histidine, resulting in the H402 risk variant [5-8]. It has been hypothesized that in the presence of the risk variant the complement system is under-regulated, thus contributing to inflammation when activated locally in association with drusen deposits at the RPE-Bruch's membrane interface [4,9]. Although drusen formation, a characteristic accumulation of protein and membranous debris in AMD tissues, may not be initiated by the complement system, an over-activated (under-regulated) complement system has been shown to contribute to drusen accumulation and exacerbation of AMD pathology [4,10]. Therefore, inhibition of the complement system is a promising strategy to slow the progression of AMD pathogenesis.

Currently, AMD is treated using monoclonal antibody–based therapies targeting vascular endothelial growth factor (VEGF), which stimulates choroidal neovascularization and induces vascular leakage [11]. However, such therapies are effective in the wet (neovascular) form of AMD, associated with vessel rupture and local

bleeding, but not in dry (atrophic) form of AMD that is characterized by the accumulation of drusen deposits and RPE atrophy. Compstatin family peptides were initially developed as inhibitors of complement-mediated autoimmune and inflammatory diseases, using phage display, functional, structural, computational studies (see review [12], and references therein). They became attractive low-molecular mass complement inhibitors for the treatment of AMD soon after the 2005 genomics studies implicated complement in AMD (see review [13], and references therein). Compstatin family peptides function by binding to complement protein C3 and sterically inhibiting the cleavage of C3 to C3a and C3b by convertase, thus impeding the formation of the chemotactic fragment C3a, the opsoninizing fragment C3b, and the propagation of the complement system through the common pathway that ultimately results in the assembly of C5b-9_n (also known as the membrane attack complex, MAC), a protein complex that forms pores on cell membranes.

One compstatin analog underwent clinical trials for AMD, and although the analog did not raise safety concerns, it did not show therapeutic efficacy. It is postulated that was likely the effects of molecular aggregation that resulted in the formation of gel-like structures [14,15] and an associated loss of functionality. This analog had been optimized over several years to have higher binding affinity than the original compstatin analogs by introducing a replacement of valine at position 4 with an aromatic amino acid, tyrosine [16,17] or tryptophan [18], and subsequently with methylated tryptophan [19]. The latter modification also increased the hydrophobic character of the peptide and presumably contributed to its aggregation in the aqueous ocular environment. Additional

compstatin analogs are currently in clinical trials for various complement-mediated diseases [20].

Recent studies have focused on increasing the solubility of compstatin peptides, using structure-based rational design, computational modeling, and optimization [21,22]. These studies have identified several analogs with N-terminal extensions that have inhibitory activities similar to those of the most potent analogs and have higher aqueous solubilities. Increased solubility was made possible by introducing two polar amino acid extensions at the N-terminus. In one analog, arginine contributed to solubility but was also shown by molecular dynamics simulations to form a salt bridge with a glutamic acid in C3, thus contributing to binding affinity as well [21,22]. In this study, we used a potent analog with arginine at position –1 and serine at position 0 [22], Peptide 1 here (or Peptide 9 in [22]), as a template to further increase solubility by incorporating two polar amino acid extensions and polyethylene glycol (PEG) blocks at the C-terminus. We demonstrate the high potency and high solubility of the new analog, using in vitro functional and solubility assays. We also demonstrate the efficacy of this peptide to inhibit complement activation in a human RPE cell–based assay that mimics AMD patho-physiology. We show that this PEGylated compstatin analog has significant promise as a therapeutic for AMD.

Materials and Methods

Peptide synthesis: Compstatin Peptides 1 and 2 (Table 1) were synthesized by WuXi AppTec (Shanghai, China). Peptide 2 has eight PEG blocks attached at the backbone of the C-terminal amino acid. Both peptides were cyclized by a disulfide bridge between the two cysteine amino acids, and they were acetylated at the N-terminus and amidated at the C-terminus. The peptides had >95% purity, as determined with high-performance liquid chromatography (HPLC) and mass spectrometry (MS).

Hemolytic assay*:* Rabbit erythrocytes (Complement Technology, Inc., Tyler, TX) were washed with PBS (1X; 3.8 mM monobasic NaH_2PO_4, 16.2 mM dibasic Na_2HPO_4, 150 mM NaCl, pH 7.4) and then resuspended in a veronal-buffered saline solution (VBS 1X; 72.8 mM NaCl, 0.9 mM sodium barbital, 1.5 mM barbituric acid, pH 7.4) containing 5 mM $MgCl_2$ and 10 mM EGTA (VBS-MgEGTA). Twofold serial dilutions of the compstatin analogs were performed in round-bottom 96-well plates and then further diluted in VBS-MgEGTA. Normal human serum (NHS; Complement Technology, Inc.) diluted in VBS-MgEGTA was added to each well followed by incubation at room temperature for 15 min. Subsequently, 30 ul of rabbit erythrocytes at a concentration of $1.25 \times 10_8$ cells/ml were added to each well. Positive controls for lysis consisted of erythrocytes in deionized water and erythrocytes in NHS diluted with VBS-MgEGTA. Negative controls for lysis consisted of erythrocytes in VBS-MgEGTA and erythrocytes in NHS diluted in VBS-EDTA (20 mM EDTA). Next, plates were incubated at 37 °C for

20 min, and then ice-cold VBS containing 50 mM EDTA was added to each well to quench hemolytic reactions. The plates were centrifuged at 1000 ×*g* for 5 min, and the supernatant was diluted 1:1 with deionized water in flat-bottom 96-well plates. Absorbance was measured spectrophotometrically at 405 nm to quantify lysis.

Apparent solubility measurements*:* Compstatin analogs were dissolved in PBS at pH 7.4 to concentrations of 10, 7.5, and 5 mg/ml. At each concentration point, the peptide solutions were shaken on a vortex mixer for 30 s and then centrifuged at 13,000 ×*g* for 5 min. The supernatant was collected and measured 5 times spectrophotometrically at 280 nm. Optical densities were converted into concentrations according to the Beer-Lambert law. An extinction coefficient of 11,125 $M^{-1}cm^{-1}$ was used for each compstatin analog as each peptide contains two tryptophan amino acids (tryptophan extinction coefficient being 5562.5 $M^{-1}cm^{-1}$).

RPE cell culture: The in vitro model of drusen biogenesis was used as previously reported [23] and used in assessing the efficacy of compstatin peptides [21,22]. Briefly, RPE cells from human fetal eyes, obtained as previously described [24], were used within the second passage were grown on laminin-coated porous inserts (Millipore, Billerica, MA) in Miller medium [25] supplemented with 5% fetal bovine serum (FBS; HyClone, Logan, UT) at 37 °C and 5% CO_2 in a humidified incubator. After culturing for 2–3 months, the cells were rinsed with PBS and treated with Miller medium containing either 5% FBS (negative control) or 10% NHS without or with the inhibitory peptides (2 uM).

The choise of the 2 μM dose for this assay was based on the intent to use double the IC_{50} concentration, which was determined to be about 1 μM. All inhibitory peptides were premixed with NHS on a rocker at room temperature for 30 min and then warmed to 37 °C before being added to the RPE cell cultures for 24 h. Next, the cells were rinsed with PBS, fixed in 4% paraformaldehyde (PFA; Electron Microscopy Sciences, Hatfield, PA) for 20 min, and stored in 0.4% PFA until use in the immunofluorescence assays.

Immunofluorescence of sub-RPE deposits*:* Basal deposits formed by the RPE cultures were visualized with immunofluorescence, as previously described [21,23]. Briefly, porous inserts were excised with a scalpel, cut into approximate 4 mm_2 pieces, and rinsed several times with PBS. Next, one half of all RPE culture inserts were embedded in 10% (w/v) agarose (Fisher, Waltham, MS) and sections at 100um using a vibratome, while the other half was subjected to decellularization (to remove the RPE monolayer) using our previously reported protocol [26,27]. Briefly, to obtain decellularized inserts, confluent RPE monolayers were incubated in Ca_{2+}, Mg_{2+}-free PBS for 30 min before treatment with a mild detergent composed of 1% Triton X-100 and 80 mM ammonium hydroxide for 5 min. The decellularized inserts were next rinsed in PBS three times before fixation with 4% PFA (20 min). Next, the vibratome sections and decellularized inserts were blocked with 5% donkey serum in PBS containing 0.5% BSA and 0.1% Triton X-100 (overnight at 4 °C) and labeled with mouse anti-C5b-9 (AbCam, Cambridge, MA; overnight at 4 °C or 2 h at room temperature), followed by labeling (2 h at room temperature) with Alexa Fluor 488-labeled anti-mouse immunoglobulin G (IgG; Life Technologies, Carlsbad, CA). The immunolabeled decellularized inserts were directly mounted in Fluoromount

(Sigma, St. Louis, MO) while the sections were counterstained with 4',6-diamidino-2-phenylindole (DAPI), a nuclear stain, before mounting.

Confocal imaging and analysis*:* Immunolabeled RPE sections and decellularized culture inserts were imaged using a Leica (Leica Microsystems, Buffalo Grove, IL) SP5 confocal microscope. Single-plane images from multiple non-overlapping areas were acquired using a 63× objective, and C5b-9$_n$ (MAC) immunofluorescence signals were quantified using ImageJ (National Institute of Health, Bethesda, MD), as we have previously reported [21]. Briefly, the color thresholding tool of ImageJ was used to analyze the intensity of C5b-9n associated fluorescence. Here, the upper intensity threshold was set such that the entire deposit area was selected for fluorescence intensity measurement while the lower intensity threshold was set to eliminate any background fluorescence. For statistical analysis, fluorescence intensity measurements of C5b-9n were averaged from multiple images and normalized with respect to the number of RPE nuclei per image (for vibratome sections) or the total image area (for decellularized whole mount samples) and then expressed as a percentage of the corresponding fluorescence intensities from samples exposed to NHS in the absence of any inhibitory peptide (positive control). All data were obtained from multiple images ($n \geq 9$) of fhRPE cells from the same donor and expressed as mean ± standard error of the mean (SEM). Statistical significance was determined using ANOVA (ANOVA), followed by Tukey's post-hoc analysis (Instat GraphPad Software Inc., La Jolla, CA). A p value of less than 0.05 was considered statistically significant.

Structural modeling: A structural model of the eight-linked PEG blocks was generated using MOLDRAW [28] and then attached to a structural model of Peptide 1 using structure editing tools in Chimera [29], to generate a structural model of Peptide 2. The structural model of Peptide 1 was derived from molecular dynamics simulations, based on the crystal structure of bound compstatin [30]. CHARMM parameters and topologies [31] were used and modified to incorporate the peptide-like bond between PEG_8 and Peptide 1. Modifications were rationally chosen based on existing amino acid parameters and topologies. Angles and dihedral angles that did not have a counterpart in existing CHARMM parameters and topologies were generated using SwissParam [32].

Molecular dynamics simulation: An explicit-solvent molecular dynamics simulation was performed, for 90 ns, using as the initial structure the modeled Peptide 2 structure. The explicit-solvent environment consisted of a water box and counterions to represent the solvated environment of the biomolecular system. The peptide was solvated in a TIP3P water box with dimensions of 75 × 57 × 67 Å, and charges were neutralized with sodium and chloride counterions at 150 mM. The TIP3P water model is a standard 3-site water model used in explicit solvent MD simulations that describes the configuration of the water molecules (rigidity/flexibility), polarization, and interactions in the simulation. Preparation steps (minimization, heating, and equilibration) were carried out to remove strain in the system, to heat the system to the desired temperature, and to relax the system prior to the production simulation dynamics, as described in a previous study [33]. Following 25,000 steps of conjugate gradient energy minimization, the system was

heated from 0 to 300 K in 62 ps with protein atoms constrained to post-minimization positions. Subsequently, the system was equilibrated through five stages for 50 ps per stage. Force constants of 41.83, 20.92, 8.368, and 4.184 kJ/mol/Å$_2$ were applied during the first four stages, respectively, to harmonically constrain all protein atoms to their post-minimization positions. During the fifth stage of equilibration, only the backbone atoms were harmonically constrained using a force constant of 4.184 kJ/mol/Å$_2$. Following equilibration, a production run was performed for 90 ns with periodic boundary conditions, SHAKE algorithm, 2 fs time steps, Langevin pressure and temperature controls, and particle-mesh Ewald electrostatics. The molecular dynamics trajectory (9,000 frames) was clustered using the root-mean-square deviation (RMSD) of the backbone or alpha carbon atoms of Peptide 2, and a representative structure from the highest-populated clusters was identified and depicted for molecular graphics visualization.

Results

The objective of this study is to optimize the aqueous solubility while maintaining the binding affinity of Peptide 1 (Table A1), our compstatin peptide that previously had the most promise to become a therapeutic for AMD. Our previous studies [21,22] focused on improving the solubility of the peptide that underwent clinical studies for AMD, with sequence Ac-I[CV(meW)QDWGAHRC]T-NH_2 [13]. This peptide had high aggregation propensity in aqueous solution, attributed to the peptide's reduced solubility compared to other less potent compstatin analogs [21]. It was first shown that adding polar dipeptides at the N-terminus (positions −1 and 0) improved solubility while maintaining potency, with the peptide Ac-RSI[CV(meW)QDWGAHRC]T-NH_2 was the most efficacious in the human RPE cell–based assay described in Methods (Peptide VI in [21]). In a subsequent study, it was deemed necessary to eliminate the methyl group from tryptophan at position 4 to further improve solubility, without compromising potency, resulting in the sequence of Peptide 1 (Peptide 9 in [22]).

To achieve our objective, we redesigned Peptide 1 by adding PEG block extensions at the C-terminus (Peptide 2; Table A1). The choice of the extension at the C-terminus of Peptide 2 was guided by the results of molecular dynamics simulations, which had shown that the C-terminus of compstatin points away from the C3-binding site toward the solvent [21,34]. Thus, we reasoned that such extensions would not interfere with the binding interface between the compstatin analog and C3. Peptide 2 contains eight PEG blocks attached at the peptide backbone in the C-terminus. The choice of PEG blocks was guided by earlier surface plasmon resonance (SPR) and enzyme-linked

immunosorbent assay (ELISA) data, which had shown that PEGylated compstatin peptides had higher solubility compared to non-PEGylated peptides with the same sequence [35]. The addition of a spacer of eight PEG blocks to compstatin analogs was deemed necessary for the SPR binding experiments to increase the space between the peptides and attachment to the streptavidin sensor chip via lysine–biotin binding. This spacer aimed to increase the mobility of the peptides, enhance their accessibility to C3, and decrease non-specific interactions, thus emulating unbound ligand states as closely as possible within the experimental constraints. The inhibitory activities of peptides with the same sequences, but without the PEG blocks, were tested using ELISAs in the same study [35]. PEGylation is an established procedure in drug design and delivery, as this procedure has been shown to increase aqueous solubility and bioavailability, including enhanced structural and chemical stability and circulation lifespan, and reduced renal clearance [36]. In addition, PEGylation has a shielding effect on drugs, typically reducing drug immunogenicity, antigenicity, and toxicity [36]. Currently, there are several PEGylated drugs in the clinic, including pegaptanib, which has been used for the treatment of age-related macular degeneration [37]. PEGylation has also been used in a compstatin variant with modified backbone, but in that case, a large (40 kDa) Y-shaped PEG structure was attached either at the N- or C-terminus [38], compared to the small (423 Da) linear 8-PEG block structure attached at the C-terminus in our study.

Figure 1 shows the dose–response curves of the complement hemolytic assay for the PEGylated Peptide 2 and the parent Peptide 1 (positive control). Peptides 1 and 2 have similar IC_{50} values within the confidence intervals from four replicate experiments,

and therefore similar potencies (Table 2).

We then tested our solubility objective. Figure A2A shows the difference between the calculated and spectrophotometrically measured (observed) concentrations in the range of 5–10 mg/ml. The concentration was experimentally measured using absorption spectroscopy at 280 nm and calculated using the weight per volume values of the dilution series, as described in Methods. Peptide 2 is much more soluble than Peptide 1 at 5 mg/ml, as the concentration difference is close to zero, the expected difference for nearly perfect solubility. In addition, Peptide 2 remains soluble up to 10 mg/ml with a slight deviation from the difference of zero, whereas the difference of Peptide 1 significantly deviates from zero and from constancy as the concentration increases. Figure 2B shows a different presentation of the same data in the form of a correlation plot between the observed and calculated peptide concentrations in millimolar. The data for Peptide 2 show much higher correlation than those for Peptide 1. In addition, the fitted straight line of the data for Peptide 2 is closer to a straight line with slope 1 that passes through the origin (Figure A2B). A straight line with slope 1 represents perfect correlation, denoting the highest solubility and the lowest aggregation. These data demonstrate that Peptide 2 has significantly higher apparent solubility, or significantly lower tendency to aggregate, than the parent Peptide 1.

We continued our study by testing the efficacy of Peptides 1 and 2 in a human RPE cell–based assay [23], which was used in previous optimizations of compstatin family peptides [21,22]. This assay is based on a human RPE cell culture that mimics the pathophysiology of AMD and can be used to interrogate the effects of complement

activation in AMD pathogenesis. The assay is useful for quantification of the effects of inhibitors on complement activation mediated by sub-RPE drusen-like deposits, typical of those present in early AMD. Figure A3 shows the deposition of deposit-associated C5b-9_n following the addition of NHS as a complement source [21,23]. Exposure of cell-free inserts to NHS did not show any evidence of C5b-9_n immunoreactivity (Supplemental Figure A1), indicating that the baseline level of alternative pathway activation in NHS does not likely contribute to this increased accumulation of sub-C5b-9_n. Confocal imaging of immunolabeled RPE culture sections (Figure A3) and (decellularized) whole mounts (Supplemental figure A2) revealed that deposit-associated sub-RPE C5b-9_n deposition is inhibited by both compstatin peptides. More specifically, quantification of anti-C5b-9 immunofluorescence from whole mounts revealed that Peptide 2 causes a remarkable 80% inhibition ($p<0.001$) of complement activation (Figure A4). The inhibitory effect of Peptide 2 was significantly greater ($p<0.001$) than that achieved by Peptide 1, which reduced C5b-9_n deposition to a lesser degree (50%; $p<0.001$).

In combination, the hemolytic assay, apparent solubility, and human RPE cell–based assay data indicate that Peptide 2 is a more promising compstatin analog for further optimization and potential clinical translation, compared to Peptide 1. The parent Peptide 1 had emerged to be the best analog until now in previous studies, in terms of solubility and affinity balance and efficacy of complement inhibition in the human RPE cell–based assay (see [21,22] and references therein for earlier optimization studies).

To gain insight into the molecular features that contribute to the structural stability and solubility of Peptide 2, we performed an extended molecular dynamics

simulation. Figure A5A shows representative conformations from the top (highest occupancy) five structural clusters derived from the molecular dynamics trajectory, using backbone atom RMSD-based clustering. These five clusters represent 79% of the conformations spanned by the peptide. The PEG_8 C-terminal extension demonstrates high local flexibility and global mobility, in essence forming a dynamic polar shell around Peptide 2. Flexibility and mobility of the PEG_8 extension are expected, given its polar character and interactions with water molecules of the solvent. This dynamic polar shell perhaps functions as a shield from self-association and aggregation of Peptide 2 owed to peptide's inherent hydrophobic features, thus contributing to the solubility of the peptide.

Figure A5B shows the conformation of the representative peptide from the structural cluster with highest occupancy, depicting key amino acid side chains for the optimization of compstatin from research in the past 20 years. These amino acids are Arg(-1), Val3, Trp4, Trp7, Ala9, and the disulfide bridge Cys2-Cys12. The Arg(-1) addition corresponds to the Arg(-1)/Ser0 extension of Peptide 1 [22], the parent analog of Peptide 2. Our latest addition in this work is the PEG_8-NH_2 (Figure A5D) extension at the C-terminus (Figure A5A–C), which results in Peptide 2, our most promising, in terms of affinity and solubility properties, lead peptide of the compstatin family until now.

Discussion

We report the design of a new compstatin peptide that has superior aqueous solubility and comparable complement inhibitory activity characteristics, compared to previously known peptides of the compstatin family. The new peptide, Peptide 2 (Table A1), is a PEGylated form of our previously most promising peptide in terms of inhibitory activity and aqueous solubility, Peptide 1 (Table A1) [22]. Peptide 2 has eight PEG blocks attached to the backbone C-terminus, accounting for an additional molecular mass of 423 Da compared to Peptide 1 (Table A1). Since the original discovery of compstatin using a phage-displayed random peptide library [39], there have been many benchmarks in the optimization of the sequence of compstatin. Initial structure-activity studies had derived a sequence template with seven amino acids being indispensable for inhibitory activity and six amino acids being optimizable [17,40]. Figure A5B shows the side chains of essential amino acids for the optimal binding and inhibitory activity of compstatin, including benchmark residue-specific optimization steps over the period of several years. Initial NMR, alanine scan, and inhibitory activity studies indicated that Val3 and Trp7 are important for binding to C3 and inhibition of complement activation [41,42]. A subsequent crystal structure of C3c in complex with a compstatin analog confirmed these findings, showing that Val3 and Trp7 are inserted in hydrophobic cavities [30]. Benchmark optimization steps include the incorporation of (i) Ala at position 9, which introduces helicity in the sequence and shifts a structural beta-turn from the central toward the C-terminal portion of the sequence [41,42]; (ii) aromatic amino acids at position 4 [16] with Trp4 being optimal [18], which was shown to participate in a

hydrophobic clustering in the crystal structure [30]; (iii) dipeptide N-terminal extensions, with Arg at position −1 being optimal because it increased solubility compared to previous peptides and introduced a new intermolecular salt bridge as shown by molecular dynamics simulations [21,22]; and in this work, (iv) C-terminal extension using an eight-block PEG construct, which greatly increases aqueous solubility, unprecedented by any other compstatin analog. In addition, acetylation at the N-terminus and amidation at the C-terminus contribute to improved activity [43]. All active peptides contain a Cys2-Cys12 disulfide bridge.

Compstatin has two surfaces, a hydrophobic and a polar one, as was pointed out by the original NMR studies [41,42], but it is the hydrophobic surface that makes the main contacts with the C3, as it was pointed out by the crystal structure [30]. It is likely that the hydrophobic surface is responsible for the aggregation properties of the compstatin analog that underwent the early clinical trials. This analog contained a methylated Trp4 residue, in which the hydrophobic methyl group had replaced the polar hydrogen of the indole amide group, making the peptide even more hydrophobic. We had reasoned in earlier optimization studies that incorporation of polar amino acid extensions at the termini would increase solubility without perturbing binding properties, and this was shown to be the case for the N-terminus [21,22] and C-terminus (Mohan RR, Gorham RD Jr, Morikis D, unpublished data). However, the analog with the best aqueous solubility is Peptide 2 of this work that incorporates an 8-PEG block construct at the C-terminus. Our earlier molecular dynamics studies had shown that the C-terminus is mobile pointing outward from the C3-peptide interface toward the solvent. Thus, we

reasoned that the 8-PEG block construct would not sterically interfere with the binding interface of the C3-peptide complex. This is evident in Figure A5, where the 8-PEG construct shows mobility around the non-binding site of Peptide 2, without specific contacts with the peptide. Therefore, PEGylation acts a solubilizer of compstatin.

To determine the potential of Peptide 2 and its parent Peptide 1 as AMD therapeutics, we evaluated the peptides in the human RPE cell–based assay. As we have reported before [36], this in vitro assay is characterized by the formation of C5b-9-rich sub-RPE deposits, a hallmark of dry AMD. Thus, this assay represents a unique testbed for screening therapeutic candidates for treatment of dry AMD. We have successfully used this assay for our recent optimization studies that resulted in the incorporation of polar N-terminal extensions in our compstatin analogs [21,22]. Here, we use this assay to demonstrate that Peptides 1 and 2 significantly inhibit the formation of C5b-9-rich sub-RPE deposits, with the PEGylated Peptide 2 exhibiting a twofold greater inhibitory effect than the parent Peptide 1. This difference in anti-C5b-9 effect may be attributed to lack of aggregation of Peptide 2, owing to its greater solubility compared to Peptide 1, which is expected to result in a higher "effective" concentration in the RPE culture. At the molecular level, the optimal solubility of Peptide 2 results from the formation of a dynamic polar shell, introduced by PEGylation, which predominantly surrounds and enhances the polar surface, and to a lesser extent the nonpolar surface of the peptide. This polar shell is designed to be a solubilizer, shielding Peptide 2 from self-association and higher-order aggregation, while leaving it unobstructed for binding the nonpolar surface.

In conclusion, we report the design of a new peptide analog of compstatin that

combines an arginine-serine N-terminal polar amino acid extension and an 8-PEG block C-terminal extension. This peptide demonstrates significantly improved aqueous solubility and efficacy in a human RPE cell–based assay that mimics the pathobiology of AMD, compared to its parent peptide, while retaining comparable inhibitory activity against complement activation as its parent peptide. The new peptide can lead to a therapeutic treatment of dry AMD, as the peptide overcomes the aggregation limitation of a previous compstatin analog that underwent clinical trials.

TABLE 1. PEPTIDE SEQUENCES.		
Peptide	**Sequence**	**Molecular mass**
1	Ac- RSI[CVWQDWGAHRC]T -NH_2	1856
2	Ac- RSI[CVWQDWGAHRC]T-PEG_8 -NH_2	2279

Table A1. Peptide 1 is a positive control with a two-polar amino acid N-terminal extension.[22] Peptide 2 is a new design that contains an 8-PEG block backbone extension. Brackets denote disulfide bridge cyclization between the two cysteine amino acids. Ac: acetylation blocking group; NH2: amidation blocking group.

TABLE 2. IC_{50} VALUES FROM HEMOLYTIC ASSAY.			
Peptide	**Mean IC_{50} (μM)**	**95% Confidence interval**	
		Upper	**Lower**
1	0.97	1.04	0.90
2	0.96	1.14	0.80

Table A2. IC50: Ligand concentration at 50% maximal inhibition. Data are from four replicate experiments (n=4).

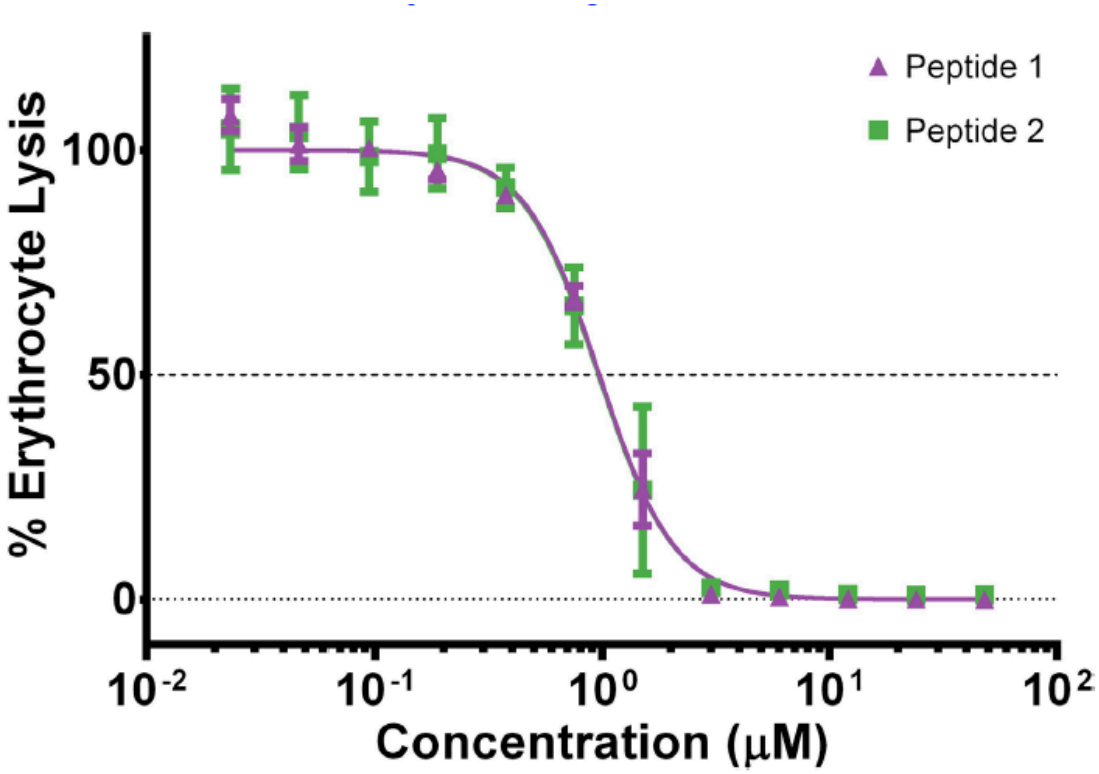

Figure A1. Concentration-dependent inhibition curves of compstatin peptides in four replicate hemolytic assay experiments. The plotted data represent the mean percent inhibition ± standard error of the mean (SEM). The dashed line intersects each inhibition curve at the IC50. Peptide 1 is the parent peptide (positive control), and Peptide 2 is the PEGylated form of the parent peptide.

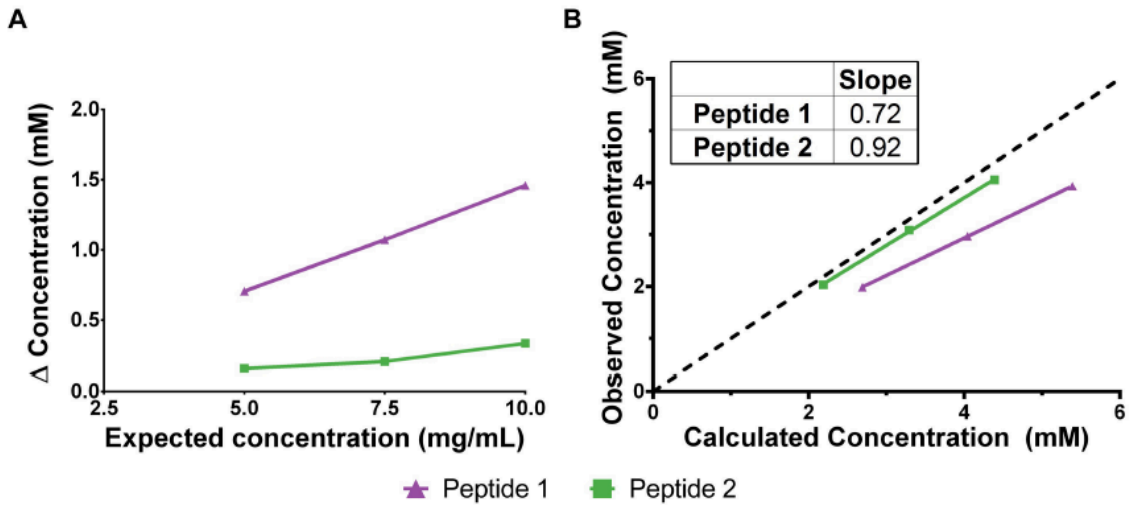

Figure A2. Apparent solubility of compstatin peptides. **A**: The difference in concentration, calculated – observed (measured), in mM, plotted against the expected concentration (in mg/ml). The actual observables are plotted, the expected concentration (in mg/ml) of the dilution series on the horizontal axis, and the observed (in mM, measured using tryptophan absorbance) minus the calculated (in mM, from the mg/ml expected concentration values) on the vertical axis. Peptide 2 is the most soluble, as the concentration difference is close to zero and remains nearly constant in the dilution series. **B**: Correlation of the observed concentration with the calculated concentration, with the concentrations presented in mM. Peptide 2 is the most soluble, as indicated by the high correlation between the observed and calculated concentrations (slope of 0.92). Each data point represents the mean measured concentration and the corresponding expected concentration with a linear regression fit to the data. A straight line of slope 1 passing through the origin is inserted to indicate the closeness of the data to perfect correlation.

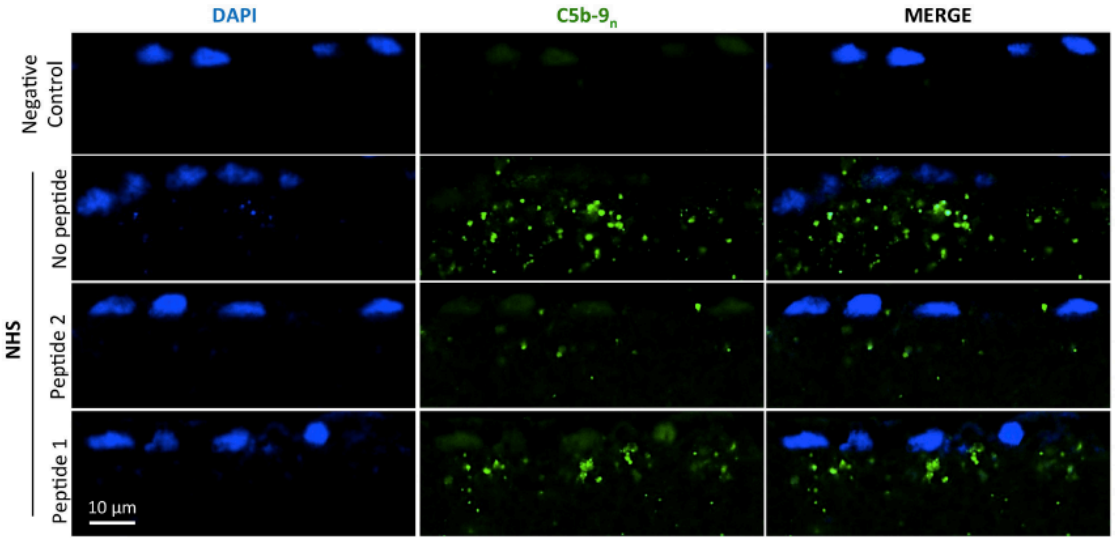

Figure A3. Human RPE cells form basal deposits rich in C5b-9n (MAC) in vitro, and inhibitory effects of compstatin peptides. Representative cross-sectional images show 3-month-old RPE cell cultures labeled with anti-C5b-9n (green) and 4',6-diamidino-2-phenylindole (DAPI; blue), following exposure to either 10% normal human serum (NHS) alone or together with Peptides 1 and 2 for 24 h. Cultures that received no NHS treatment served as a negative control. Scale bar = 10um.

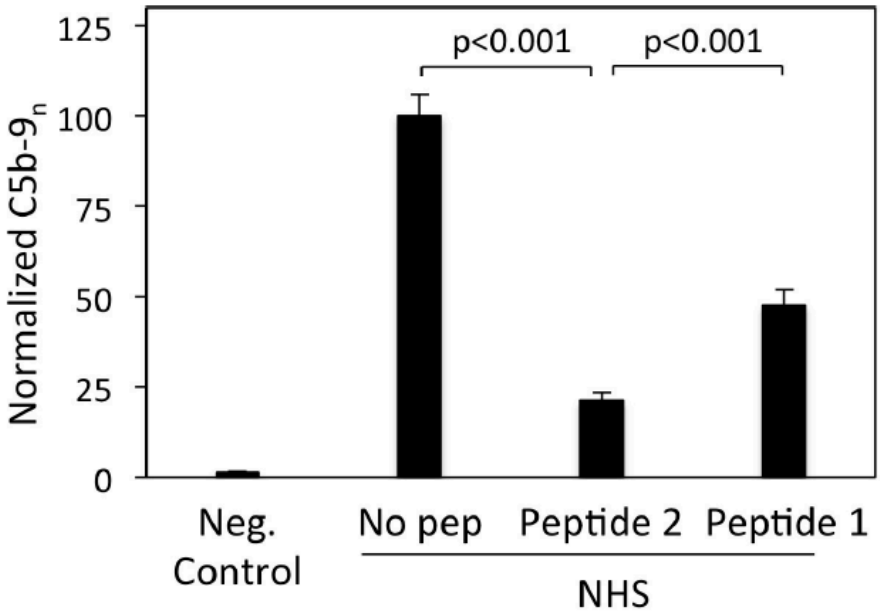

Figure A3. Compstatin peptides inhibit complement-induced C5b-9n deposition in RPE culture. Fluorescence intensity measurements from anti-C5b-9n-labeled (decellularized) whole mount samples (n > 9) were normalized with respect to human serum (NHS)-treated samples and plotted as mean ± standard error of the mean (SEM). Data analyses show that Peptide 2 causes 80% reduction in NHS-induced basal C5b-9n deposition by RPE cells. Peptide 1 exhibits a weaker inhibitory effect, reducint C5b-9n deposition by 50%. Bars indicare mean ± SEM.

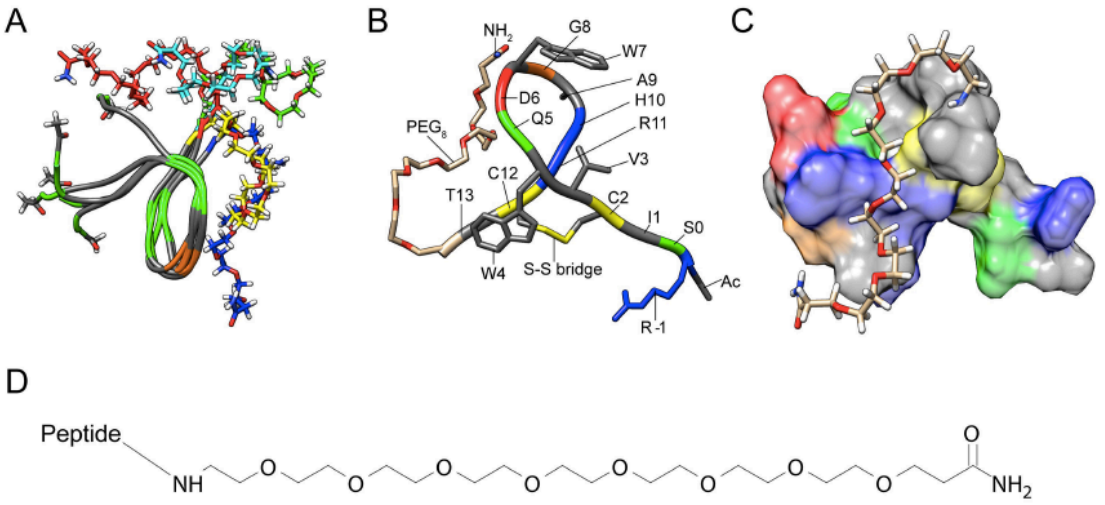

Figure A5. Molecular structure of Peptide 2. **A**: Representative conformers of Peptide 2 from the five highest-populated root-mean-square deviation (RMSD) clusters of the molecular dynamics trajectory, with occupancies of 38%, 12%, 10%, 10%, and 9%. The peptide backbone is shown in a tube representation, colored by the amino acid property type: gray for hydrophobic, green for polar, and brown for glycine. Cys2 and Cys12 are marked as hydrophobic because they form a disulfide bridge. The PEG8 C-terminal extensions are shown in stick models of different colors for each conformer. The acetyl and amide terminal blocks are shown in stick models, colored by atom type: gray for carbon, white for hydrogen, blue for nitrogen, and red for oxygen. **B**: The major conformer of Peptide 2 (38% occupancy) in backbone tube representation, with key side chains in compstatin peptide optimization in stick representation. The location of all amino acids is marked. The following color code is used: gray for hydrophobic, green for polar neutral, blue for basic, red for acidic, yellow for cysteines and the disulfide bridge, and brown for glycine. The PEG8-NH2 C-terminal extension is shown in stick

representation without hydrogens, with carbons depicted in brown, oxygens in red, and nitrogen in blue. **C**: Surface representation of Peptide 2, with the PEG8-NH2 extension shown in stick representation (including hydrogens). The color code is as in Panel **B**, with the added hydrogens of PEG8-NH2 shown in white. **D**: The chemical structure of PEG8-NH2.

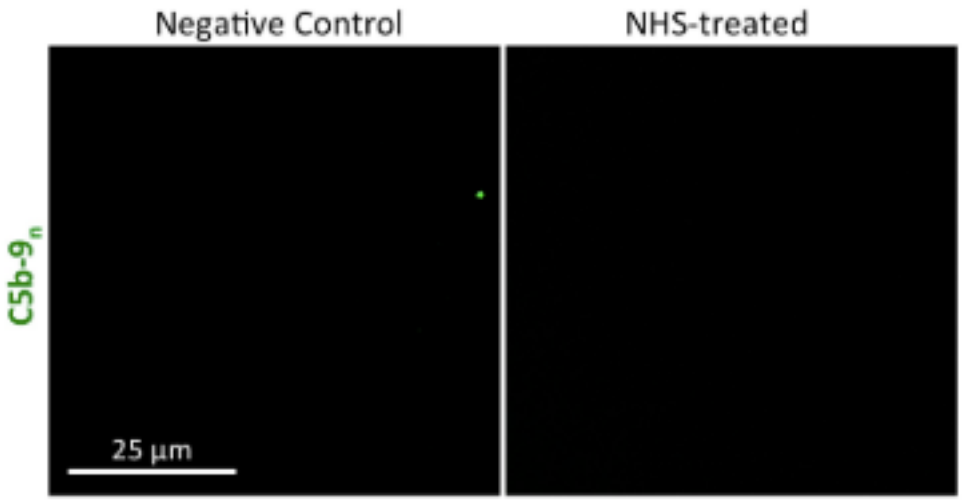

Supplemental Figure A1. Representative whole-mount images show 'cell-free' culture inserts labeled with anti-C5b-9n (green) following exposure to 10% NHS for 24h. No evidence of C5b-9n immunoreactivity is seen in the absence of RPE cells.

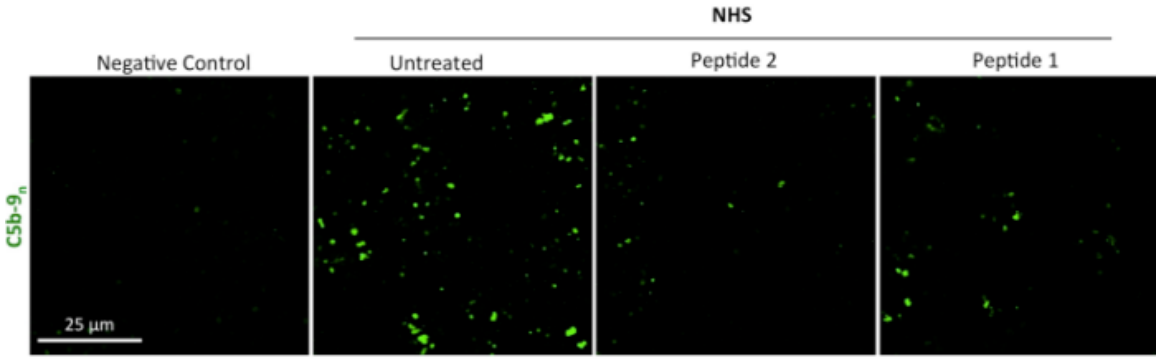

Supplemental Figure A2. Representative whole-mount images show two month-old RPE cell cultures labeled with anti-C5b-9n (green) following exposure to either 10% NHS alone or together with peptides 1 and 2 for 24h. Cultures that received no NHS treatment served as a negative control. Scale bar: 25um.

References

1. Liszewski MK, Atkinson JP. Complement regulators in human disease: lessons from modern genetics. J Intern Med 2015; 277:294-305.

2. Schramm EC, Clark SJ, Triebwasser MP, Raychaudhuri S, Seddon JM, Atkinson JP. Genetic variants in the complement system predisposing to age-related macular degeneration: A review. Mol Immunol 2014; 61:118-25.

3. Black JRM, Clark SJ. Age-related macular degeneration: genome-wide association studies to translation. Genet Med 2016; 18:283-9.

4. Anderson DH, Radeke MJ, Gallo NB, Chapin EA, Johnson PT, Curletti CR, Hancox LS, Hu J, Ebright JN, Malek G, Hauser MA, Rickman CB, Bok D, Hageman GS, Johnson LV. The pivotal role of the complement system in aging and age-related macular degeneration: Hypothesis re-visited. Prog Retin Eye Res 2010; 29:95-112.

5. Hageman GS, Anderson DH, Johnson LV, Hancox LS, Taiber AJ, Hardisty LI, Hageman JL, Stockman HA, Borchardt JD, Gehrs KM, Smith RJH, Silvestri G, Russell SR, Klaver CCW, Barbazetto I, Chang S, Yannuzzi LA, Barile GR, Merriam JC, Smith RT, Olsh AK, Bergeron J, Zernant J, Merriam JE, Gold B, Dean M, Allikmets R. A common haplotype in the complement regulatory gene factor H (HF1/CFH) predisposes individuals to age-related macular degeneration. Proc Natl Acad Sci USA 2005; 102:7227-32.

6. Klein RJ, Zeiss C, Chew EY, Tsai J-Y, Sackler RS, Haynes C, Henning AK, SanGiovanni JP, Mane SM, Mayne ST, Bracken MB, Ferris FL, Ott J, Barnstable C, Hoh J. Complement Factor H Polymorphism in Age-Related Macular Degeneration. Science 2005; 308:385-9.

7. Haines JL, Hauser MA, Schmidt S, Scott WK, Olson LM, Gallins P, Spencer KL, Kwan SY, Noureddine M, Gilbert JR, Schnetz-Boutaud N, Agarwal A, Postel EA, Pericak-Vance MA. Complement Factor H Variant Increases the Risk of Age-Related Macular Degeneration. Science 2005; 308:419-21.

8. Edwards AO, Ritter R, Abel KJ, Manning A, Panhuysen C, Farrer LA. Complement Factor H Polymorphism and Age-Related Macular Degeneration. Science 2005; 308:421-4.

9. Hollyfield JG. Age-Related Macular Degeneration: The Molecular Link between Oxidative Damage, Tissue-Specific Inflammation and Outer Retinal Disease The Proctor Lecture. Invest Ophthalmol Vis Sci 2010; 51:1276-81.

10. Anderson DH, Mullins RF, Hageman GS, Johnson LV. A role for local inflammation in the formation of drusen in the aging eye. Am J Ophthalmol 2002; 134:411-31.

11. Lai K, Landa G. Current choice of treatments for neovascular AMD. Expert Review of Clinical Pharmacology 2015; 8:135-40.

12. Morikis D, Lambris JD. Structure, dynamics, activity, and function of compstatin and design of more potent analogues. Structural Biology of the Complement System 2005:317–40.

13. Ricklin D, Lambris JD. Compstatin: A Complement Inhibitor on its Way to Clinical Application. In: Lambris JD, editor. Current Topics in Complement Ii. Vol 6322008. p. 273–92.

14. Zarbin MA, Rosenfeld PJ. PATHWAY-BASED THERAPIES FOR AGE-RELATED MACULAR DEGENERATION An Integrated Survey of Emerging Treatment Alternatives. Retina-the Journal of Retinal and Vitreous Diseases 2010; 30:1350-67.

15. Yehoshua Z, Rosenfeld PJ, Albini TA. Current Clinical Trials in Dry AMD and the Definition of Appropriate Clinical Outcome Measures. Semin Ophthalmol 2011; 26:167-80.

16. Klepeis JL, Floudas CA, Morikis D, Tsokos CG, Argyropoulos E, Spruce L, Lambris JD. Integrated computational and experimental approach for lead optimization and design of compstatin variants with improved activity. J Am Chem Soc 2003; 125:8422-3.

17. Morikis D, Soulika AM, Mallik B, Klepeis JL, Floudas CA, Lambris JD. Improvement of the anti-C3 activity of compstatin using rational and combinatorial approaches. Biochem Soc Trans 2004; 32:28-32.

18. Mallik B, Katragadda M, Spruce LA, Carafides C, Tsokos CG, Morikis D, Lambris JD. Design and NMR characterization of active analogues of compstatin containing non-natural amino acids. J Med Chem 2005; 48:274-86.

19. Katragadda M, Magotti P, Sfyroera G, Lambris JD. Hydrophobic effect and hydrogen bonds account for the improved activity of a complement inhibitor, compstatin. J Med Chem 2006; 49:4616-22.

20. Morgan BP, Harris CL. Complement, a target for therapy in inflammatory and degenerative diseases. Nat Rev Drug Discov 2015; 14:857-77.

21. Gorham RD Jr, Forest DL, Tamamis P, Lopez de Victoria A, Kraszni M, Kieslich CA, Banna CD, Bellows-Peterson ML, Larive CK, Floudas CA, Archontis G, Johnson LV, Morikis D. Novel compstatin family peptides inhibit complement activation by drusen-like deposits in human retinal pigmented epithelial cell cultures. Exp Eye Res 2013; 116:96-108.

22. Gorham RD Jr, Forest DL, Khoury GA, Smadbeck J, Beecher CN, Healy ED, Tamamis P, Archontis G, Larive CK, Floudas CA, Radeke MJ, Johnson LV, Morikis D. New Compstatin Peptides Containing N-Terminal Extensions and Non-Natural Amino Acids Exhibit Potent Complement Inhibition and Improved Solubility Characteristics. J Med Chem 2015; 58:814-26.

23. Johnson LV, Forest DL, Banna CD, Radeke CM, Maloney MA, Hu J, Spencer CN, Walker AM, Tsie MS, Bok D, Radeke MJ, Anderson DH. Cell culture model that mimics drusen formation and triggers complement activation associated with age-related macular degeneration. Proc Natl Acad Sci USA 2011; 108:18277-82.

24. Hu J, Bok D. A cell culture medium that supports the differentiation of human retinal pigment epithelium into functionally polarized monolayers. Mol Vis 2001; 7:14-9.

25. Maminishkis A, Chen S, Jalickee S, Banzon T, Shi G, Wang FE, Ehalt T, Hammer JA, Miller SS. Confluent monolayers of cultured human fetal retinal pigment epithelium exhibit morphology and physiology of native tissue. Invest Ophthalmol Vis Sci 2006; 47:3612-24.

26. Yang X, Scott HA, Monickaraj F, Xu J, Ardekani S, Nitta CF, Cabrera A, McGuire PG, Mohideen U, Das A, Ghosh K. Basement membrane stiffening promotes retinal endothelial activation associated with diabetes. FASEB 2016; 30:601-11.

27. Yang X, Scott HA, Ardekani S, Williams M, Talbot P, Ghosh K. Aberrant cell and basement membrane architecture contribute to sidestream smoke-induced choroidal endothelial dysfunction. Invest Ophthalmol Vis Sci 2014; 55:3140-7. [PMID: 24713480].

28. Ugliengo P, Viterbo D, Chiari G. MOLDRAW - MOLECULAR GRAPHICS ON A PERSONAL-COMPUTER. Z Kristallogr 1993; 207:9-23.

29. Pettersen EF, Goddard TD, Huang CC, Couch GS, Greenblatt DM, Meng EC, Ferrin TE. UCSF chimera - A visualization system for exploratory research and analysis. J Comput Chem 2004; 25:1605-12.

30. Janssen BJC, Halff EF, Lambris JD, Gros P. Structure of compstatin in complex with complement component C3c reveals a new mechanism of complement inhibition. J Biol Chem 2007; 282:29241-7. [

31. Brooks BR, Brooks CL, Mackerell AD, Nilsson L, Petrella RJ, Roux B, Won Y, Archontis G, Bartels C, Boresch S, Caflisch A, Caves L, Cui Q, Dinner AR, Feig M, Fischer S, Gao J, Hodoscek M, Im W, Kuczera K, Lazaridis T, Ma J, Ovchinnikov V, Paci E, Pastor RW, Post CB, Pu JZ, Schaefer M, Tidor B, Venable RM, Woodcock HL, Wu X, Yang W, York DM, Karplus M. CHARMM: The biomolecular simulation program. J Comput Chem 2009; 30:1545-614.

32. Zoete V, Cuendet MA, Grosdidier A, Michielin O. SwissParam: A Fast Force Field Generation Tool for Small Organic Molecules. J Comput Chem 2011; 32:2359-68.

33. Mohan RR, Gorham RD Jr, Morikis D. A theoretical view of the C3d:CR2 binding controversy. Mol Immunol 2015; 64:112-22.

34. Tamamis P, Lopez de Victoria A, Gorham RD Jr, Bellows-Peterson ML, Pierou P, Floudas CA, Morikis D, Archontis G. Molecular Dynamics in Drug Design: New Generations of Compstatin Analogs. Chem Biol Drug Des 2012; 79:703-18.

35. Lopez de Victoria A, Gorham RD Jr, Bellows-Peterson ML, Ling J, Lo DD, Floudas CA, Morikis D. A New Generation of Potent Complement Inhibitors of the Compstatin Family. Chem Biol Drug Des 2011; 77:431-40.

36. Kang JS, DeLuca PP, Lee KC. Emerging PEGylated drugs. Expert Opin Emerg Drugs 2009; 14:363-80.

37. Li WJ, Zhan P, De Clercq E, Lou HX, Liu XY. Current drug research on PEGylation with small molecular agents. Prog Polym Sci 2013; 38:421-44.

38. Risitano AM, Ricklin D, Huang YJ, Reis ES, Chen H, Ricci P, Lin ZE, Pascariello C, Raia M, Sica M, Del Vecchio L, Pane F, Lupu F, Notaro R, Resuello RRG, DeAngelis RA, Lambris JD. Peptide inhibitors of C3 activation as a novel strategy of complement inhibition for the treatment of paroxysmal nocturnal hemoglobinuria. Blood 2014; 123:2094-101.

39. Sahu A, Kay BK, Lambris JD. Inhibition of human complement by a C3-binding peptide isolated from a phage-displayed random peptide library. J Immunol 1996; 157:884-91.

40. Morikis D, Lambris JD. Structural aspects and design of low-molecular-mass complement inhibitors. Biochem Soc Trans 2002; 30:1026-36.

41. Morikis D, Assa-Munt N, Sahu A, Lambris JD. Solution structure of Compstatin, a potent complement inhibitor. Protein Sci 1998; 7:619-27.

42. Morikis D, Roy M, Sahu A, Troganis A, Jennings PA, Tsokos GC, Lambris JD. The structural basis of compstatin activity examined by structure-function-based design of peptide analogs and NMR. J Biol Chem 2002; 277:14942-53.

43. Sahu A, Soulika AM, Morikis D, Spruce L, Moore WT, Lambris JD. Binding kinetics, structure-activity relationship, and biotransformation of the complement inhibitor compstatin. J Immunol 2000; 165:2491-9.